RL-TR-94-113
Final Technical Report
August 1994

CLASSICAL ANALYSIS METHODS FOR DESIGNING AND DEVELOPING DOWNLOOKING RADARS

NTL Technologies, Inc.

George Skahill

APPROVED FOR PUBLIC RELEASE; DISTRIBUTION UNLIMITED.

Rome Laboratory
Air Force Materiel Command
Griffiss Air Force Base, New York

This report has been reviewed by the Rome Laboratory Public Affairs Office (PA) and is releasable to the National Technical Information Service (NTIS). At NTIS it will be releasable to the general public, including foreign nations.

RL-TR-94-113 has been reviewed and is approved for publication.

APPROVED: Michael J. Callahan

MICHAEL J. CALLAHAN
Project Engineer

FOR THE COMMANDER: Luke L. Lucas

LUKE L. LUCAS, Colonel, USAF
Deputy Director
Surveillance & Photonics

If your address has changed or if you wish to be removed from the Rome Laboratory mailing list, or if the addressee is no longer employed by your organization, please notify RL (OCDS) Griffiss AFB NY 13441. This will assist us in maintaining a current mailing list.

Do not return copies of this report unless contractual obligations or notices on a specific document require that it be returned.

REPORT DOCUMENTATION PAGE

Form Approved
OMB No. 0704-0188

1. AGENCY USE ONLY (Leave Blank)	2. REPORT DATE	3. REPORT TYPE AND DATES COVERED
	August 1994	Final Sep 92 - Apr 94

4. TITLE AND SUBTITLE
CLASSICAL ANALYSIS METHODS FOR DESIGNING AND DEVELOPING DOWNLOOKING RADARS

5. FUNDING NUMBERS
C - F30602-92-C-0080
PE - 62702F
PR - 4506
TA - 14
WU - PA

6. AUTHOR(S)
George Skahill

7. PERFORMING ORGANIZATION NAME(S) AND ADDRESS(ES)
NTL Technologies, Inc.
159 Clay Pitts Road
Greenlawn NY 11740

8. PERFORMING ORGANIZATION REPORT NUMBER
N/A

9. SPONSORING/MONITORING AGENCY NAME(S) AND ADDRESS(ES)
Rome Laboratory (OCDS)
26 Electronic Pky
Griffiss AFB NY 13441-4514

10. SPONSORING/MONITORING AGENCY REPORT NUMBER
RL-TR-94-113

11. SUPPLEMENTARY NOTES
Rome Laboratory Project Engineer: Michael J. Callahan/OCDS/(315) 330-4441

12a. DISTRIBUTION/AVAILABILITY STATEMENT
Approved for public release; distribution unlimited.

12b. DISTRIBUTION CODE

13. ABSTRACT (Maximum 200 words)
This report describes analytical methods for characterizing the distributions of surface clutter as observed by downlooking radars over spherical planets, taking the classical, pencil and paper, methods of analytic geometry and calculus as far as possible before turning to computer based numerical evaluations. General expressions describing surface clutter power distributions in range and range-rate coordinates are developed in closed form and evaluated for several low PRF, phased array configurations.

Information contained in this document formed the subject matter for a series of eight lectures at Rome Laboratory, under this contract, to relative newcomers to the study of clutter limited radar. With the classicial analysis tools, they were able to quickly obtain results which compared favorably with those from elaborate simulations evolved by teams of experts over periods of many years.

14. SUBJECT TERMS	15. NUMBER OF PAGES
Radar, Airborne Radar, Space Based Radar, Radar Clutter, Earth Surface Clutter	96
	16. PRICE CODE

17. SECURITY CLASSIFICATION OF REPORT	18. SECURITY CLASSIFICATION OF THIS PAGE	19. SECURITY CLASSIFICATION OF ABSTRACT	20. LIMITATION OF ABSTRACT
UNCLASSIFIED	UNCLASSIFIED	UNCLASSIFIED	SAR

FOREWORD

This report was prepared under Contract F30602-92-C-0080, entitled Classical Analysis Methods for Designing and Developing Downlooking Radars. It was submitted in compliance with CLIN0002 Data Item A003 of the contract. The Rome Laboratory Project Engineer was Mr. Michael J. Callahan of Rome Laboratories/OCDS.

Section 1 is an introduction to the concept and the advantages of formulating computer models for the examination of terrain clutter effects on downlooking radars using the classical methods of calculus, analytical geometry and electromagnetic theory. In this approach, paper and pencil analyses are pursued stubbornly before transitions to computer based evaluations are begun.

Development of a closed form integral expression for the earth's surface clutter power received by a monostatic downlooking radar, including antenna and waveform effects, is given in Section 2. Examples of evaluation methods and results are described in Section 3 for airborne radars at altitudes of two and ten kilometers. The effects of antenna and waveform parameter selection are introduced. The occasionally devastating effects on accuracy of inadequate formulations - usually associated with the altitude line effects - are explored. Section 4 contains discussion of conclusions reached during the course of this effort and recommendations for future work.

Appendix A summarizes the geometrical relationships used in formulating clutter integrals. Appendix B explores some aspects of the transformation of surface clutter density from its conventional description in terms of grazing angle to radar coordinates.

CONTENTS

ILLUSTRATIONS

1. SUMMARY

This report introduces and advocates the use of classical methods of analysis in characterizing the clutter environments of downlooking radars as an essential first step in fashioning versatile, accurate, and easy-to-use computer simulations. It summarizes the content of a series of lectures presented to selected members of the Rome Laboratory staff in 1992 and 1993, sponsored by RL/OCDS.

The subject matter evolves from rudimentary concepts of electromagnetic theory (Section 2). Integral expressions for the clutter power received from the earth's surface are derived and transformed into closed form equations expressed entirely in waveform coordinates of range and range-rate, or Doppler. Analysis results based on ordinary radars and slowly varying clutter densities feature intricate and difficult to interpret clutter power distributions, providing further evidence that these effects are not entirely caused by spatial and temporal variations internal to the clutter. For example, Figure 1.1 depicts a highly structured velocity distribution of clutter power for a sidelooking, airborne phased array radar observing a smooth, featureless earth with an orthodox burst waveform.

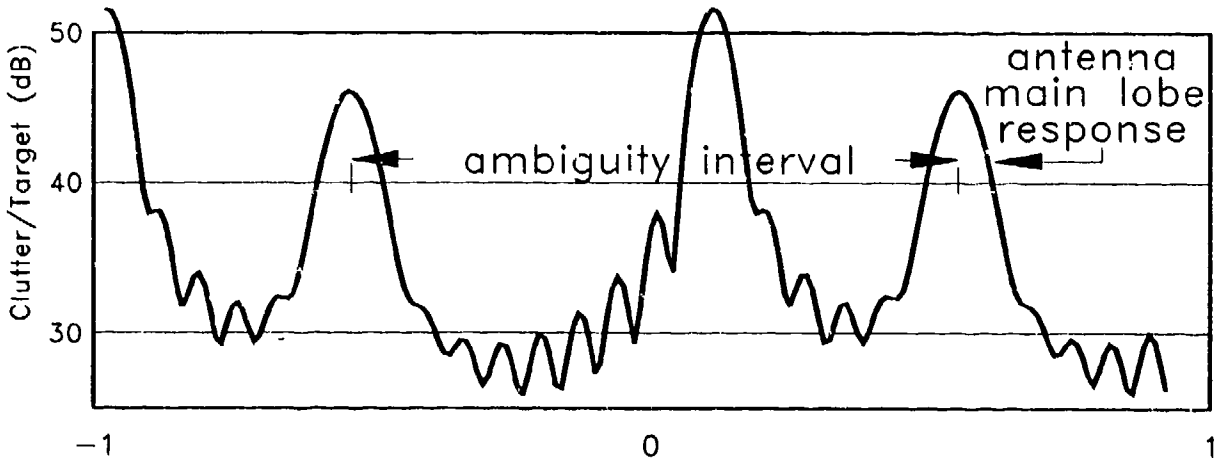

Figure 1.1 Velocity Distribution of Earth Surface Clutter

Analysis tools include concepts of electromagnetic theory, analytical geometry, trigonometry, and integral calculus at undergraduate levels plus some basic antenna and waveform concepts. Each discipline contributes to the development of relationships from which range and Doppler distributions of earth clutter are easily generated. None of the concepts is advanced or difficult, but the benefits of the approach depend on all of them being dealt with at the same time. This has proven to be unexpectedly difficult for many, in part because the clutter environment of a downlooking radar is exceedingly complex just because of its range/Doppler perspective.

This work evolved from studies of space based radar where earth curvature is conspicuous and investigators had to examine its effects carefully, only to discover that they were more significant in airborne than spaceborne radars, that many of the early studies had not been adequately formulated and/or did not have the accuracy needed to handle the effects properly. Its power has been validated by newcomers to the study of radar who have quickly generated results comparing favorably with those of computer simulations developed by teams of experts over periods of many years. A leading contributor to these achievements has been the ease with which the methods handle the singularity of clutter density - in waveform coordinates - that extends along the radar's ground track as well as the limiting conditions at the horizon that have diminished accuracy in many simulations.

The introductory nature of this work is embedded in a number of restrictive assumptions about the clutter and the radars observing them, not in the methods employed. Monostatic radar antennas are assumed to be side looking arrays in tangential motion, without crab angle, above a smooth spherical earth. The only clutter contributor is reflection from the earth's surface, presumed to be a slowly varying function of grazing angle only. Preliminary studies of scenarios including more realistic clutter, other platform directions, more challenging waveforms and bistatic encounters - not addressed in this report - have been encouraging.

The range equation was developed in these studies from simple antenna and communications concepts, and monostatic radar was evolved as a special case of bistatic radar. This, plus their superiority in managing the unwieldy spherical geometries, make the classical methods the first choice for credible analysis of bistatic encounters.

2. RADAR RANGE EQUATION

Any equation used to evaluate the power returned to and received by a radar as the result of reflection of its transmitted power by remote objects is a version of the 'radar range equation.' In this section antenna and communication concepts are used to evolve an integral equation that is particularly useful for calculating the power returned from distributed objects. The eventual purpose is to quantify the power reflected from the surface of a smooth spherical planet that returns to and is received by an airborne or spaceborne radar.

Every antenna radiates more intensely in some directions than others in accordance with its gain function which describes how it distributes the energy it radiates into two dimensional angle space (Figure 2.1). A radiation pattern is a plot of the gain function in a single angle dimension. The conceptually useful isotropic radiator, which exhibits unity gain in all directions, cannot actually be achieved.

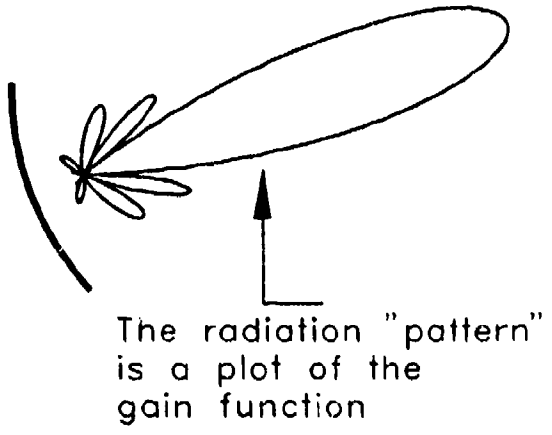

Figure 2.1 Antenna Gain Function

A radiation sphere centered on a source of electromagnetic radiation is one that is large enough that the density of power passing through its surface is decaying as the square of its radius. The distribution of power density on a radiation sphere of radius R is (Figure 2.2):

$$density = \frac{(transmitted\ power)\ (antenna\ gain)}{4\ \pi\ R^2}.$$

The total power radiated is obtained by integrating over the surface of the sphere, using any spherical coordinate system centered on the antenna and must,

$$\int_{sphere} power\ density\ da = \int_{sphere} \frac{P_t\ G}{4\pi R^2}\ R^2\ \sin\theta\ d\theta\ d\phi$$

of course, equal the power radiated by the antenna. For the hypothetical isotropic antenna with unity gain in all directions, the integral reduces trivially to the comforting conclusion that power radiated equals power radiated. With realizable antennas the gain varies with direction, but conservation of energy must endure, and any region in space in which the gain is greater than unity must be compensated by another where the gain is less. It is for this reason that the main lobe of a high gain antenna may only extend over a small fraction of the total angle space.

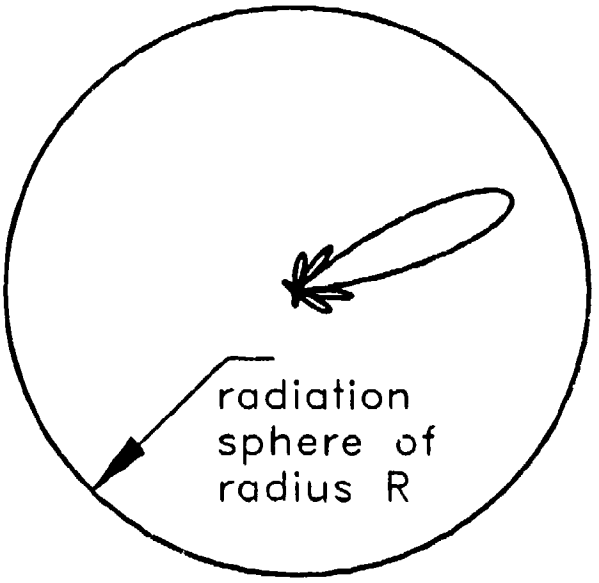

Figure 2.2 Power Density on a Radiation Sphere is $p = (P_tG)/(4\pi R^2)$

Antenna gain is defined relative to the total power actually radiated. A measured value of antenna gain can never be quite this large because of the inevitable losses between the antenna's "feed point" and the point along its feed path where the gain is measured. Since the power at that point must be larger than the total radiated power in the same amount as the gain has diminished, the same result for power density is obtained, provided that consistent values of power and gain are always used.

An antenna's ability to extract power from an incident plane wave is measured by its "effective area" which is defined so that the product of the power density of the incident wave at the antenna and its effective area equals the power

received. An antenna's effective area varies with direction of arrival in exactly the same way its gain function does, and they are related via the relationship:

$$effective\ area = \frac{gain * (wavelength)^2}{4\pi}.$$

This is the antenna reciprocity relationship which has the practical effect that no distinctions are needed between the transmitting and receiving functions in the analysis or design of any antenna or related optical sensor.

In evolving a range equation for radar, it is useful to characterize some of the aspects of the exchange of power between two widely separated antennas comprising a simple communications system. It consists of an antenna with gain function G_t radiating power P_t and a second, remote antenna at distance R with an effective area function A_r. The second antenna intercepts a fraction of the power transmitted by the first and delivers it to a receiver. The power density at the receive antenna was described previously as $(P_tG_t)/(4\pi R^2)$, and power is removed in proportion to its effective area so that the transfer of power between the two entities is described by:

$$P_r = \frac{P_t\ G_t\ A_r}{4\pi R^2}$$

In this simplest form of the communications equation, power exchange appears not to depend on frequency. However, this result is achieved only in those occasional circumstances where the product of the transmit antenna's gain and the receiving antenna's effective area exhibit no dispersions. Systems employing constant gain antennas, such as dipole or log-periodic designs, in collaboration with constant area antennas, such as reflectors, are able to exhibit this behavior.

Systems using two reflector antennas or two log-periodic antennas would exhibit dispersive behaviors in accordance with (λ = wavelength):

$$P_r = \frac{P_t\ A_t\ A_r}{(\lambda R)^2} \qquad \text{or} \qquad P_r = \frac{P_t\ G_t\ G_r\ \lambda^2}{(4\pi R)^2}.$$

These equations quantify the power transferred in straightforward radio communications (Figure 2.3). In some instances, a repeating element is added (Figure 2.4) for extended range or for communicating around corners.

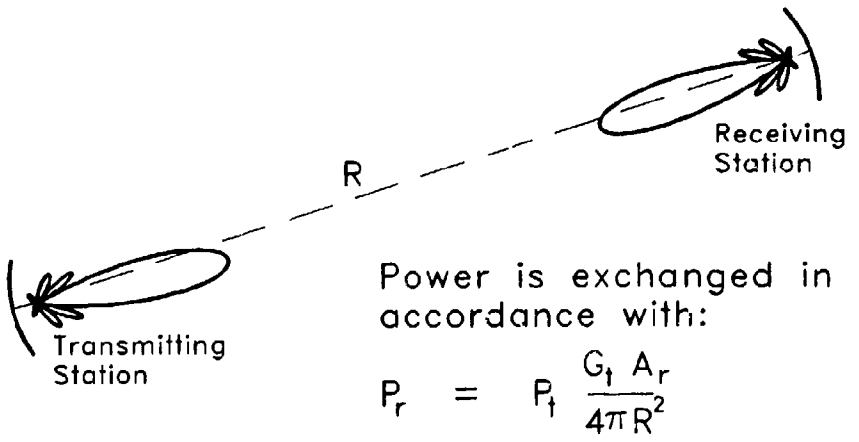

Figure 2.3. A Transmitter - Receiver System

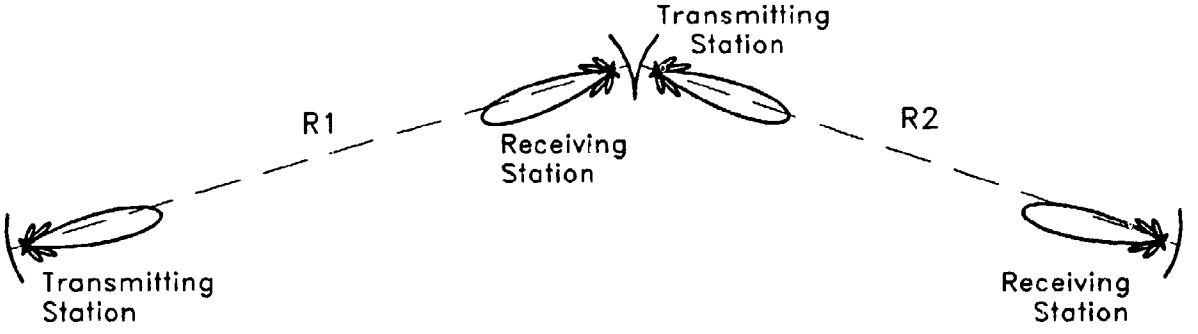

Figure 2.4 Communications System with Repeater

The repeater receives power from the transmitting station, optionally amplifies it, and re-transmits it to the receiving station. In this case, successive applications of the communications equation lead to an expression for the power relayed to the receiving station via the repeater, using the subscript x for repeater parameters:

$$P_r = \frac{P_t G_t A_x}{4\pi (R1)^2} \; gain_x \; \frac{G_x A_r}{4\pi (R2)^2} \; .$$

The transition from a communications system with repeater to a radar configuration is straightforward, requiring only revised interpretations of what some of the system elements are, not what they do. In the bistatic radar configuration of Figure 2.5, the repeater has simply been replaced with a target, and the

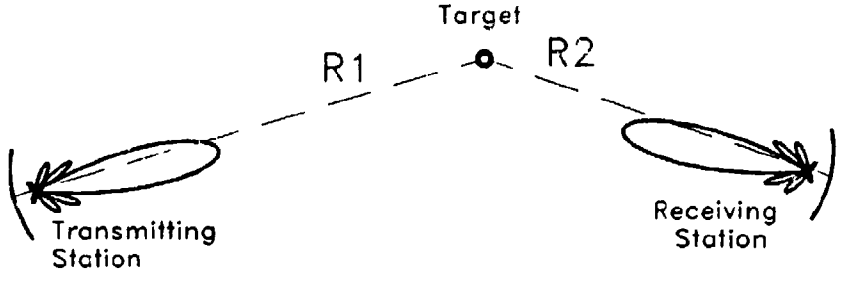

Figure 2.5 Bistatic Radar Configuration

repeater parameters of its receiving antenna's effective area, A_x, its transmitting antenna's gain, G_x, and its amplification, $gain_x$, are coalesced into the target's bistatic radar cross section, $\sigma = A_x \; gain_x \; G_x$, leading immediately to this form of the bistatic radar range equation:

$$P_r = \frac{P_t G_t}{4\pi (R1)^2} \; \sigma \; \frac{A_r}{4\pi (R2)^2} \; .$$

The target intercepts a fraction of the transmitter power in proportion to its effective area and reradiates some or all of that power in accordance with its gain. Functionally, it replicates a communications repeater except that it may absorb some of the incident energy and, in that case, the amplification factor denoted $gain_x$ in the communications encounter becomes an attenuation factor.

Detailed studies of radar cross section have to accommodate depolarization effects in the interactions of targets with electromagnetic waves. For the present purposes, the scalar representation is satisfactory.

To obtain a range equation for a monostatic radar with collocated transmitter and receiver, the bistatic range equation needs only to be updated by using the symbol r for the distance from radar to target and noting that r = R1 = R2. Even though the nature and the complexity of analyzing a target's cross section is enormously different for this case than for the bistatic one, there is no impact on the range equation. These simplifications lead immediately to either of these well-known forms of the radar range equation. The latter one can be simplified further

$$P_r = \frac{P_t\, G_t}{4\pi r^2}\ \sigma\ \frac{A_r}{4\pi r^2}\ ; \qquad P_r = \frac{P_t\, G_t\, G_r\, \lambda^2}{(4\pi)^3\, r^4}\ \sigma .$$

when the same antenna configuration is used for both transmit and receive functions by using the symbol G in place of both G_t and G_r.

These forms can be employed to evaluate the power received from targets by monostatic radars. However, only by comparing the target power with other quantities such as noise or clutter power can estimates of utility be inferred.

In this study, the emphasis is given to the task of distinguishing targets from clutter for which the ratios of target power to clutter power are needed, not on radar sizing issues for which signal to noise estimates are demanded. For this reason, issues of signal to noise are not addressed directly in this report. However, occasional "sanity checks" with respect to radar sizing are strongly recommended lest effort be wasted evaluating radar designs that are able to resolve targets from clutter efficiently but exhibit deficient ratios of signal to noise.

Sensible discussion of target and clutter signals and their ratios necessitate awareness of what is meant by the words target and clutter. A non-trivial response is that all of the observables we wish to observe are targets while those that we wish not to observe are clutter. This report emphasizes airborne and spaceborne surveillance radars for which surface and air vehicles constitute targets and the earth's surface is the important source of clutter. Other sources of clutter - not addressed here - include animals, birds, insects, atmospheric and meteorological effects, airborne pollution, etc. Some of these qualify as targets for other types of radar for which the surface and air vehicles of our concern may be defined as part of the clutter. In some surveillance, only military vehicles qualify as targets while their civilian counterparts are clutter, leading to some of the advanced radar techniques of discriminating targets and clutter designated target identification.

2.1 RANGE EQUATION FOR EARTH CLUTTER

The concern of this section is quantifying the clutter contributed to an elevated downlooking monostatic radar by the surface of the earth. The scenario is illustrated in Figure 2.6. A radar in circular orbit (or in level flight) observes

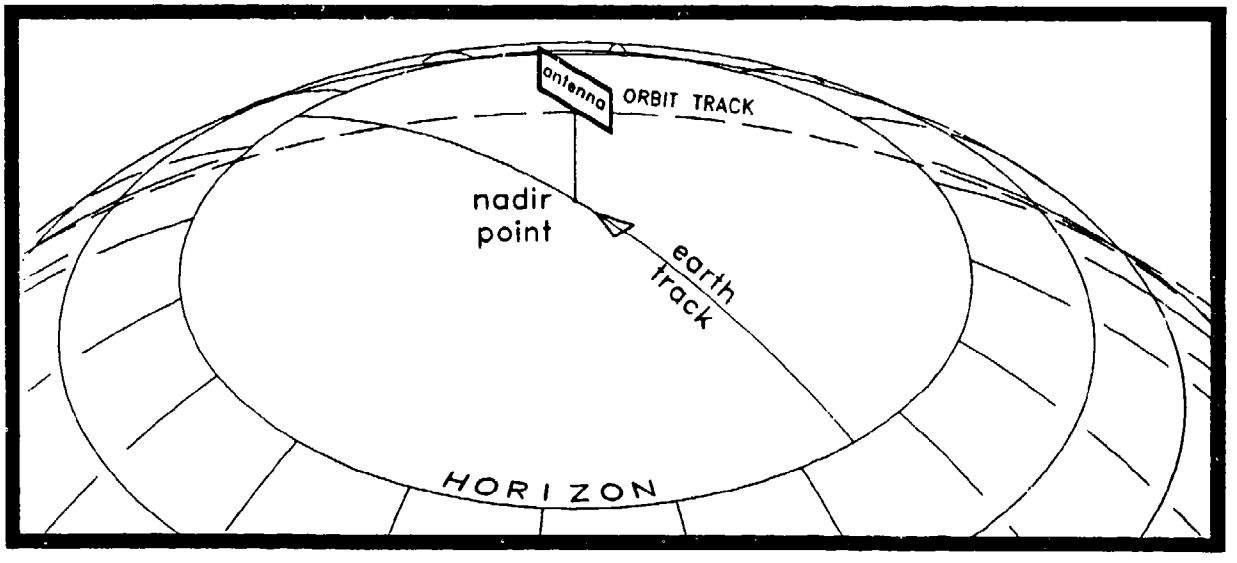

Figure 2.6 Spaceborne Radar in Orbit

the earth. The radar's antenna is shown aligned with its earth track which differs from its satellite or aircraft track by the crab angle. Its mission is to detect the vehicular targets, but it must distinguish them from the earth surface clutter, in this case the reflections from the surface of a featureless, perfectly spherical earth. The geometrical relationships are depicted in Figure 2.7. The area of observation

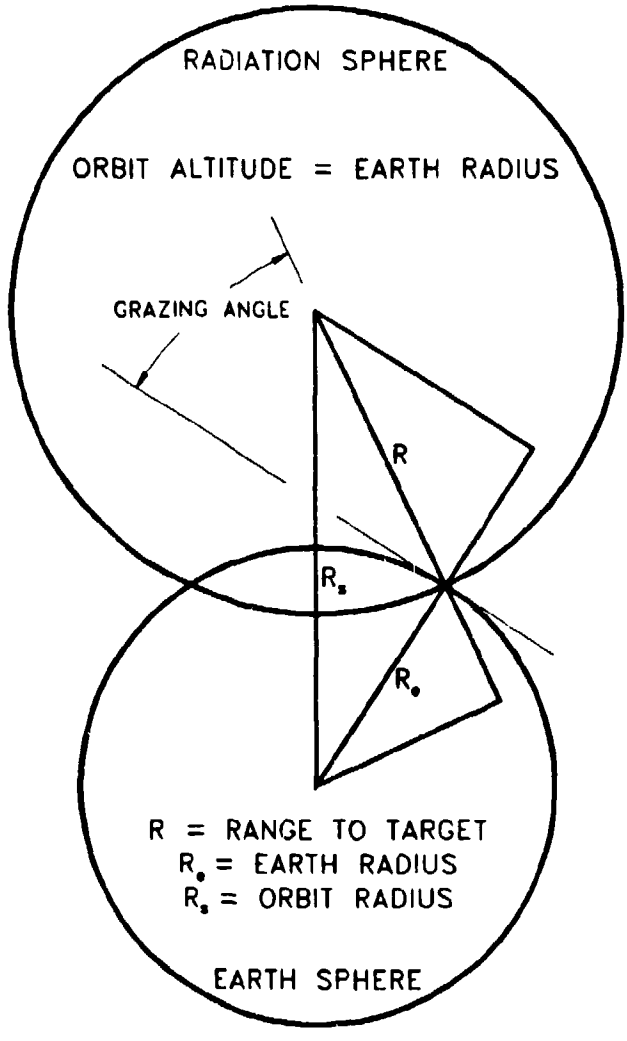

Figure 2.7 Geometrical Relationships for Radar Altitude = Earth Radius

is at the intersection of the earth sphere and a radiation sphere of radius r, shown in finer detail in Figure 2.8 to highlight the relationship between the differential area elements on their surfaces:

$da_r = da_e \sin(\text{graze})$.

Clearly, a clutter patch on the earth's surface appears as a foreshortened - projected - element on the radiation sphere and their areas are related by the sine of the grazing angle as indicated.

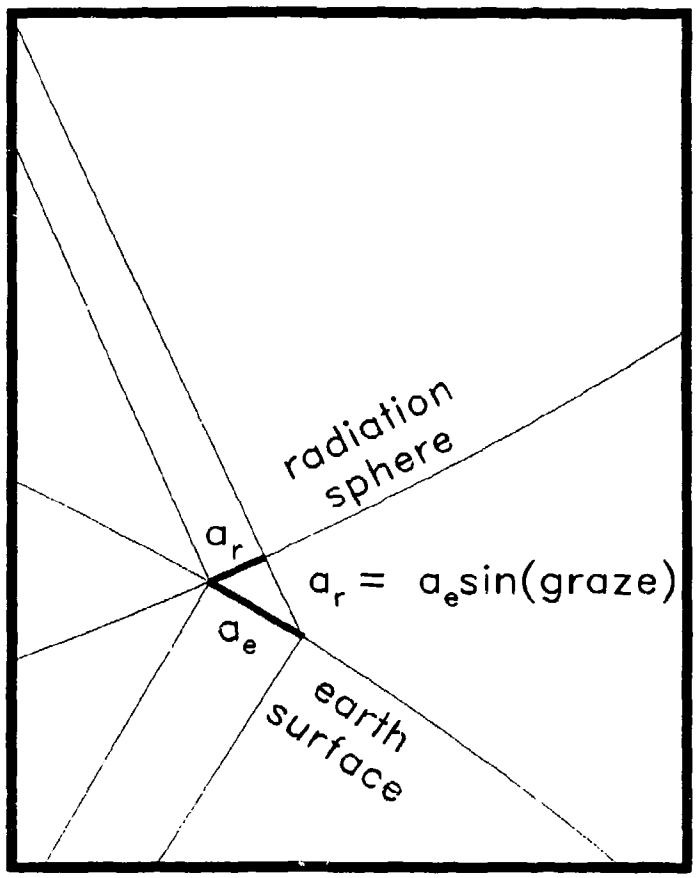

Figure 2.8 Differential Area Elements on Surfaces of Earth and Radiation Spheres

The radar cross section of a differential area element on the radiation sphere is the product of its area, $da = R^2 \sin\theta \, d\theta \, d\phi$ using any suitable spherical coordinate system, and the "clutter density," σ^c, of the surface at that point, a property of the surface that is interpreted as that fraction of the power incident on it that is retroreflected or backscattered toward the radar, with other portions being scattered or absorbed differently (Figure 2.9).

The radar range equation for the differential power received by the radar as the result of retroreflection from a differential patch of surface clutter is evolved from the monostatic range equation on page 2-6 as:

$$dP_r = \frac{P_t \, G_t \, G_r \, \lambda^2}{(4\pi)^3 \, r^4} \, \sigma^c \, da_r .$$

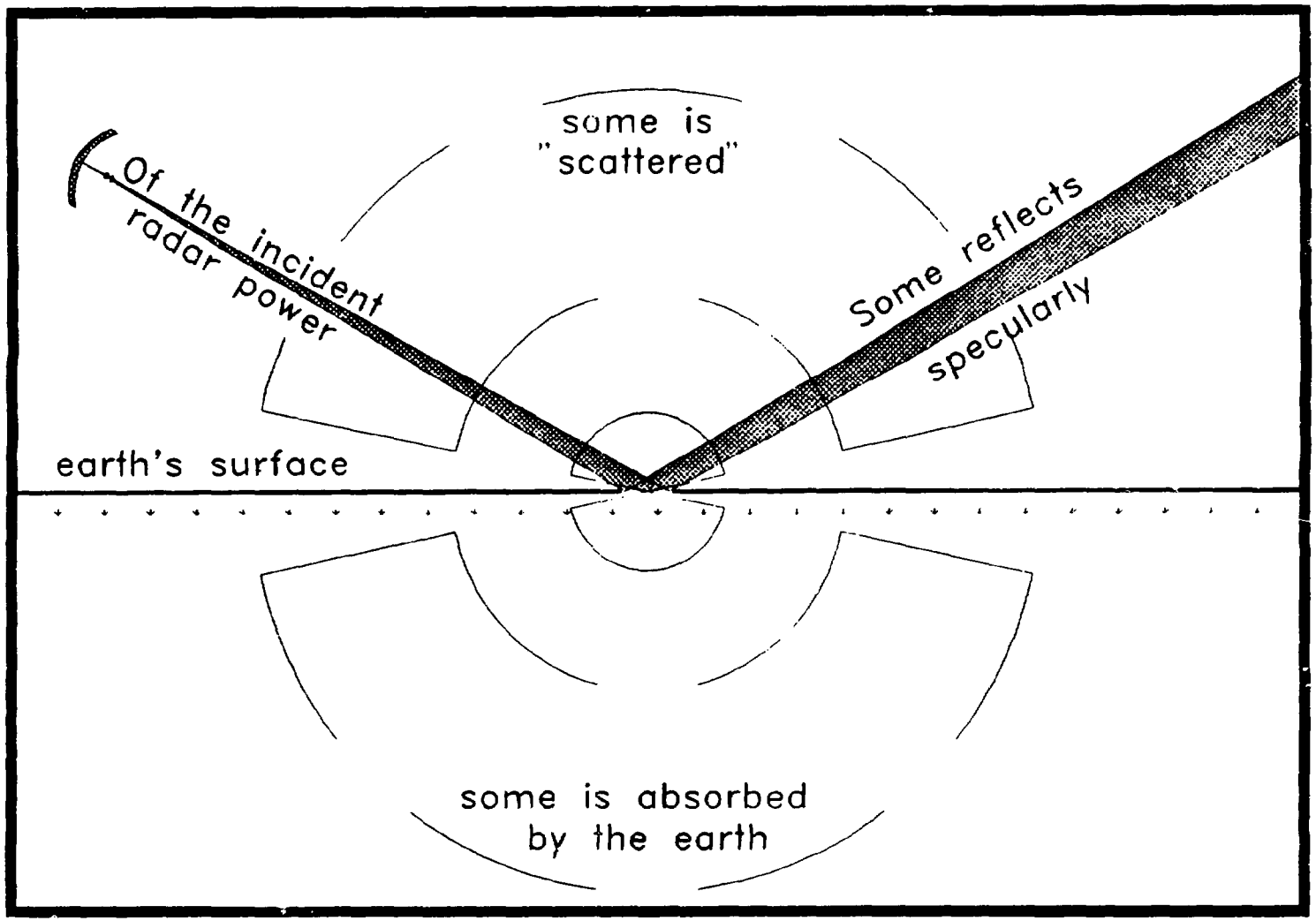

Figure 2.9 Energy Incident on the Earth's Surface is Partly Absorbed, Partly Reflected and Partly Scattered

This is represented in any conventional spherical coordinate system (r,θ,ϕ) centered on the radar by:

$$dP_r = \frac{P_t\, G_t\, G_r\, \lambda^2}{(4\pi)^3\, r^4}\, \sigma^c\, r^2\, \sin\theta\, d\theta\, d\phi$$

so that the total surface clutter power is represented by an integral over the visible surface of the earth:

$$P_r = \int_{earth's\ surface} \frac{P_t\, G_t\, G_r\, \lambda^2}{(4\pi)^3\, r^2}\, \sigma^c\, \sin\theta\, d\theta\, d\phi .$$

This representation can be simplified even more by introducing a normalizing point target. Comparing the surface clutter power received with the power received from this target provides a form in which the dispersions and all constant terms have been eliminated. Updating notations to accommodate this procedure:

r_t, σ_t = range and radar cross section of normalizing point target.

r_{cl}, σ^{cl} = range to and cross section clutter density of a differential area element on a radiation sphere at its intersection with the earth.

G_1, G_2 = the gain functions of the collocated transmit and receive antennas evaluated in the direction of the target or of the clutter patch as appropriate.

θ_{cl}, ϕ_{cl} = latitude and longitude coordinates of the clutter patch in <u>any</u> spherical coordinate system centered on the radar.

dR = the differential element of power returned to the radar as a result of backscatter from the clutter patch - normalized by the power returned from the target.

R = the normalized clutter power returned to the radar from an extended area on the surface of the earth, sometimes but not necessarily the entire surface visible from the radar.

$$= \int_{earth's\ surface} dR.$$

$$= \int_{earth's\ surface} \frac{(G_1G_2)_{cl}}{(G_1G_2)_t} \frac{\sigma^c r^4_t}{\sigma_t r^2_{cl}} \sin\theta_{cl} d\theta_{cl} d\phi_{cl}.$$

This expression accounts for the effects of the relative antenna transmit and receive patterns, of the variations of the surface clutter density with the location of the clutter patch and of the encounter geometry in quantifying the (normalized) clutter power received by a continuous wave radar. Because of the normalization, it exhibits no overt frequency dependence and it is independent of transmitter power, receiver noise figure and the absolute as opposed to relative antenna patterns.

It formalizes that the only resource available for diminishing clutter signals relative to target signals, in the continuous wave case, is the antenna pattern. Actually, the absolute clutter power received changes very little as the antenna design parameters are adjusted whereas a target's returns can be substantially enlarged by increasing the antenna gain in its direction by pointing or scanning the antenna's main lobe. Only with the incorporation of radar waveforms operating in synergy with the antenna patterns is a meaningful ability to resolve target and clutter signals achieved. Waveforms operate in the domain of target (or clutter) range and range-rate. The waveform function is designated Æ and, like the antenna pattern functions, it acquires the subscript cl or t depending on whether it is applied to a patch of clutter or to a point target. The expression for normalized clutter over a designated portion of the earth's surface is augmented to account for waveform effects as:

$$R = \int_{earth's\ area} \frac{(G_1G_2)_{cl}}{(G_1G_2)_t} \frac{Æ_{cl}}{Æ_t} \frac{\sigma^c}{\sigma_t} \frac{r_t^4}{r_{cl}^2} \sin\theta_{cl}\, d\theta_{cl}\, d\phi_{cl}$$

This expression, including both antenna pattern functions and waveform functions, includes all the tools available for "extracting" target signals from clutter signals.

Its generality is limited by several assumptions embedded in its development; that the surface clutter is completely uncorrelated, that the radar and the objects of its regard are widely enough separated to validate the use of the electromagnetic theory's radiation condition, and by the implicit assumption that the evaluation of the clutter integral will take place in, or through the agency of some (any) conventional spherical coordinate system. Note that the integrand consists of several groupings of factors, each encouraging the analysis towards a different coordinate selection: 1) the antenna patterns, 2) the waveforms, 3) clutter cross section densities which include characterization of clutter's "internal motions", and 4) the encounter geometry which includes characterization of its "external motions." The external motions account for the gross variations of clutter patch range-rate across the surface of the earth, illustrated by contours of constant range-rate (isodops) which, for the case of a radar in level flight above a spherical earth, exhibit mirror symmetry (Figure 2.10) about the ground track vector.

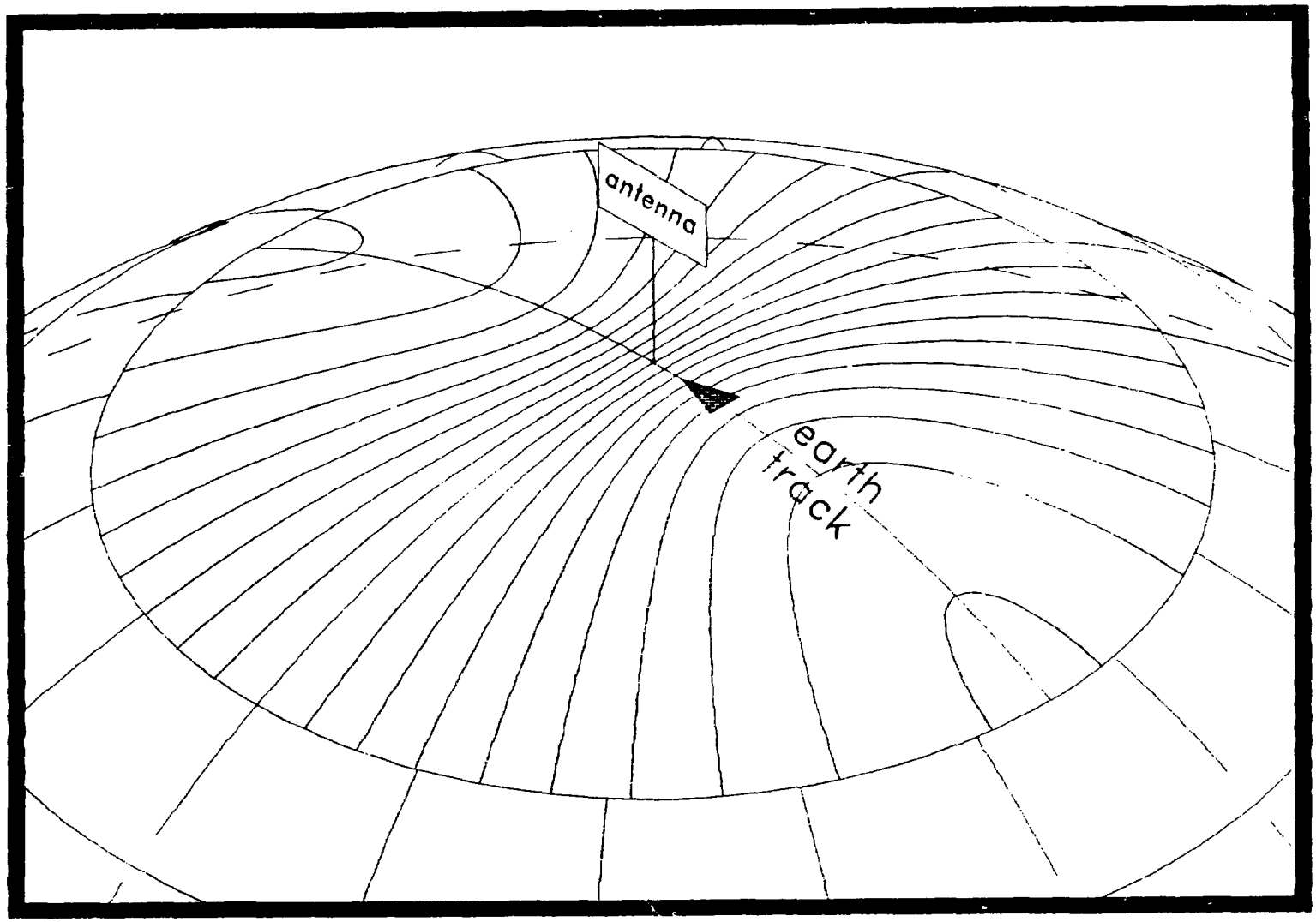

Figure 2.10 Contours of Constant Range Rate on the Planet's Surface Exhibit Mirror Symmetry About the Ground Track

2.2 Coordinate Systems

Appendix A examines the geometry of downlooking radar and introduces a number of relationships among important distances and angles. It also describes and interrelates three spherical coordinate systems that have been used in various applications of the surface clutter integral to several downlooking configurations. All three of these systems are closely tied to a Cartesian coordinate system centered on a radar in level flight oriented so that (Figure 2.11): the x-coordinate is aligned with a side looking vector with respect to the earth track, the

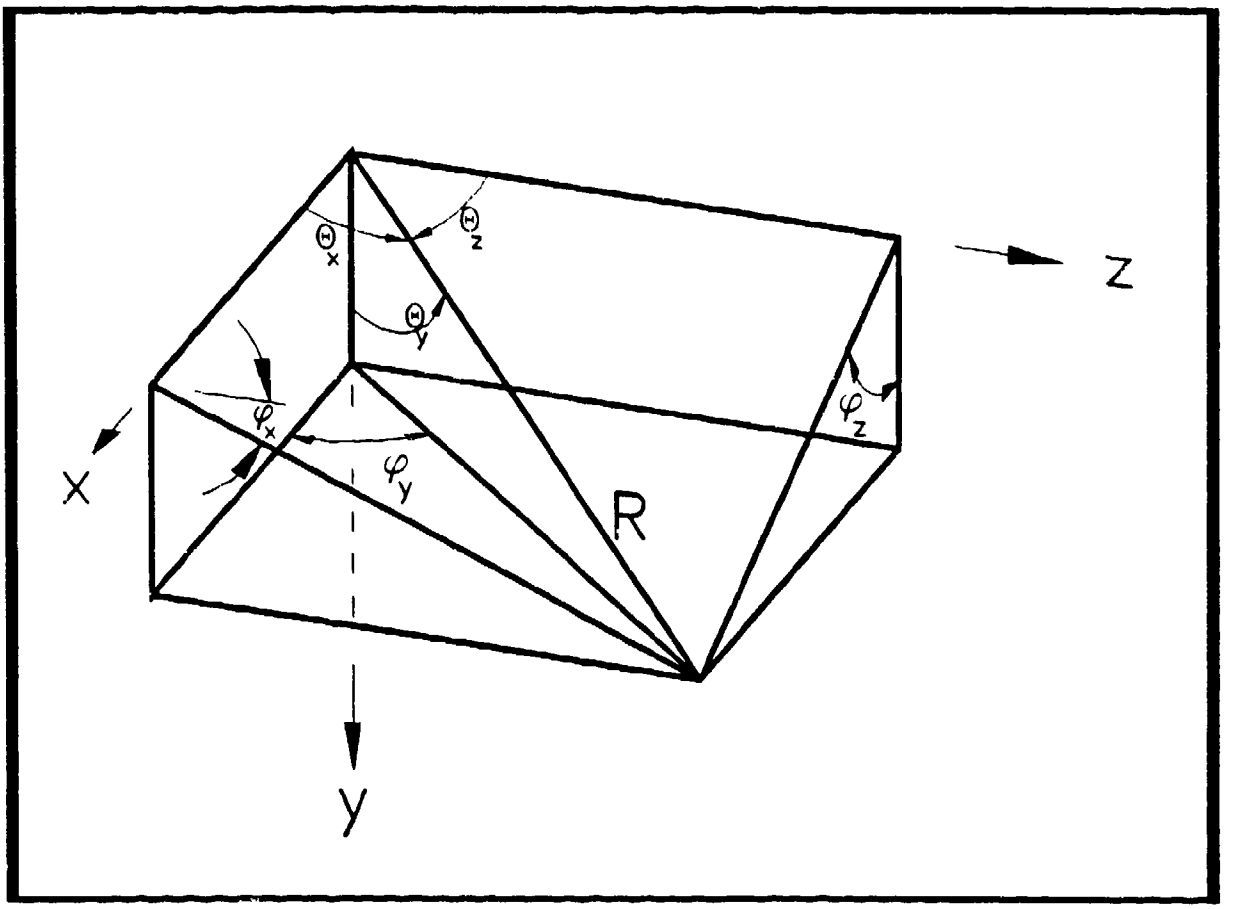

Figure 2.11 Spherical Coordinate Systems with x, y, and z Axis Poles

y-coordinate is aligned with a down looking vector, and the z-coordinate is aligned with a forward looking vector with respect to earth track. The three spherical systems are those with poles aligned with each of the three axes, x, y, z with polar and azimuthal angles designated (θ_x, ϕ_x), (θ_y, ϕ_y), and (θ_z, ϕ_z). Note that the three polar angles (θ_x, θ_y, and θ_z) constitute the set of direction angles in the selected Cartesian coordinate system and their cosines the set of direction cosines.

Of these, the θ_y ,ϕ_y coordinate system is the one usually selected for the low and medium PRF, sidelooking radar clutter analysis. θ_y is an ordinary elevation angle measured from the nadir; ϕ_y is the azimuth angle measured from the side-looking boresight. The expression for integrated clutter becomes:

$$R = \int_{earth's\ area} \frac{(G_1G_2)_{cl}}{(G_1G_2)_t} \frac{Æ_{cl}}{Æ_t} \frac{\sigma^c\, r_t^4}{\sigma_t\, r_{cl}^2} \sin\theta_y\, d\theta_y\, d\phi_y$$

with the angle variables interpreted as defining the direction to a patch of surface clutter. The domain of the integrand, a clutter density in the selected coordinate system, covers a full circle in azimuth and is bounded by the nadir point and the horizon in elevation. In the integration, the contribution of each clutter patch is modified appropriately by the geometry of the encounter, by its own clutter properties, by the filtering actions of the antenna and the waveform in its direction.

This can be transformed to a coordinate system based on the clutter patch range and range-rate. This transformation makes use of normalized clutter range and range-rate variables ρ and μ:

and new configurational parameters:

$$\rho = \frac{r_{cl}}{r_h}; \qquad \mu = \frac{rdot_{cl}}{v_s}$$

r_h = range from radar to horizon,

rdot = range-rate of a patch of surface clutter as observed from the radar,

v_s = tangential velocity of the radar.

It is accomplished with the aid of the following relationships among the angles to a patch of clutter and its range, range-rate as observed by the radar, based on the smooth spherical earth model (refer to Appendix A for geometrical details),

$$\sin\theta_y \, d\theta_y = \frac{1 - \rho^2}{2 \rho^2 \left(\frac{r_s}{r_h}\right)} \, d\rho$$

$$\mu = \cos\theta_z = \sin\theta_y \sin\phi_y$$

$$d\mu = \cos\theta_y \sin\phi_y \, d\theta_y + \sin\theta_y \cos\phi_y \, d\phi_y$$

$$d\phi_y = \frac{d\mu}{\cos\theta_x} + \frac{\mu \, d\rho}{\rho \cos\theta_x} \frac{(1 + \rho^2)(1 - \rho^2)}{1 - 2\rho^2 \left(\frac{r_s^2 + r_e^2}{r_h^2}\right) + \rho^4}$$

leading to the following closed form expression for the earth surface clutter power, more precisely a clutter-to-target ratio, received by an elevated radar.

$$R = \int_{\rho,\mu} \frac{1}{2} \frac{(G_1 G_2)_{cl}}{(G_1 G_2)_t} \frac{Æ_{cl}}{Æ_t} \frac{\sigma^c \, r_t^4}{\sigma_t \, r_s r_h} \frac{1-\rho^2}{\rho^4} \frac{d\rho \, d\mu}{\sqrt{1 - \mu^2 - \frac{1+\rho^2}{2\rho\left(\frac{r_s}{r_h}\right)}}}$$

In this expression, all the factors describing the effects of the geometrical configuration have been expressed in coordinates of the range and range-rate of the observed clutter. The waveform function is, of course, naturally expressed in that way, and, to the extent that the clutter RCS density function σ^c and the antenna pattern functions can also be formulated in these terms, it can be used directly to quantify the surface clutter power received by the radar. The integrand is a clutter density in the new coordinate system of (normalized) clutter range and clutter range-rate, ρ and μ. It can exhibit a singularity when:

$$\sqrt{1 - \mu^2 - \frac{1+\rho^2}{2\rho(\frac{r_s}{r_h})}} = \cos\theta_x = 0$$

which corresponds to the ground track along the surface of the earth. The domain of the integrand, corresponding to either the left or right half of the earth's surface viewed from the radar, extends from the nadir point to the horizon in ρ and from the potential singularity along the ground track ahead to the one along the ground track behind in μ. The complete clutter calculation requires, in this formulation, successive integrations over the right and the left half of the earth's surface.

In manipulating electromagnetic equations describing radio or radar system power densities, it is unusual, to say the least, to encounter singularities. The explanation for this one is that the power density has been transformed into a non-orthogonal coordinate system. Along the singularity the range and range-rate coordinates of the clutter become parallel in physical space so that a finite amount of clutter power is observed in what appears to be zero area. Actually, for any non-zero resolving power in these dimensions, the integrated clutter power is finite as it clearly must be. However, the singularity's effects on observed clutter distributions can be quite remarkable as described in Section 3.

In some circumstances the effects of the singularity are canceled by an antenna pattern null that extends along the ground track. A perfectly oriented, sidelooking vertical aperture will often exhibit a $\cos\theta_x$ (voltage) element factor which will completely overcome the $\cos\theta_x$ power factor in the denominator of the clutter density. Even a slight misalignment of such a pattern null and the ground track can result in the reappearance of extraordinary effects, however.

In the transformation from locating each patch of surface clutter in angular dimensions (Figures 2.6 and 2.10) to locating it in the ρ,μ domain (Figure 2.12), the ground track is mapped into the horseshoe shaped curve with the nadir point (directly below the radar) at its center and the fore/aft horizon points at the two ends. The horizon, extending over an azimuth semi-circle from directly ahead to directly behind, is mapped into the straight line at horizon range in the clutter range, range-rate domain. The term altitude line is used by some to describe the

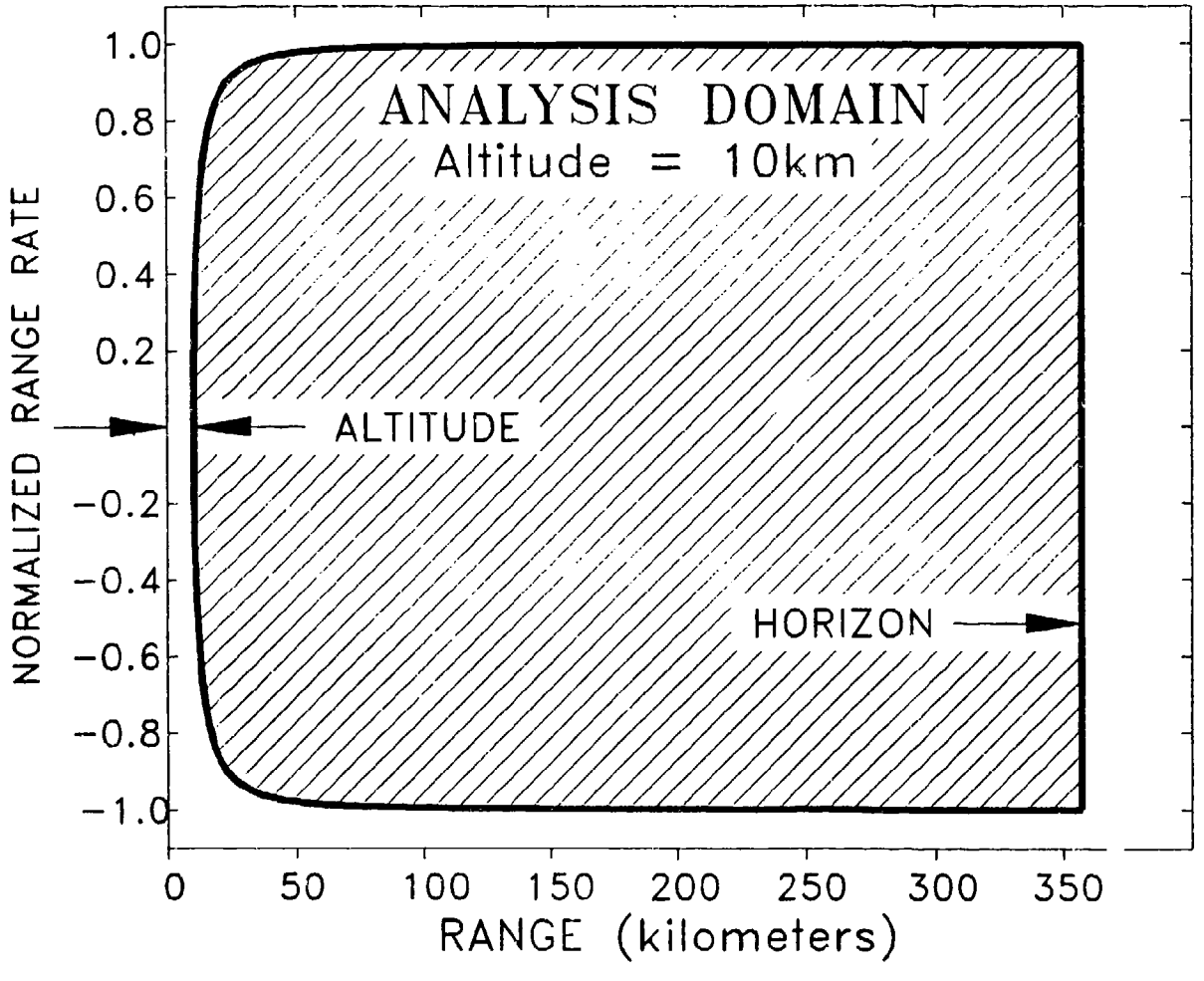

Figure 2.12 Range, Range-rate Domain

exceptionally large clutter density associated with the nadir point "at altitude range"; others use it to describe the totality of unusual clutter effects observed along the ground track, from horizon to horizon.

Close examination of the integrand of the previous formula, the surface clutter density in the ρ,μ coordinate system, designated D,

$$D = \frac{1}{2} \frac{(G_1G_2)_{cl}}{(G_1G_2)_t} \frac{Æ_{cl}}{Æ_t} \frac{\sigma^c r_t^4}{\sigma_t r_s r_h} \frac{1-\rho^2}{\rho^4} \frac{1}{\sqrt{1 - \mu^2 - \frac{1+\rho^2}{2\rho(\frac{r_s}{r_h})}}}$$

immediately reveals that several factors conspire to amplify its nadir response to large levels, particularly in light of the fact that the surface clutter RCS density, σ^c, usually grows very quickly as ρ approaches its minimum value (Appendix B).

2.3 Antenna and Waveform Contributions

2.3.1 Antenna Patterns. Most radar antennas can point their main lobe within a large angle field. A sidelooking airborne radar may incorporate a phased array antenna capable of directing its main lobe independently over an azimuth window of $\pm$60 degrees relative to its boresight and over an elevation window extending from a few degrees above to about 30-degrees below the horizon. If the antenna's aperture lies in the vertical plane and is aligned with the ground track, then the azimuth and elevation steering are separately controlled in the θ_z, θ_y directions, the direction cosines with respect to the aperture's vertical and horizontal axes. Note that azimuth boresight $\pm$60 degrees corresponds to an interval of 90$\pm$60 degrees in θ_z and that an elevation interval from boresight +10/-30 degrees corresponds to an interval of 90+10/-30 degrees in θ_y. Note also that θ_z and θ_y are perpendicular only near boresight and become parallel in the y-z plane, the plane of the aperture.

The antenna pattern exhibits a spatial dependence which does, of course, depend on its pointing. An expression for a normalized voltage pattern of a phased array antenna might take the form, using angles shown in Figure 2.11:

$$\textit{element factor} = \sin\theta_y \cos\theta_x$$

$$\textit{azimuth array factor} = \frac{\sin\left\{ n_z \pi d_z \left(\frac{\cos\theta_z}{\lambda} - \frac{\cos\theta_{z0}}{\lambda_0} \right) \right\}}{n_z \sin\left\{ \pi d_z \left(\frac{\cos\theta_z}{\lambda} - \frac{\cos\theta_{z0}}{\lambda_0} \right) \right\}}$$

$$\textit{elevation array factor} = \frac{\sin\left\{ n_y \pi d_y \left(\frac{\cos\theta_y}{\lambda} - \frac{\cos\theta_{y0}}{\lambda_0} \right) \right\}}{n_y \sin\left\{ \pi d_y \left(\frac{\cos\theta_y}{\lambda} - \frac{\cos\theta_{y0}}{\lambda_0} \right) \right\}}$$

$$\textit{array factor} = (\textit{azimuth array factor}) * (\textit{elevation array factor})$$

$$\textit{antenna pattern} = (\textit{element factor}) * (\textit{array factor} + \textit{errors})$$

presuming that all the antenna elements are the same, that they are excited equally and distributed on a planar, rectangular grid with spacings d_z and d_y, that their number is n_z and n_y in the respective directions, and that their common element pattern is that of a vertical dipole located in front of a ground screen. Deployment and excitation error effects are embedded in the error term. The pointing angle is identified to be θ_{z0}, θ_{y0} at an operating wavelength of λ_0. The formulation accounts for the scanning of the pointing angle as wavelength changes, an expected dispersion in array antennas in which the phase of every element is controlled to implement scanning.

The example antenna pattern formula corresponds to uniform excitation of the antenna elements, a common design for transmitting purposes because of efficiencies it allows in implementing distributed RF power generation. On receive, weighting functions are often applied to excitation amplitudes to diminish sidelobes at the expense of reduced antenna gain. These modify the functional representations of the array factors but not the underlying variables. Some of the examples presented in Section 3 use more elaborate weighting techniques to achieve very low side lobes in narrow angle windows.

The antenna operates as a spatial filter, selectively intensifying or diminishing the energy retro-reflected from every clutter patch on the surface of the earth in accordance with its two-way pattern. With the smooth spherical earth presumptions embedded in the formulation, a one-to-one correspondence can be made between the angle, angle domain naturally used in representing the pattern and the geometrical distribution of clutter in terms of its range and range-rate relative to the radar. Alignment of the antenna and the platform's ground track serves to simplify evaluations of the integral because of the attendant simplifications in the transformations between the antenna's angle variables and the surface clutter range and range-rate variables.

2.3.2 Waveform Functions. The calculations of earth surface clutter are exemplified with the use of conventional coherent pulse burst waveforms, time series of equally spaced rectangular pulses. Essential features are the duration of each pulse, t, the interval between pulses, τ, and the number of pulses, n. The burst duration, T, is $(n-1)\tau + t$, approximately $(n-1)\tau$. Analogously with the

antenna pattern expressions listed on page 2-21, its frequency spectrum can be represented as a product of an "element factor," the Fourier transform of an individual pulse, and an "array factor," the Fourier transform of the periodic burst. The transform of a uniform or rectangular pulse is $\sin(\pi ft)/(\pi ft)$ with a main lobe which exhibits a half-power width in the frequency domain of 0.886/t, nominally 1/t. The transform of an untapered periodic train of n pulses is:

$$\frac{\sin(n\pi\tau f)}{n\sin(\pi\tau f)}$$

which has nominal frequency domain resolution of 1/T and a repetitive spectral response with ambiguous lobes separated by $1/\tau$ = PRF (Figure 2.13).

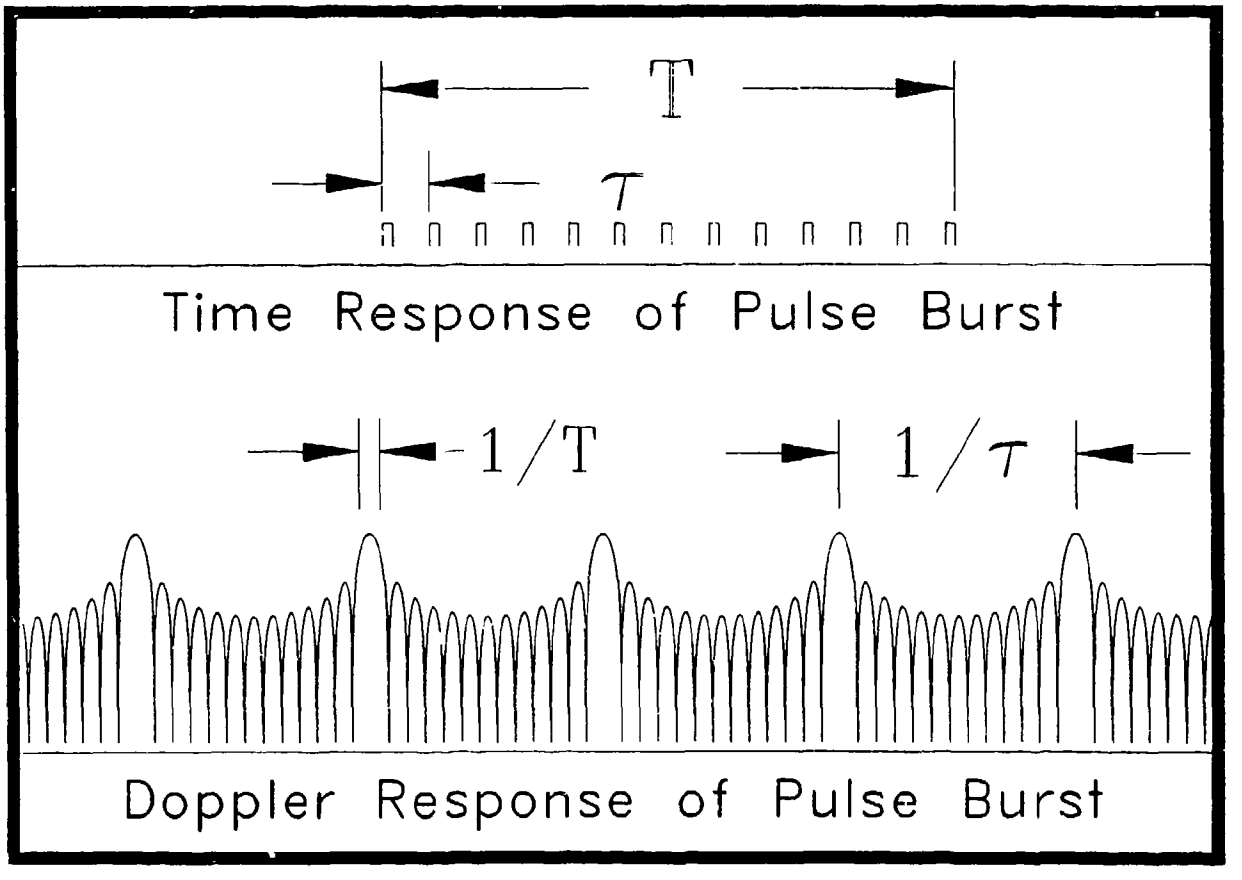

Figure 2.13 Low PRF Waveform Response

Tapered pulse bursts are achieved by imposing weighting functions on the burst amplitudes and/or phases to achieve lower sidelobes at the expense of diminished frequency domain resolution. These weighting functions can be imposed during burst transmission or they can be imposed as part of the receive subsystem's processing. Tapering on transmit is not common practice because of difficulties encountered in its implementation. Tapering on receive is much simpler, but it must be repeated for every range, range-rate resolution cell evaluated. As with the antenna, weightings modify the functional representations of the waveform but not the underlying variables nor its ambiguity properties.

The waveform processing operates as a filter, selectively intensifying or diminishing the energy retro-reflected from every target on the surface of the earth in accordance with the received time-frequency characteristics which, in turn, correspond to the target's range and range-rate with respect to the radar. With the smooth spherical earth presumptions embedded in the formulation, every clutter patch location can be expressed in terms of either its angle, angle with respect to the radar, naturally used in representing the antenna pattern, or its range and range-rate relative to the radar, naturally used in representing the waveform. Alignment of the antenna and the platform's ground track simplifies evaluations of the clutter integral by simplifying the transformations between them.

For the airborne radar designs considered in this report, a low PRF waveform is one whose interpulse period is large enough to ensure that all earth returns from one pulse have been received prior to transmission of the next. Equivalently, it receives reflections from only one range interval on the earth's surface at one time. Equivalently, it has no ambiguous range responses within the horizon. The selection of which particular range within an unambiguous interval the radar responds to is completely arbitrary. In fact, its signal processing subsystem is able to and regularly does generate independent responses to objects at all possible ranges. Interpulse periods of several milliseconds, corresponding to PRFs of several hundred Hertz, are common in low PRF airborne radars.

The exclusion of ambiguous results in the range dimension in practical airborne radars is necessarily accompanied by ambiguous results in the Doppler or range rate dimension through the agency of the ambiguous lobes illustrated in Figure 2.13. For every range interval selected for processing, the signal

processing subsystem is able to and regularly does generate independent responses to objects at a number of range-rates, approximately the ambiguous range rate interval divided by the resolution. The domain of the clutter integration is shown (Figure 2.14) with a typical low PRF waveform function overlaid at a selected range. For the selected processing range and range rate, the clutter power (more precisely the clutter to target ratio) is calculated in accordance with the previously evolved integral equation with its limits selected for summation of surface clutter contributions from the entire visible surface. The horseshoe shaped domain in the range, range-rate coordinate system represents half of the visible earth, either the right or the left half as partitioned by the ground trace.

A high PRF waveform is one whose ambiguous spectral lobes, separated by the PRF, are so far apart that only one can respond to earth targets. The targets extend over a velocity spectrum of approximately $\pm$(platform velocity plus maximum target velocity). The exclusion of range-rate ambiguities in practical airborne radars requires PRFs of tens or even hundreds of kiloHertz and is necessarily accompanied by multiple ambiguities in range.

A medium PRF waveform, intermediate between high and low PRF, is accompanied by ambiguities in both dimensions with the combined total number a constant. The signal processing subsystem regularly generates responses to objects at all reasonable values of both. In early phases of this effort, targets were located near the horizon, implying that range ambiguous waveforms would receive additional clutter power from less than target range at much higher power levels. In later phases, including all of the examples of this report, targets were located at a small fraction of horizon range and any range amibuities were located far beyond target range, contributing additional clutter power at much reduced levels.

In all results, a perfectly rectangular pulse shape has been presumed and the waveform effects in range are approximated by restricting the integration limits in ρ from the entire domain to the selected range $\pm$ half of the range resolution. This assumption allows the computer resources required in evaluating the integral to be reduced substantially, and, according to test cases, diminishes data integrity imperceptibly. The presumption of a uniform pulse in range rather that one with a sin(x)/x or other more realistic range response demands substantially larger bandwidth than is usually associated with a stated range resolution.

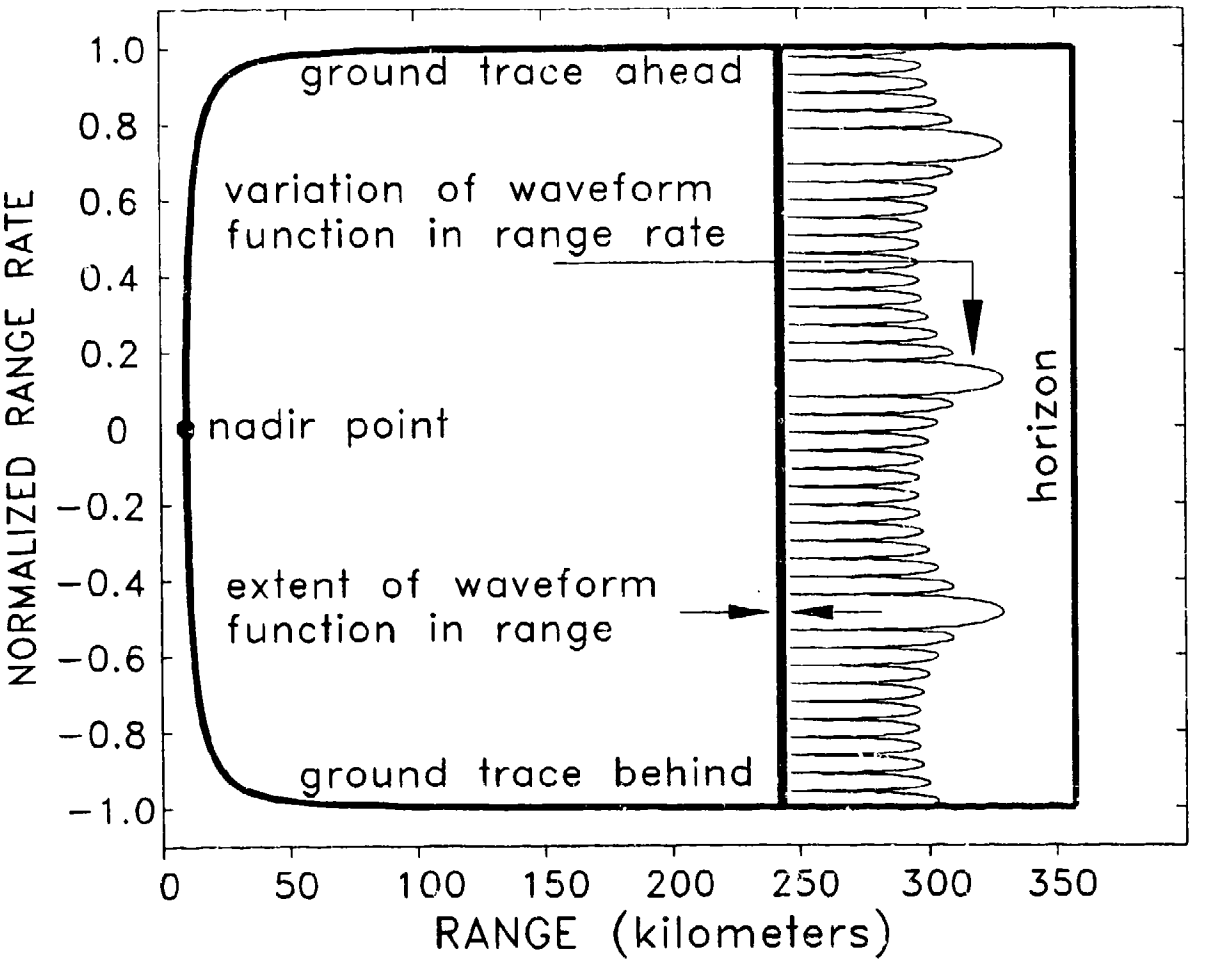

Figure 2.14 Waveforms Consisting of Pulses with Sharp Skirts Permit Integrations over the Entire Surface Clutter Domain to be Approximated by Integrations over Narrow Range Windows

Conventional waveforms, such as those from the sin(x)/x family, respond at all ranges of course, and suitable concern for accuracy is necessary when restricting their extent to small regions on either side of the peak response. In all cases tested to date, this limitation has not led to perceptibly diminished accuracies. When these studies are expanded to include non-alignment and other waveforms than low PRF, further testing of accuracy will be needed.

One of the illustrative cases considered in the following section was based on a radar altitude of 10 km and a nominal target range of two tenths of horizon range. The integrand was limited to a domain which extended over a single range resolution interval in ρ, for which the appropriate integration limit in μ varies as:

$\mu_{max} = \sin\theta_y$ = 0.9858902 at nominal target range minus 10 km,
= 0.9890874 at nominal target range minus 1 km,
= 0.9893694 at nominal target range, 71.459 km,
= 0.9896398 at nominal target range plus 1 km,
= 0.9916393 at nominal target range plus 10 km.

For many antenna pattern/waveform pattern combinations, the integration results were not affected much by how closely the μ limit approached its maximum. In those cases an arbitrary value of $\mu_{max} = 0.95$ was just as accurate as those where it approached arbitrarily close to its theoretical value. This was the situation in the encounters reported in Figures 3.1 through 3.4. In other cases, where either the antenna or the waveform pattern had ambiguous responses at main lobe levels in the direction of the ground trace singularity, accuracy suffered unless the limits of integration approached very closely to the singularity. In Figures 3.5 through 3.7 a value of 0.989 was close enough to the exact value to generate results with excellent accuracy whereas a value of 0.95 was not. (In these examples, the integration in μ was performed at the nominal target range where the selected value of 0.989 is sufficiently less than the exact value of 0.9893694 to preclude problems at the singularity. The two range values correspond to an elevation angle difference of 0.144-degrees.)

These examples were based on PRF values of 600 and 900 Hz, corresponding to range ambiguity intervals of 250 and 167 kilometers respectively. This ensured that any range ambiguous clutter was retroreflected from significantly farther ranges than target range and experienced substantial range related attenuations. The specific values of 600 and 900 Hz have no particular significance for this encounter. In subsequent examples where the radar altitudes was 2 kilometers, the PRF of 900 Hz is barely unambiguous in range.

2.3.3 Specific Antenna/Waveform Functions. Results reported in this document were based on the use of uniformly illuminated transmit antenna configurations and waveforms. Uniform illumination functions were employed for the antenna receive

configurations and waveform processing in some situations, and tapered functions were employed in others. The subtleties of the trades among resolution, sidelobe response and gain of different taper functions are extensive and no attempt at their exposition is attempted here. The use of 'gable' and related taper functions have been emphasized because their transforms are easily evaluated and their sidelobes are unusually wide. The large sidelobe extent facilitates uncomplicated construction of antenna and waveform pattern pairs in which the entire extent of the main lobe response of one coincides with a low side lobe region of the other (Section 3.4), an essential ingredient in minimizing the clutter integral. The penalty for the gable waveform's straightforward formulations is suboptimum trades among the performance parameters.

An equally spaced sequence of n uniform pulses transforms according to:

$sink(x,n) = \frac{\sin(nx)}{n \sin(x)}$. A sequence of m pulses, with the same spacing but with a gable distribution, as 1-2-3-4-5-6-7-6-5-4-3-2-1, transforms according to:

$gabl(x,m) = sink^2(x,\frac{m+1}{2}), \quad m \text{ odd.}$ Simple combinations of several uniform and gable illumination functions can be used to synthesize antenna and waveform patterns that reduce levels of the clutter density functions in the regions of the antenna/waveform main lobe responses. These combinations are especially simple to formulate when all of their components share a common phase center, allowing the individual transforms to be added without phase compensation.

A composition of this sort, identified as Taper Function Synth2, is used in Section 3.4. It consists of four terms:

- a 13 element gable distribution is the dominant contributor,
- two much smaller, out of phase, 15 element uniform distributions with the same spacings contribute to diminishing the sidelobe response in a selected region; each has its own amplitude and offset from the gable main lobe,
- another much smaller, out of phase, 2 element (10 x spacing) uniform distribution, with its amplitude and offset from the gable main lobe selected to diminish the sidelobe response in the selected region even more.

This function and others like it were generated by a trial and error approach in which the effects of changes on plots of the round trip antenna pattern, waveform function and the azimuth density function were monitored visually. While it lacks the power of matrix inversion methods in optimizing performance of specific configurations, it provides invaluable, detailed insights into the process of formulating configurations to be optimized in an optimal way. It supports preliminary explorations into the selection of antenna/burst extents as functions of presumed target offset and their relationships to the extents of sidelobe space to be minimized, to the selection of element spacings and the uses of spacing diversity, to evaluations of frequency selection and bandwidth. It fosters identification of and comparisons among all the criteria eligible for use in adaptive clutter reduction procedures.

3. SELECTED RESULTS

During the development of the analytical constructs described in Section 2, requirements for advanced downlooking radar cycled through a number of applications and parameters, ranging in frequency from L-Band to X-Band and in altitude from 2 to 800 km. L-Band and S-Band airborne radars at altitudes of 2 and 10 km were studied in some detail, and the example data presented in this section were from those efforts, mostly from the L-Band lower altitude encounters.

3.1 Encounter Configurations and Parameters

In every case reported, the radar was in level flight without crab angle, over a perfectly spherical half-earth, corresponding to one of the two horseshoe shaped analysis domains characterizing the visible earth. The surface clutter density consisted of a nadir spike plus isotropic diffuse scattering at -20dBsm/sm: $\sigma^c = 0.01 + 0.99 * \sin^{299}(\text{grazing})$ with $\sigma^0 = \sigma^c * \sin(\text{grazing})$ as explained in Appendix B. Aircraft velocity was 100 meters per second. The antenna was an array of sixteen vertical columns with each column containing eight individual radiating elements. Column excitation was uniform and the array factor (elevation plane) voltage pattern of each column was of the form sin(nx)/sin(x), usually directed at target range. Column spacing was 0.65-wavelength.

In every example the target range was 20 percent of horizon range and there were no shorter range ambiguities. In a few cases, ambiguities existing at ranges beyond target range were ignored after a brief study indicated that, for the restrictive assumptions used, they added a small amount to the received clutter distributions without affecting their character in any way. All results correspond to integration in only one of the two horseshoe shaped analysis domains that make up the visible earth. Contributions from the other half of the earth were ignored, as if the planet were bisected along the ground trace into a right half with surface clutter and a left half that was perfectly absorptive. Effects of this latter short cut can be seen very clearly in some of the results (for example, Figure 3.7) Both of these steps were taken to diminish the computer time used in generating results.

3.2 Computer Evaluation Methods

Prior to this lecture series, NTL Technologies had worked exclusively with Fortran language computer methods and had evolved software for accurately evaluating surface clutter integrals, using integration grids of as many as 100,000 points for each range ring, accounting for almost all antenna and waveform effects. Methods of devising synergistic antenna pattern and waveform functions for purposes of substantially reducing clutter/target ratios, using low PRF waveforms, had been demonstrated.

RL/OCDS requested that, for the current effort, computer evaluations be performed with a mathematics software package named MathCAD as a way of increasing student participation in the analytical, as opposed to the computer cranking, process. With trepidation, this was attempted. It succeeded very well and every result in this document was obtained using MathCAD. Routines were developed and improved during lecture and discussion periods and the transitions from the paper and pencil analyses of Section 2 to computer evaluations was unusually swift and painless. Because of that and also to promote the more complete understanding that program development cultivates, guidance on specific program development has not been included in this document although a few general comments follow.

Compared with Fortran, the MathCAD methods appear to provide equivalent processing power and speed with minimal programming requirements. Accuracy problems encountered in Fortran executions were encountered, with haunting similarities, in MathCad executions. Fortran documentation of cases evaluated is definitely superior, mainly because of the way it encourages separation of executable routines and data; in MathCAD, adequate documentation of cases evaluated can be a pain.

The most vital difference between the two is in the implementation of integrals. With Fortran, the process is completely in the hands of the analyst who decides on approximation methods, numerical techniques, sample intervals, and everything else. With MathCAD, the integral is formulated, a parameter that vaguely controls the trade of execution time versus accuracy is set and away it goes. With time and effort, good results are forthcoming but the seemingly total

inaccessibility of debugging information can be disconcerting to those accustomed to more traditional methods. (The most frustrating examples are those where an integral evaluation computes for hours or days and then declares, with no diagnostic data available anywhere, that it is 'not converging.')

3.3 Calculated Results for Altitude of 10 km

The first example corresponded to the case of all sixteen of the vertical column subarrays described in Section 3.1 being energized uniformly both on transmit and receive. The pattern of each of the (8 high x 16 wide) array elements was isotropic. An azimuth steering phase was imposed to scan the beam 84.26-degrees from the aircraft velocity vector (the z-axis), corresponding to a z-axis direction cosine of 0.1. Altitude was 10 km. The waveform was a uniform burst of sixteen pulses of 0.05 milli-second duration, and the PRF was 600 Hertz.

Evaluation of the expression for clutter/target ratio for these conditions produced a typical velocity spectrum (Figure 3.1) that could be generated by the radar's signal processing subsystem. The antenna pattern peak is located at a normalized velocity of 0.1, and a velocity filter centered there would generate a peak response as shown. Any velocity filter offset from the pattern peak by the velocity ambiguity interval also generates peak response, accounting for the three lobed spectrum. Velocity filters that are offset from the antenna peak response by lesser amounts in the clutter velocity domain exhibit reduced response because of the misalignment of the antenna pattern and waveform functions. The filter offset by half of the ambiguity interval is diminished about 25dB relative to the peak, clearly indicating that chances of finding a target are best if it is located at the peak of the antenna pattern with a radial velocity component, compared to clutter at the same location, of half of the velocity ambiguity interval.

Increasing the PRF from 600 to 900 Hertz increases the separation between the response peaks (Figure 3.2). Using antenna array elements with the patterns of a vertical dipole in front of the ground screen, sin(elevation) * cos(side) = $\sin\theta_y \cos\theta_x$, has very little impact on this result (Figure 3.3). Relocating the antenna pattern peak to 0.55 (normalized velocity) does not change the characteristic much for PRF = 600 (Figure 3.4) but does for the PRF of 900 HZ (Figure 3.5)

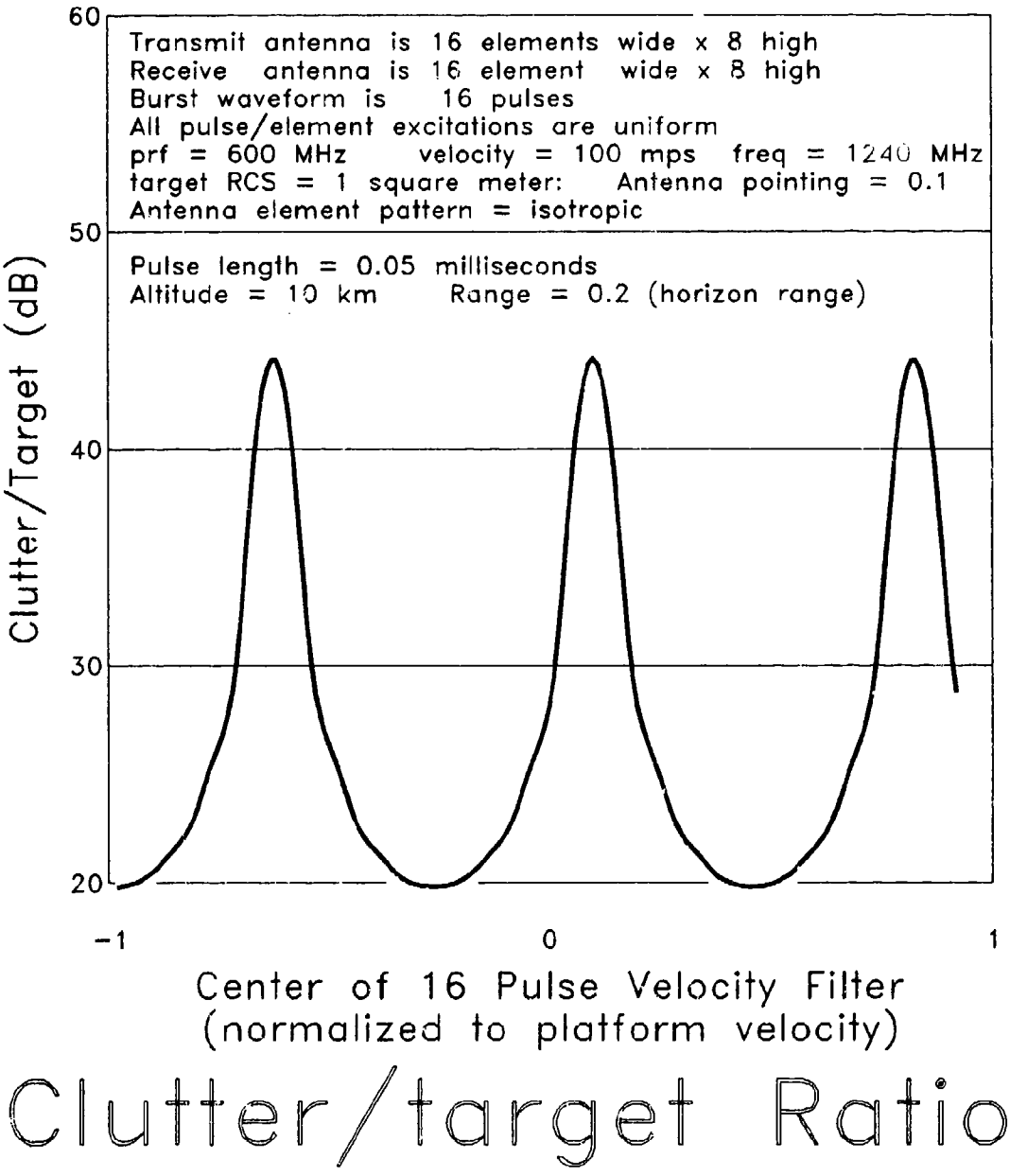

Figure 3.1 Velocity Distribution of Clutter for Isotropic Array Elements and PRF = 600 Hz

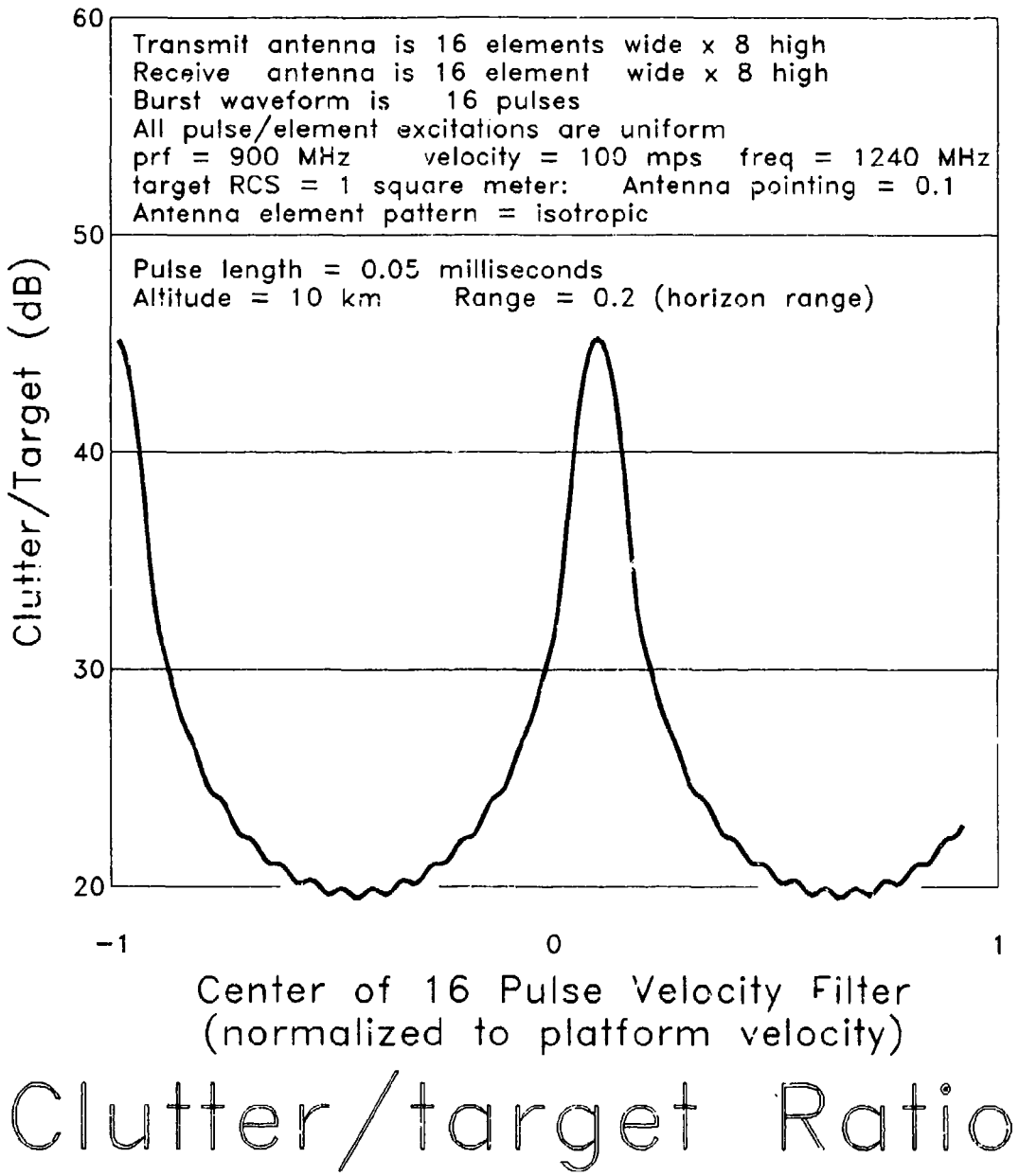

Figure 3.2 Velocity Distribution with PRF Increased to 900 Hz

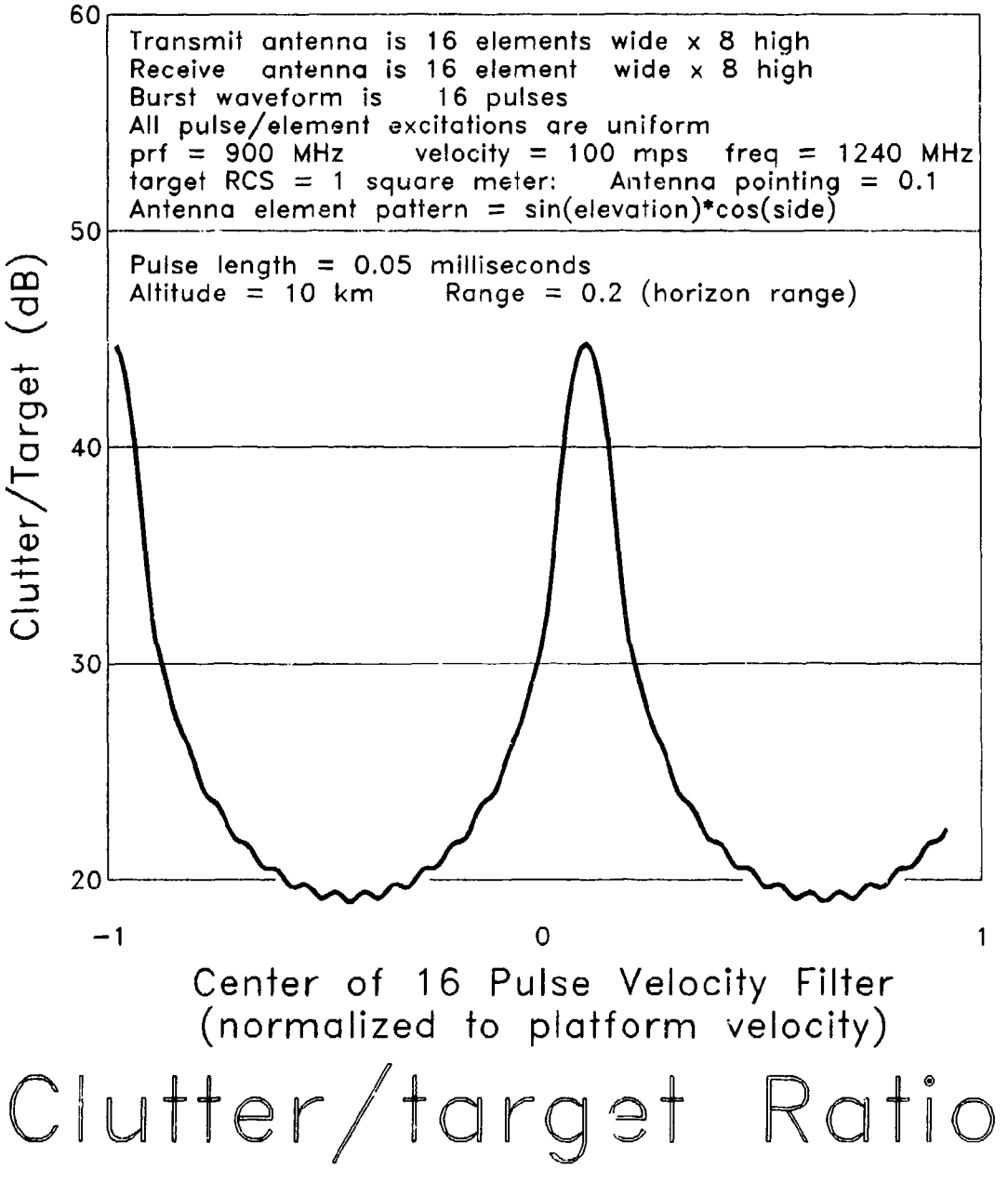

Figure 3.3 Velocity Distribution for $\sin\theta_y \cos\theta_x$ Element Patterns and PRF = 900 Hz

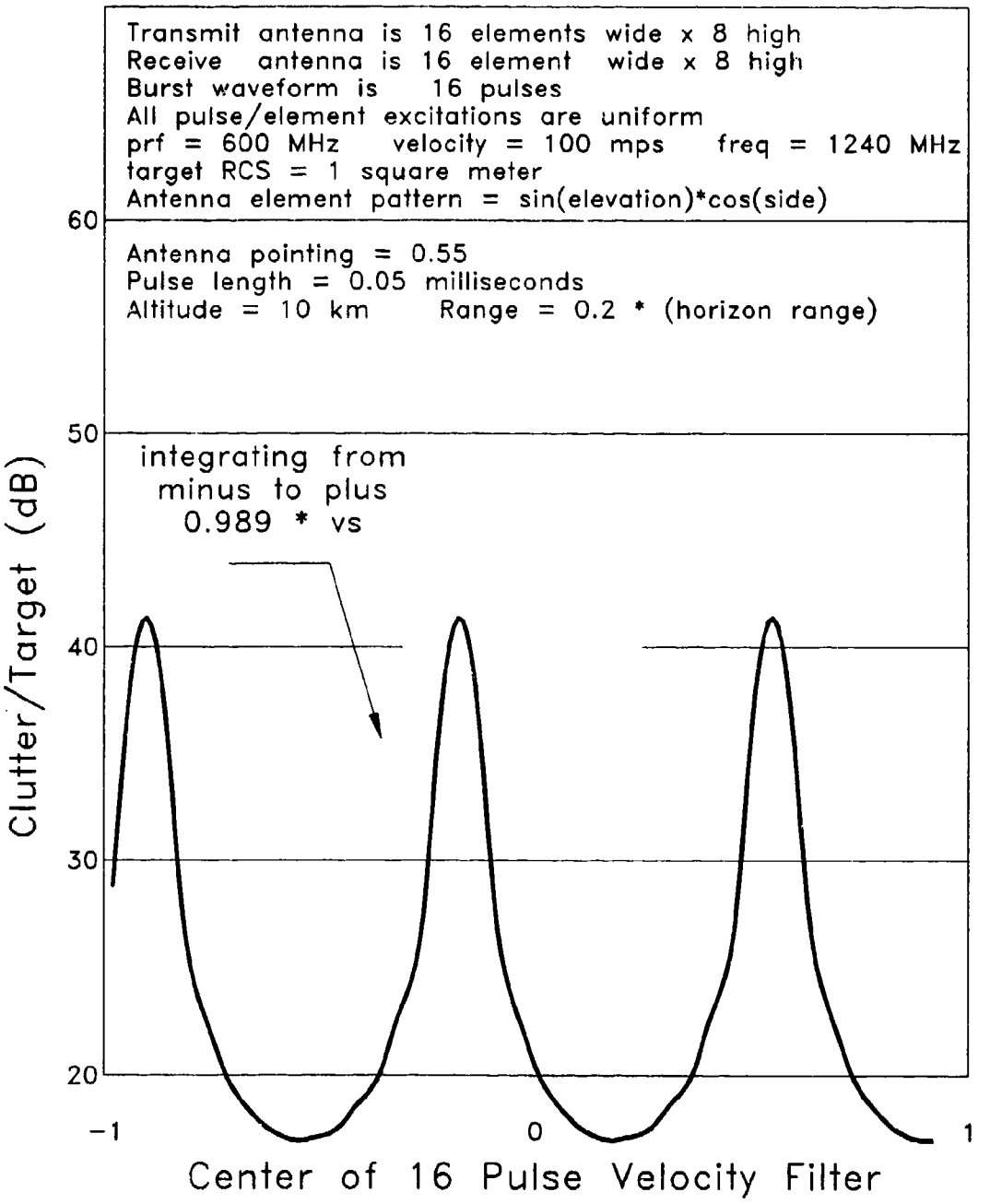

Figure 3.4 Velocity Distributions with Antenna Pattern Pointing Changed to 0.55, PRF = 600 Hz

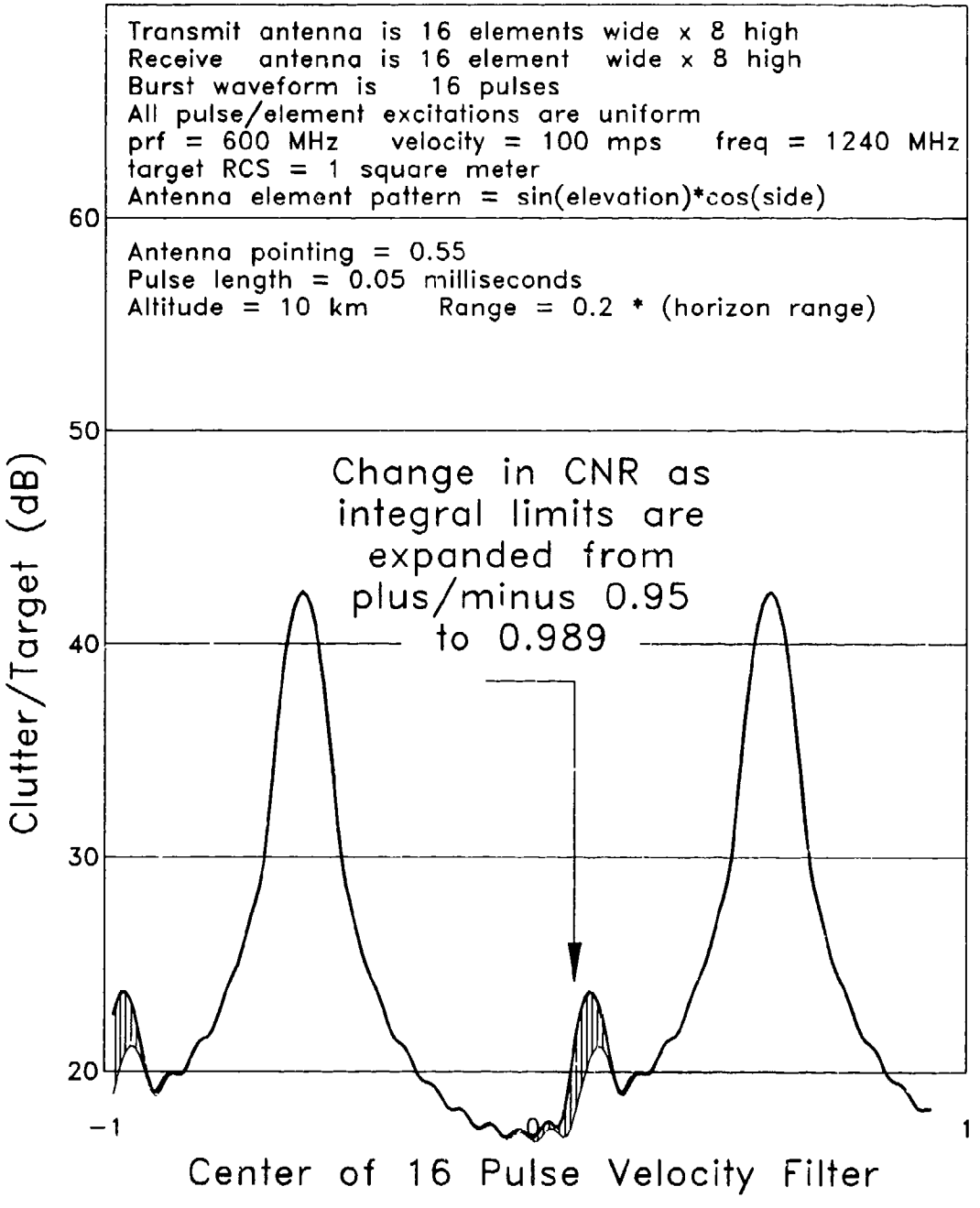

Figure 3.5 Velocity Distributions with Antenna Pattern Pointing Changed to 0.55, PRF = 900 Hz

In the latter result, unlike the previous ones, a discernable difference is obtained when the limits of integration are enlarged slightly to approach more closely to the singularity along the ground trace. The effect is magnified many times by redefining the antenna elements to isotropic, both for the PRF of 900 Hz (Figure 3.6) and 600 Hz (Figure 3.7). Clearly, in these latter examples substantial clutter power is received by the radar from a very narrow swath along the ground trace.

The explanation of these effects is found by examining the density of the clutter integral around the range half-circle and its factors for the last example featuring the PRF = 600 Hz, antenna pointing = 0.55, and isotropic element patterns (Figures 3.8 through 3.15). In each of these illustrations, the round trip antenna pattern is the same; the waveform function is also the same but translated slightly from page to page, corresponding to different velocity filters; the clutter density, the integrand of the clutter integral, is the product of these two as well as the geometry and the clutter RCS density factors. A waveform ambiguity a little to the right of the antenna main lobe in Figure 3.8 has shifted well to its left in Figure 3.15. In every case, because of the antenna's end fire grating lobe, the clutter density function is very large along the ground trace for all conditions, most especially when it coincides with a range-rate ambiguity (Figure 3.12). The transition from a two lobed spectrum to four (Figures 3.2 and 3.5/6) as the antenna scans and the grating lobe develops is simply the result of the interaction of the ambiguous waveform and the ambiguous antenna pattern with maxima at 0.55 and -1. The use of antenna element factors with a zero along the ground trace can diminish these effects considerably but cannot eliminate them (Figure 3.5).

A c[illegible]r lesson to be learned from these results is to avoid configurations where the antenna array factor generates a grating lobe, even if it appears to be suppressed by the element factor. Not only does it cause antenna impedance problems, it can allow unduly large clutter power from the ground trace to enter the receiver. Even when the element factor suppresses these pattern effects in theory, caution is advised because pattern prediction models are often inaccurate at large angles from boresight.

W[illegible] grati[illegible]obes must be permitted, PRF diversity is available to avoid alignments of antenna and waveform ambiguities. Adaptive methods of controlling element/pulse excitations for diminishing clutter should include this diversity.

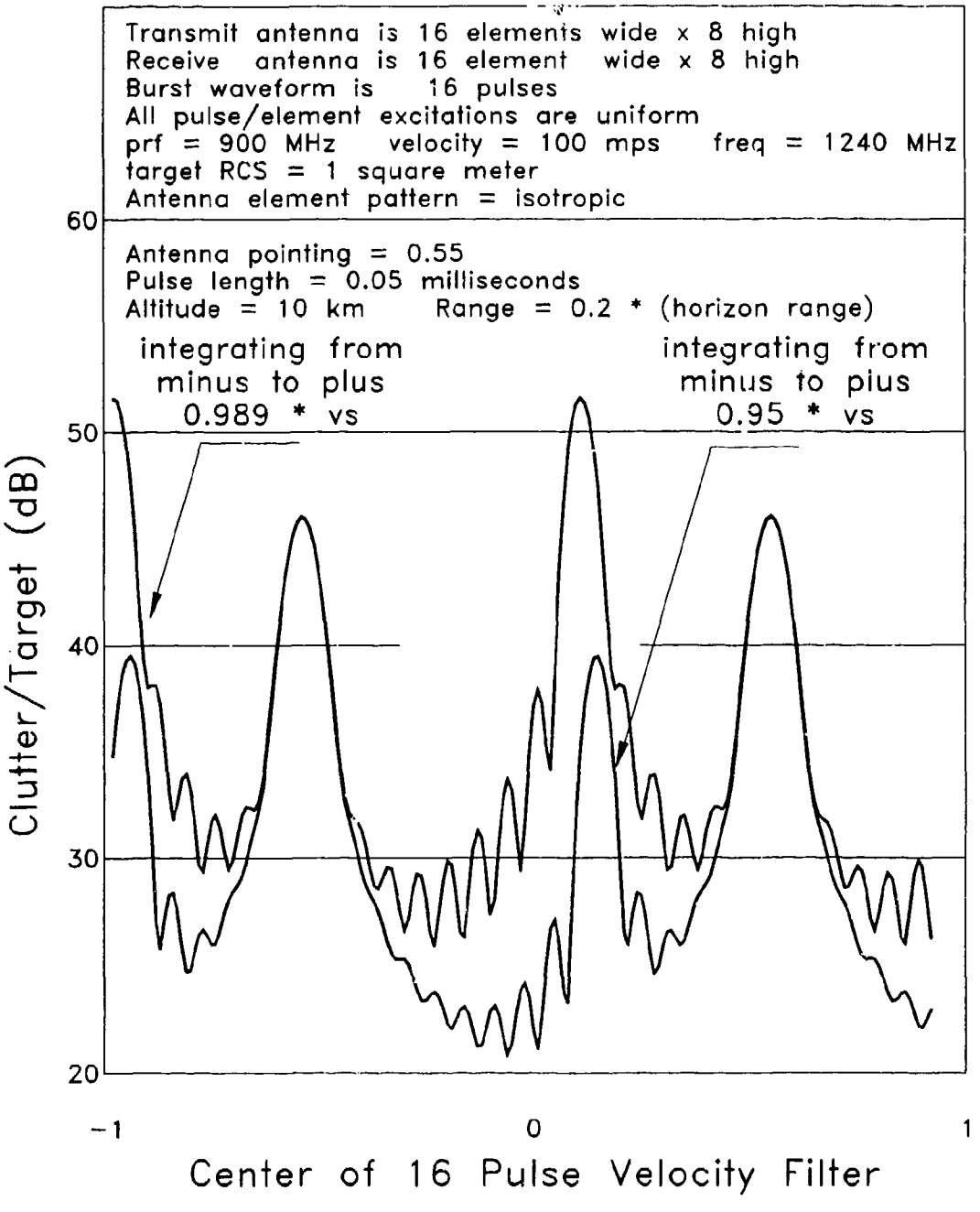

Figure 3.6 Velocity Distributions for Antenna Pattern Pointing of 0.55, PRF = 900 Hz, Isotropic Element Pattern

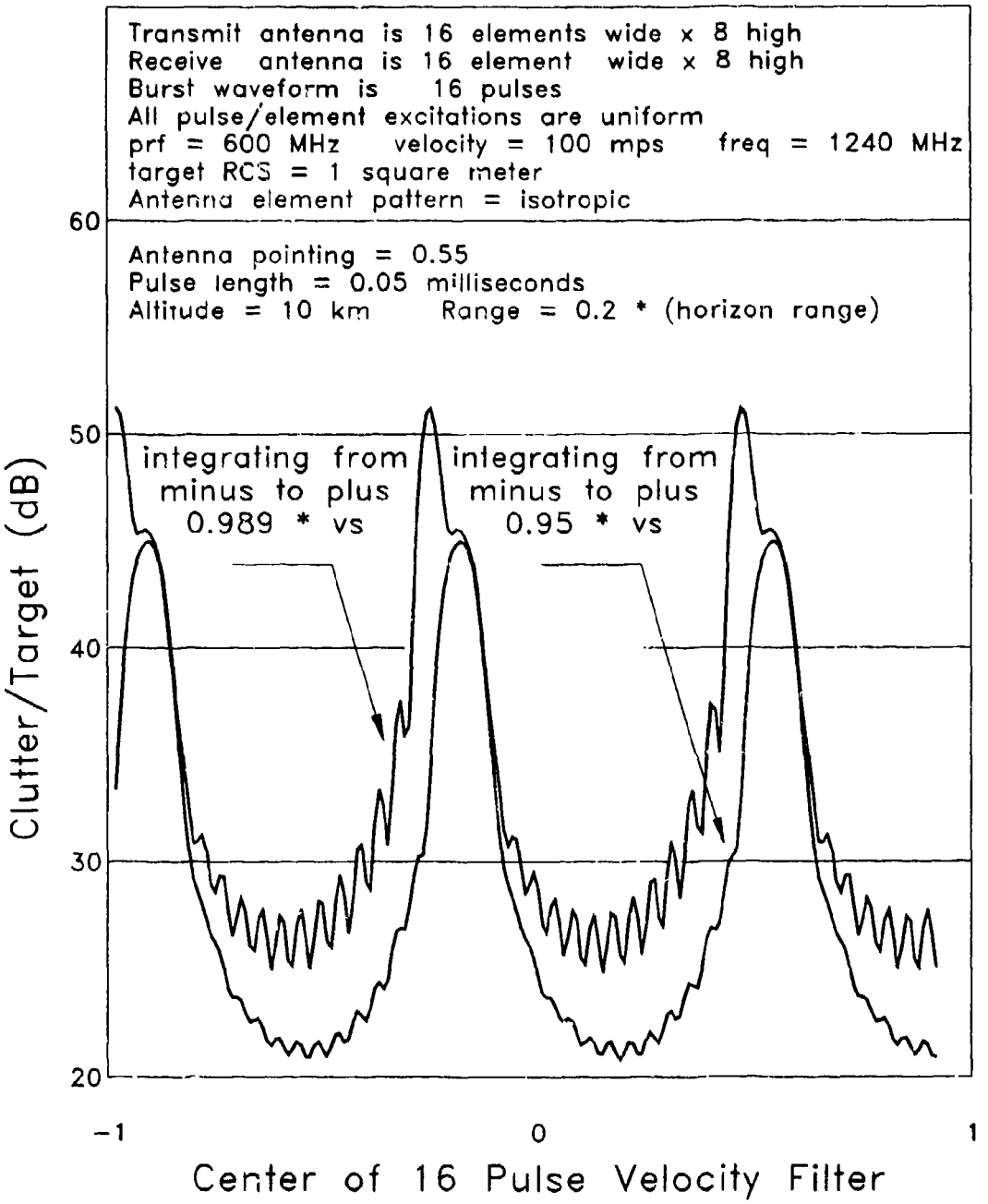

Figure 3.7 Velocity Distributions for Antenna Pattern Pointing of 0.55, PRF = 600 Hz, Isotropic Element Pattern

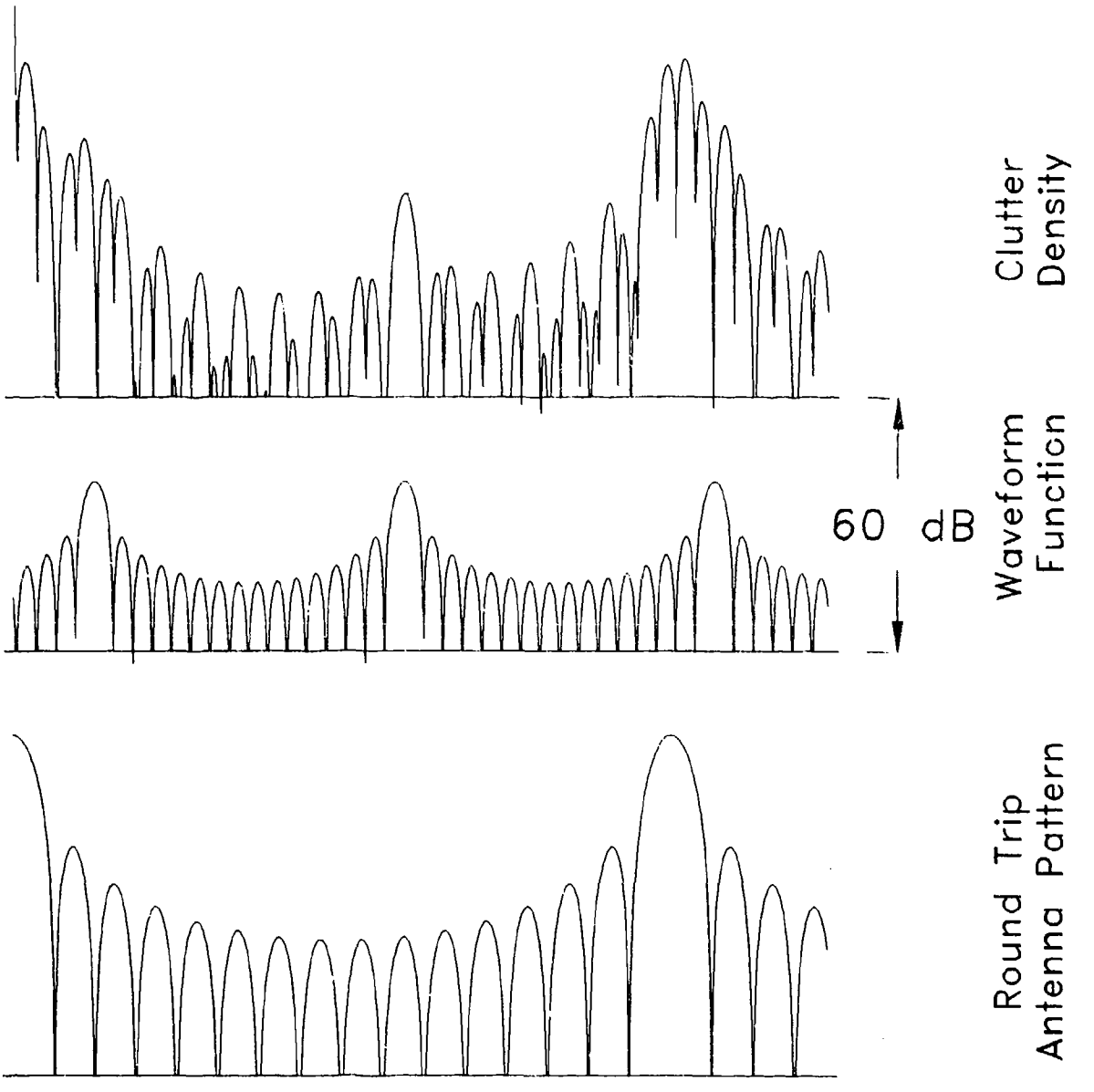

Figure 3.8 Antenna, Waveform(#1) and Clutter Density Functions for Pattern Pointing of 0.55, PRF = 600 Hz

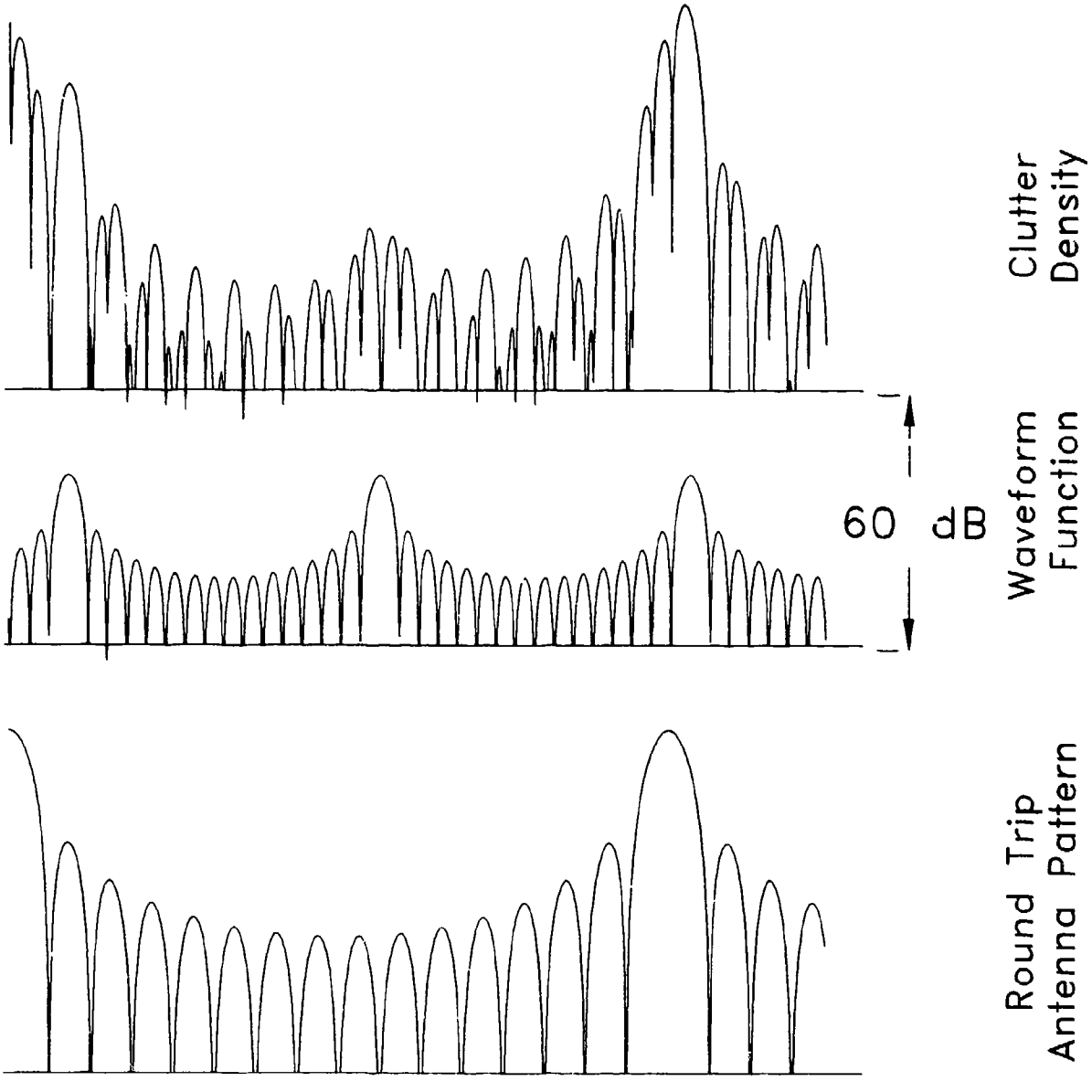

Figure 3.9 Antenna, Waveform(#2) and Clutter Density Functions for Pattern Pointing of 0.55, PRF = 600 Hz

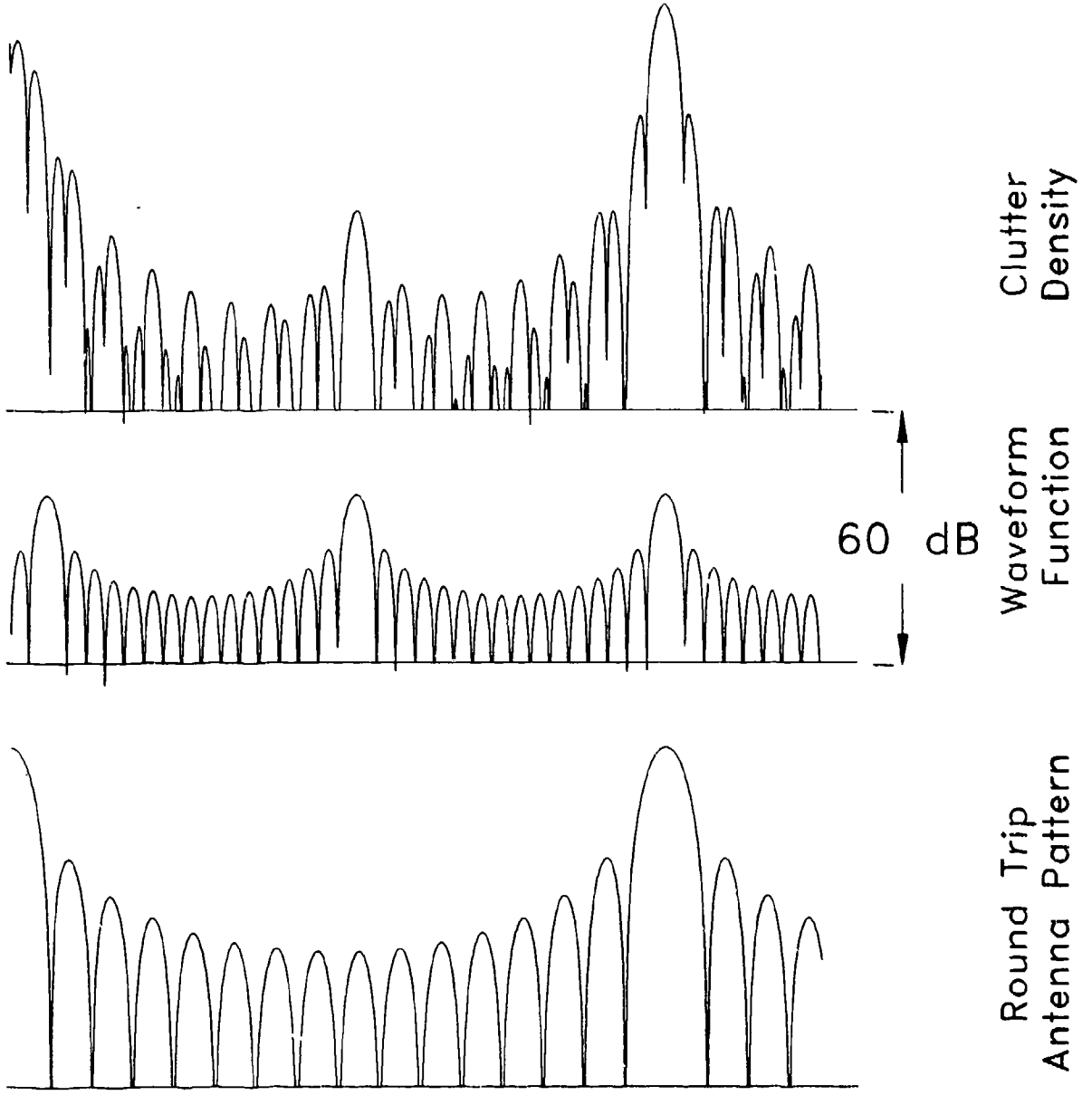

Figure 3.10 Antenna, Waveform(#3) and Clutter Density Functions for Pattern Pointing of 0.55, PRF = 600 Hz

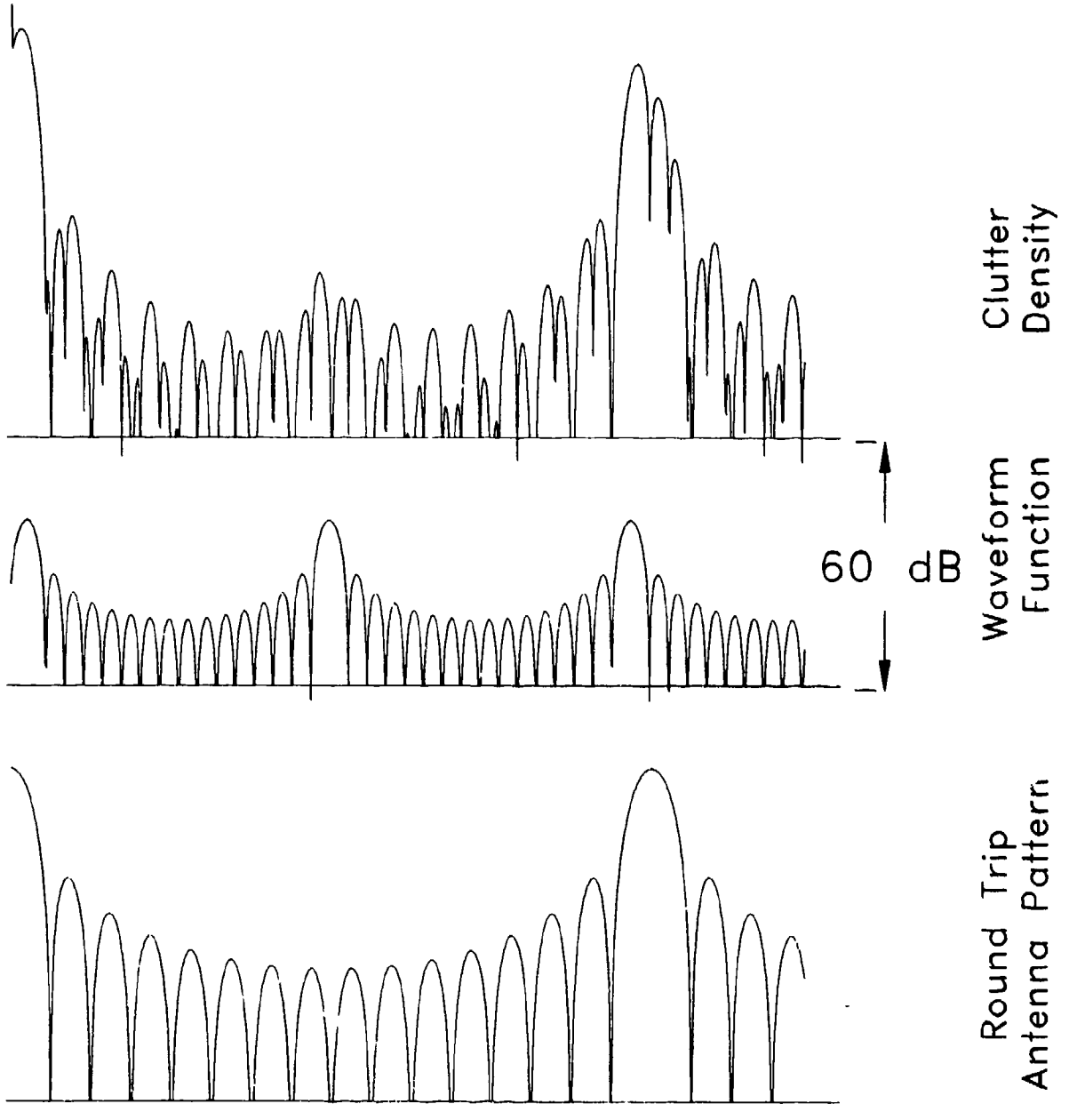

Figure 3.11 Antenna, Waveform(#4) and Clutter Density Functions for Pattern Pointing of 0.55, PRF = 600 Hz

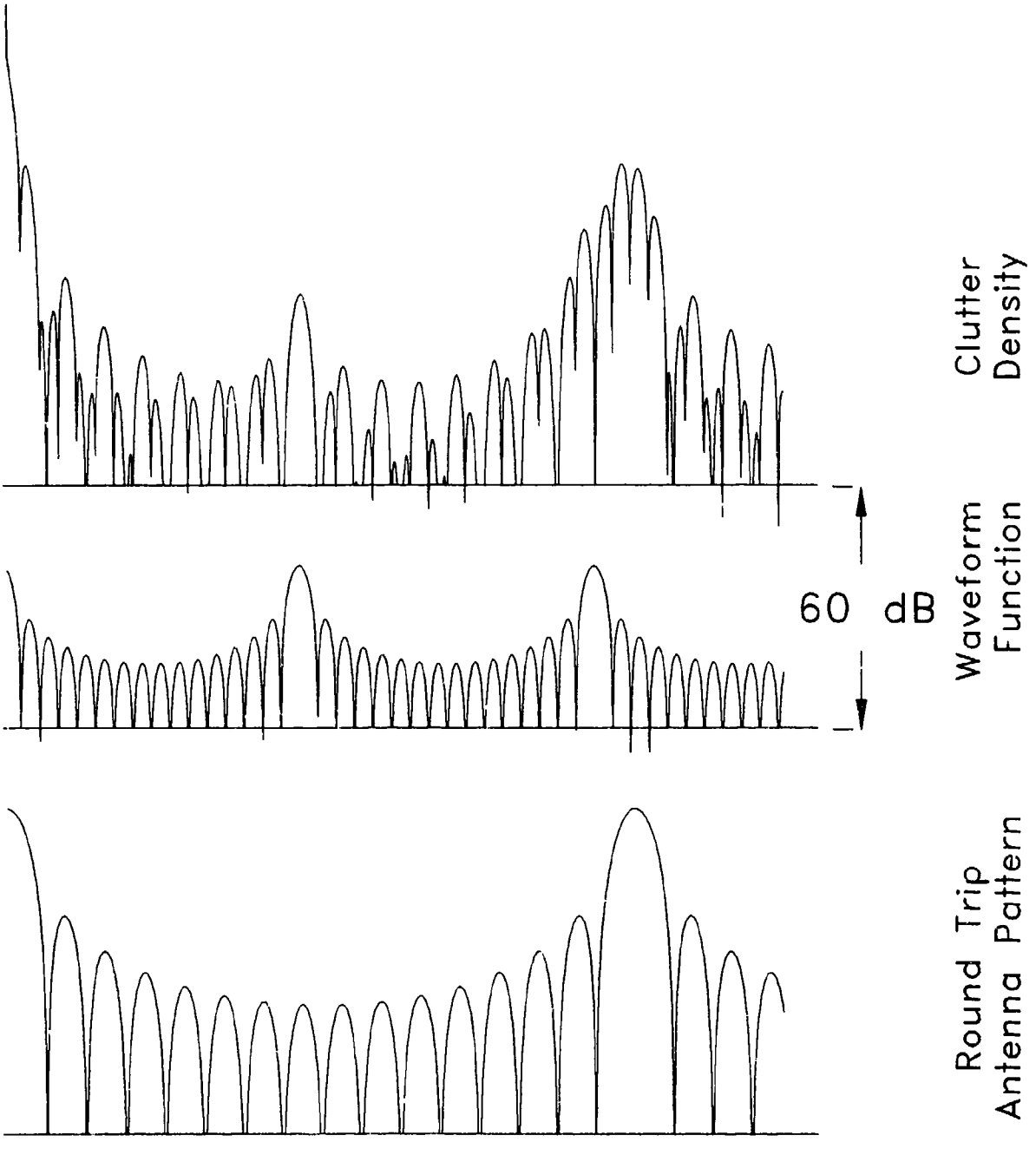

Figure 3.12 Antenna, Waveform(#5) and Clutter Density Functions for Pattern Pointing of 0.55, PRF = 600 Hz

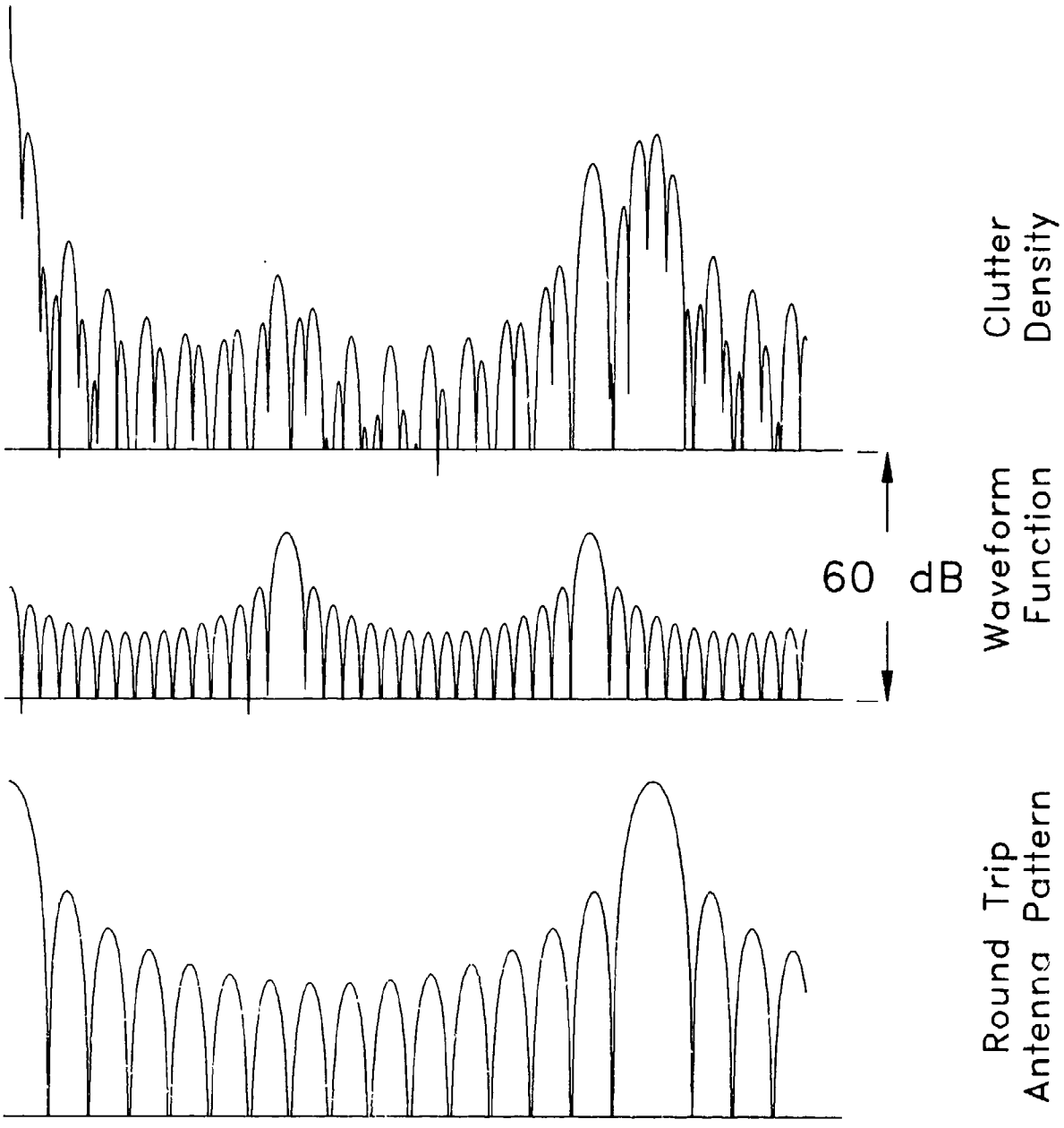

Figure 3.13 Antenna, Waveform(#6) and Clutter Density Functions for Pattern Pointing of 0.55, PRF = 600 Hz

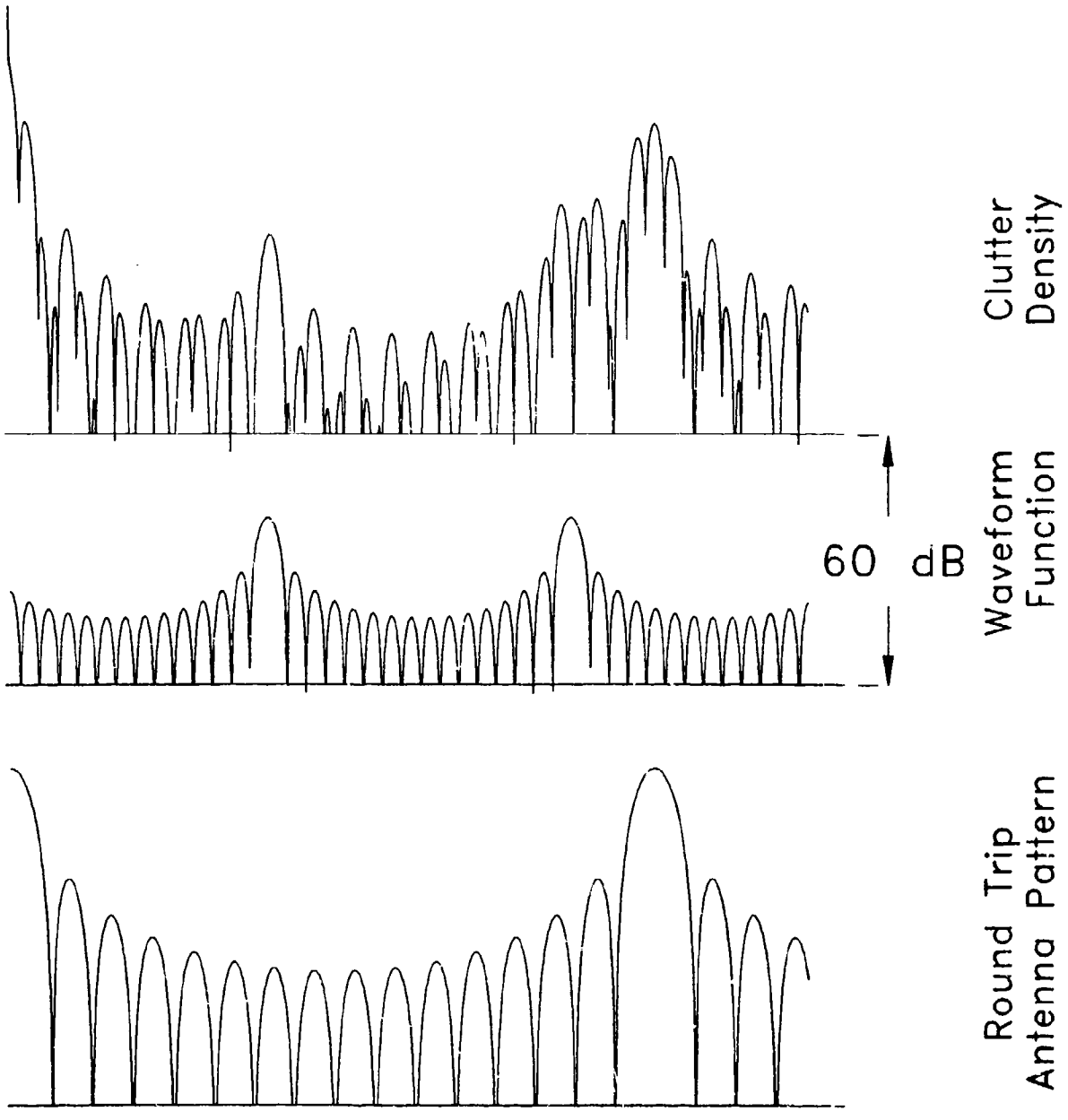

Figure 3.14 Antenna, Waveform(#7) and Clutter Density Functions for Pattern Pointing of 0.55, PRF = 600 Hz

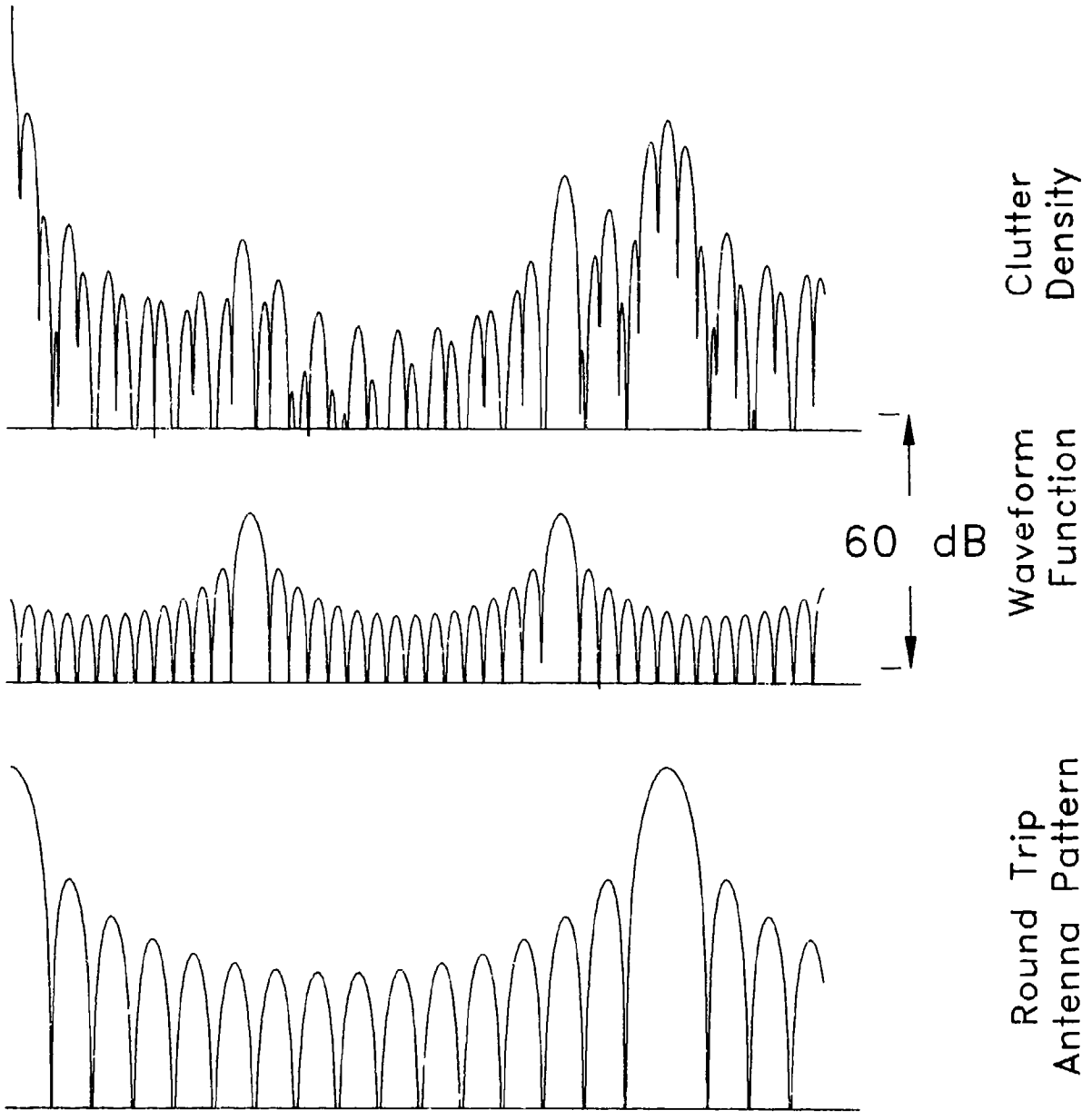

Figure 3.15 Antenna, Waveform(#8) and Clutter Density Functions for Pattern Pointing of 0.55, PRF = 600 Hz

3.4 Calculated Results for Altitude of 2 km

In the following examples, the same radar is used with its altitude changed to 2km where a PRF of 900 Hz is barely unambiguous in range. Tapered antenna illumination and tapered waveform processing are used to reduce their sidelobe levels at the expense of coarser resolutions. An example uses uniform illumination of the antenna's vertical column arrays on transmit and specially tailored tapering of antenna illumination and waveform processing on receive. The density plots for this case (Figure 3.16) with antenna pointing of 0.05 and velocity filter maximum at -0.25 demonstrate clearly the intent of aligning the maximum antenna response with a minimum waveform response - that extends over most of the antenna main lobe - and vice versa to minimize the clutter integral. The formulation, analysis and synthesis of families of discrete element antenna/waveform functions with appropriately wide and synergetic nulls is an important element of advancing the capabilities of downlooking radar. They must adapt to the clutter environment together, composing a joint response that minimizes the integral of the product of (antenna pattern) * (waveform function) * (clutter RCS density) * (geometrical factors). Eventually, closed loop processes will be used to execute the adaptation. For now, clearer understanding of the interactions of these factors will help to compose radar systems from which the adaptive procedures will be able to derive maximum benefit.

Density plots for the same configuration with antenna pointing of 0.25 and waveform maximum located at -0.13 and -0.34 clearly expose that a velocity filter able to provide respectable clutter reduction at one range rate need not be very good at another (Figures 3.17 and 3.18). The difference in integrated level for the two filters is over 20 dB. The velocity spectrum for this particular pair of functions is shown at the right side of Figure 3.19 which presumes that the same waveform weighting is employed for every velocity filter. The reference spectrum on the left is based on a conventional tapered burst excitation (-26 dB first sidelobe) of both the receive antenna and the waveform.

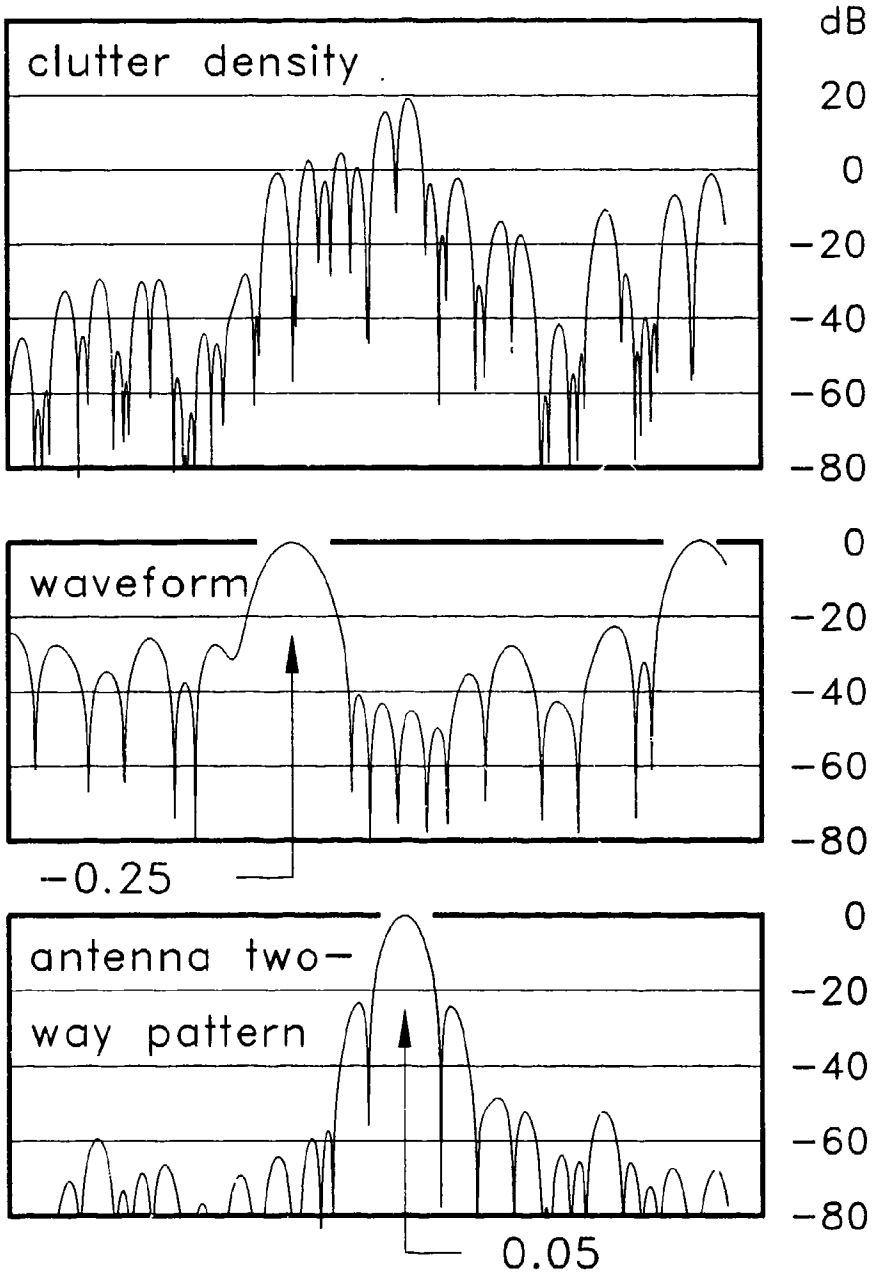

Figure 3.16 Antenna, Waveform and Clutter Density Functions for Antenna Pointing of 0.05 and Waveform Pointing of -0.25 using Taper Function Synth2

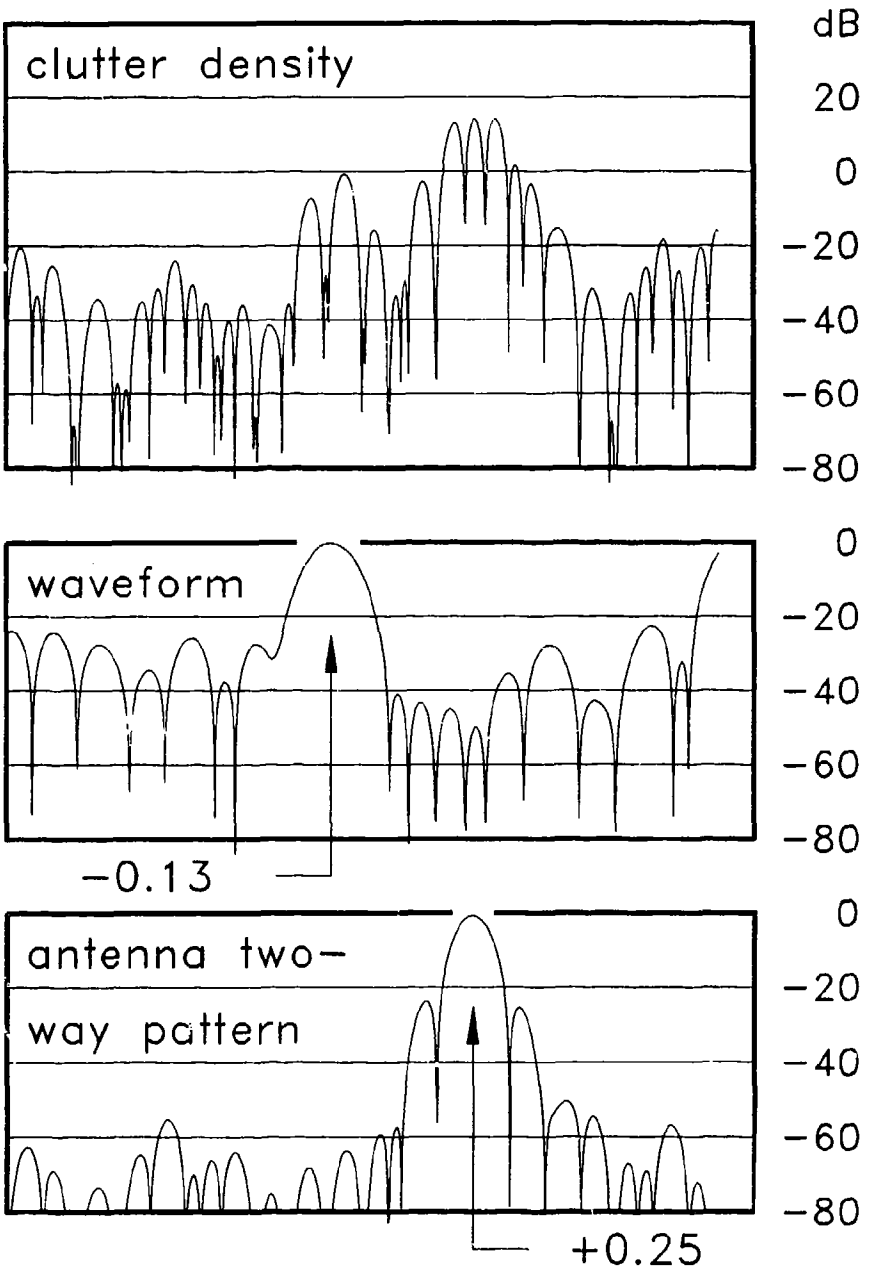

Figure 3.17 Antenna, Waveform and Clutter Density Functions for Antenna Pointing of 0.25 and Waveform Pointing of -0.13 using Taper Function Synth2

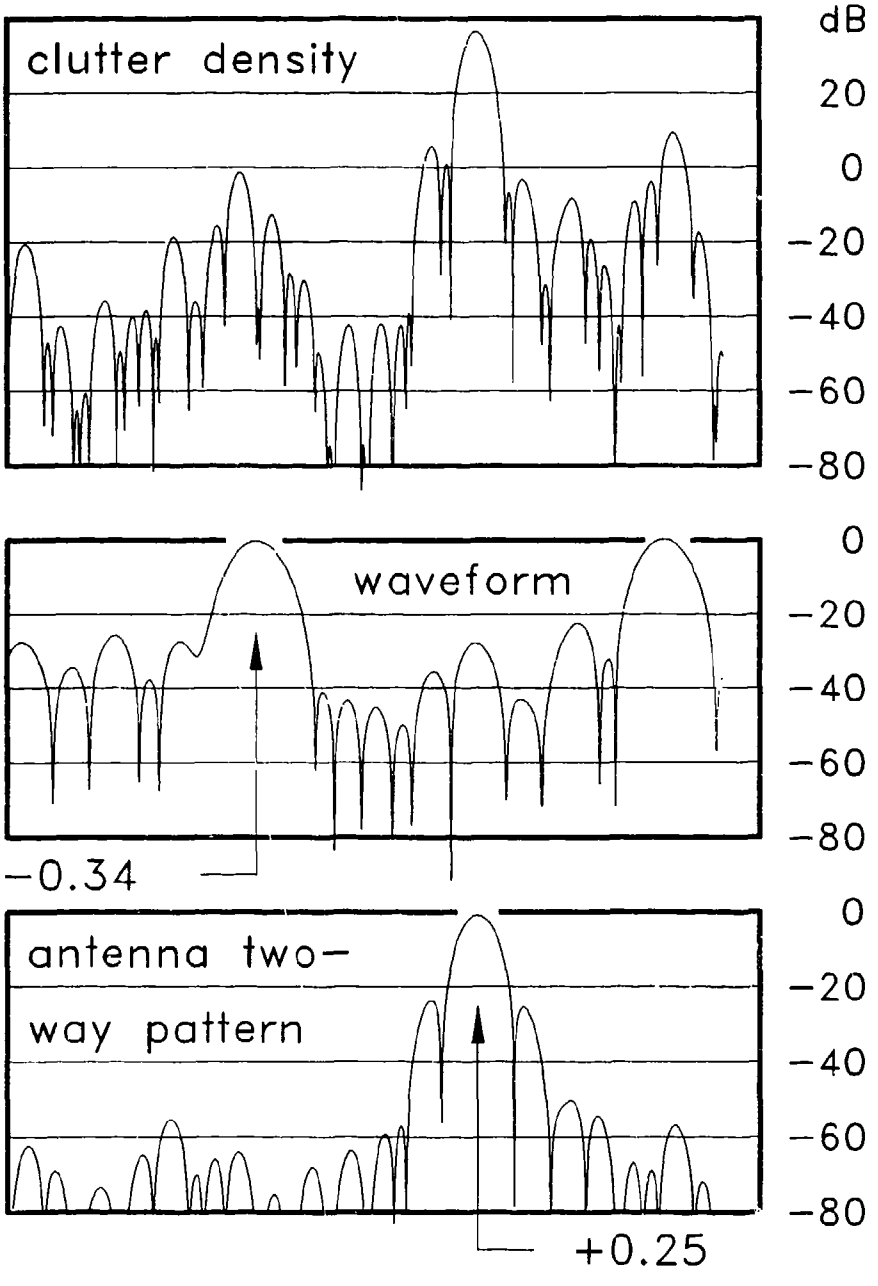

Figure 3.18 Antenna, Waveform and Clutter Density Functions for Antenna Pointing of 0.25 and Waveform Pointing of -0.34 using Taper Function Synth2

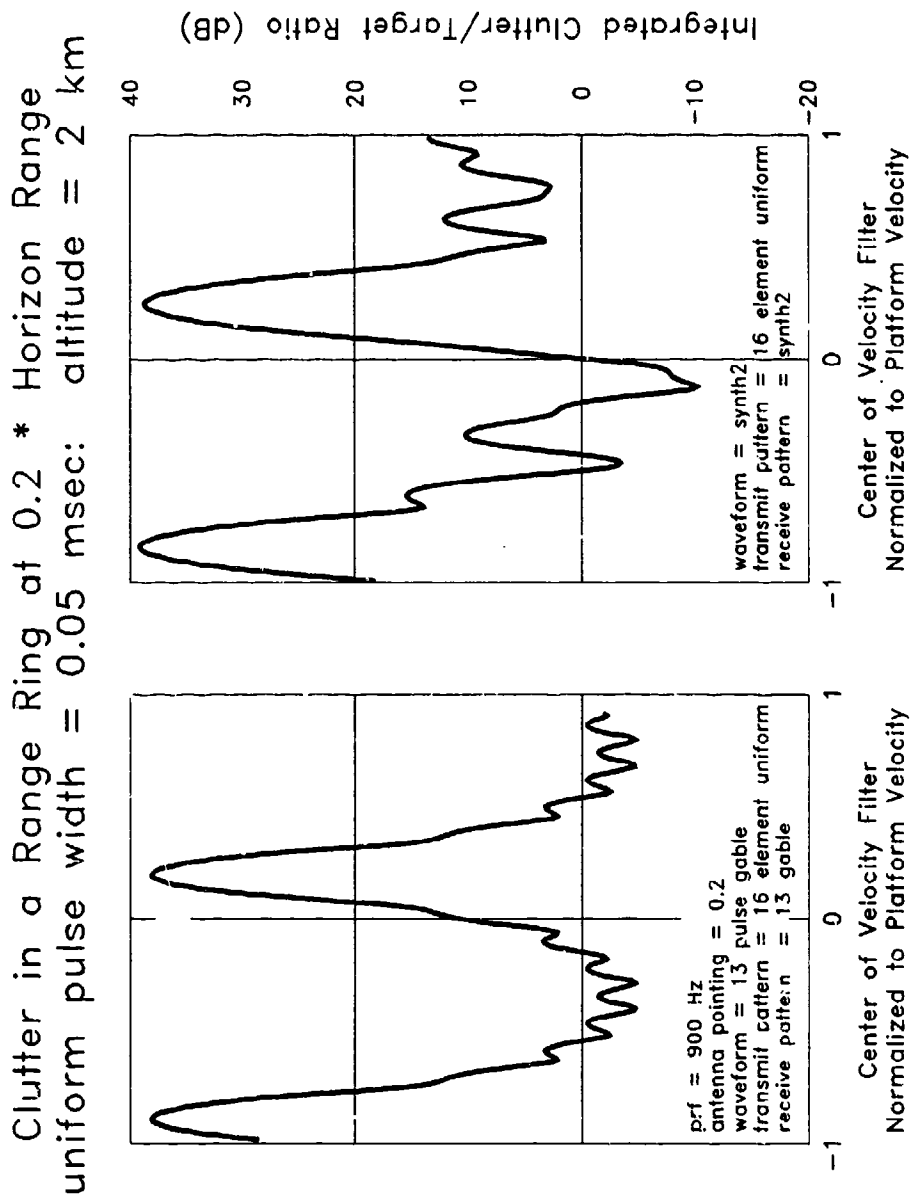

Figure 3.19 Velocity Distributions for Antenna Pointing of 0.25 using Taper Function Synth2 on Antenna and Waveform Receive Processing

4. CONCLUSIONS AND RECOMMENDATIONS

Section 4.1 describes our conclusions and recommendations regarding the classical analysis methods, how effective they've been and how their continued application to clutter research can lead to high payoff results, particularly in bistatic radar. Section 4.2 examines the value of the contract in advancing RL/OC analysis and design skills and recommends their continued cultivation in a design study of candidate bistatic radars configurations and deployments.

4.1 Classical Analysis Methods

The methods reported in this document evolved from studies of space based radar for surveillance of the earth and its atmosphere, studies that demanded the perspective of a radar elevated above a spherical planet. An analytic geometry for space based encounters was developed (Appendix A), motivated by significant inaccuracies in the "back of envelope" estimates commonly used in preliminary radar studies. Invariably the inaccuracies resulted from apparently sensible, but in fact erroneous, applications of flat earth intuitions to spherical earth problems. This spherical earth geometry was quickly applied to estimating the effects of smoothly distributed surface clutter, naturally leading to a calculus problem in which total clutter power was obtained by integrating a continuum of suitably weighted clutter density over the visible surface of the earth (Section 2).

Initial studies, which excluded waveform effects, proceeded uneventfully. However, with the introduction of waveforms and attendant transformations of the clutter integral into the range, range-rate coordinate system, occasional accuracy problems were encountered, problems that were aggravated as radar altitudes and target ranges diminished. Their association with the ground trace was particularly evident in cases where the altitude was reduced to those of airborne as opposed to spaceborne radar (Section 3). These findings resulted from the expenditure of a few person-years of effort over a period of less than a decade.

Similar insights had been evolved in Air Force airborne radar studies of the past 40 years, studies which consumed lifetimes of dedicated effort. They evolved from flat earth airborne radar studies of the 1940s and 1950s, and their earliest

examinations of spherical earth encounters coincided with, and were strongly influenced by, the onset of the computer age. Only in recent years have they accurately reported the complex structures of surface clutter in the range/range-rate distributions that the classical methods uncovered right away. It is our judgment that the decades of delay were the result of attempts to cope concurrently with the novelties of computer aided analysis and the seemingly inexplicable complexities in the observed distributions of clutter phenomena.

It is also our judgment that the problem addressed in this study, smoothly distributed surface clutter, is one that lends itself to formulations using the continuum methods of classical physics, followed by computer aided evaluations. The current tendency to compose this particular problem using the quantum methods of computer simulation is not inherently flawed, of course, but it can be plagued with difficult to find and difficult to fix accuracy problems caused in part by the clutter phenomenolgy, in part by the computer methods. It may be appropriate to save the simulation methods for other clutter phenomena.

4.1.1 Conclusions. The application of college level calculus to the study of the surface clutter of downlooking radars has contributed analyses which, after a total investment of a few person-years, has competed favorably with analyses developed by the entire radar community over the last forty years. The classical method leads to superior results because it nurtures insights into the underlying physical processes and discourages the representation of clutter effects which happen to be deterministic as statistical processes.

4.1.2 Recommendations. Two areas of radar clutter analysis deserve the immediate attention of classical methods because of potentially huge payoffs: one is simplification in formulating bistatic radar encounters, the other is exploration of partially coherent reflectivity of the earth's surface as a contributor to the seemingly statistical behavior of its clutt The goal of both efforts is to is to provide analytical alternatives to the currently total reliance on elaborate clutter models, theories, data banks, and simulations.

4.2 Training and Development of Systems Analysts

4.2.1 Conclusions. A major purpose of this contract was to familiarize selected members of the staff of Rome Laboratory with analysis methods suitable for characterizing the parameter and performance trades of downlooking, clutter limited radar. Participants did develop better appreciations for and insights into what is involved in theoretical radar studies and the remarkable breadth of technology that must be invoked - all at the same time - in determining what tasks a radar configuration can perform and how well. They discovered that an important feature of the study of radar is the need for current, advanced know-how in many areas, electromagnetics, transmitters, receivers, waveforms, antennas, propagation, microwaves, estimation, signal processing, data processing, computers, recording, etc.

The effort was less successful in imparting immediate and comprehensive understandings of the subject matter, mainly because none of the participants had adequate blocks of uninterrupted time to devote to serious theoretical studies during the lecture series, and none felt comfortable about having enough time in the future to continue them. The issue of uninterrupted time is crucial in all analytical studies, particularly during apprenticeships, particularly with a topic that demands proficiency in a large number of supporting subsystems and technologies.

What can be done to nurture the development of staff to provide long term capabilities and continuity in analytical radar studies? The first step is to identify suitable candidates with aptitudes for the mathematics of physics and engineering and the skill to perform and evaluate trade studies and analyses that extend across a very large number of parameter and performance dimensions. After individuals bring willingness and aptitude, success depends on management's willingness and ability to cultivate the evolution of needed capabilities with a nurturing work environment, consisting of three elements: (1) task assignments that foster analytical maturity, (2) enough uninterrupted time and adequate expert help to develop analytical skills and good instincts for the issues, and (3) continuing hierarchical guidelines, clearly delineating the relationships among the radar system and supporting subsystem activities, clearly delineating the role of the radar in its user environment, and how it fits into its command and control architecture.

The last of these elements contains an issue of substance: very often the needed guidelines are evolved from the studies they are intended to direct, studies that include examination of utilization strategies and command and control issues as well as trades among radar sizing, parameters and performances. Seasoned analysts may occasionally take on these political/management/public relations/ marketing/user related/consensus building responsibilities in addition to their analysis tasks, basically adding systems engineering functions to their analysis activities. For beginning analysts these activities can represent overwhelming distractions from the task at hand.

4.2.2 Recommendation. Our suggested approach is to compose project teams consisting of two or more staff members and to assign to each the combined systems engineering/systems analysis responsibilities for their project. The division of responsibilities and leadership among team members, and the apportionment of the free time needed for analytical advancement, can be adjusted according to the aptitudes and desires of each, with management oversight as required. Management cooperation in making adequate amounts of time available to each team member, as needed, is important. Various mixes of senior and junior staff can, in the long run, expose everyone to a large number of experiences and responsibilities. Of course, some individuals gravitate to the management/systems engineering responsibilities, others to the analytical responsibilities, and a few veterans manage to do both. This type of program structure, often involving larger teams, is typical of how much of the industry operates.

Specifically, current and long range goals can be fostered in a design effort in which a selected team of the RL/OC staff evaluates all of the cost, utilization, configuration, technical, performance, parameter and political trades involved in creating a complete, coherent and useful description of an airborne bistatic radar system. Enhanced systems engineering and analysis skills will be achieved through participation of the team's members, variously acting as a group, in directed subpanels, or as individual spokespersons, in:

- negotiations of performance objectives of search, track, signature, ...
- preliminary systems engineering studies for candidate bistatic designs,
- documentation of trades among deployments, configurations, cost, utility,
- development of a universal analytic geometry for bistatic encounters,
- analytical characterization of the earth's bistatic surface clutter.

APPENDIX A
GEOMETRICAL AND COORDINATE RELATIONSHIPS

The encounter of an elevated surveillance radar with targets and clutter on and near the surface of the earth is influenced strongly by its curvature. As the altitude of the radar diminishes, the more important it becomes to factor the spherical earth influences into the radar analyses - to avoid serious deficiencies in accuracy - particularly with respect to surface clutter. At first glance this appears to contradict common sense since anyone can see that a radar in orbit must be affected by the curvature effects while a low altitude radar encounter can be closely represented with a plane earth approximation. The problem is the extraordinary difficulty of visualizing the low altitude encounter because of the short range to the horizon compared with the earth radius.

The way to the facts is careful and accurate analysis, and the best procedure is to develop generally applicable analytical tools, using easy to visualize space based radar configurations (Figure A.1). With good analysis tools, the altitude can be reduced parametrically to support examinations of the airborne radars. Even then, uncommon care in numerical evaluation is needed to maintain accuracy at the lower altitudes, particularly along the ground trace and near the horizon.

The coordinate system adopted for this study is a Cartesian x,y,z system which is centered on the antenna's phase center and aligned with its aperture which is in tangential motion, without crab angle, above a spherical planet. The x-axis is the sidelooking direction relative to the ground trace. The y-axis is the down looking direction, passing through the center of the earth and intersecting its surface at the nadir point. The z-axis is the forward looking direction, parallel to the ground trace. The x-y axis intersects the earth along the zero Doppler contour, and the y-z axis along the ground trace. The orientation of the reference system allows surface clutter integrals to be composed in a convenient range, range-rate domain. The particular selection of the x or y and z axes is to permit the reference "patch" of surface clutter to be located in positive x, y and z directions.

Three different spherical coordinate systems are defined with their poles

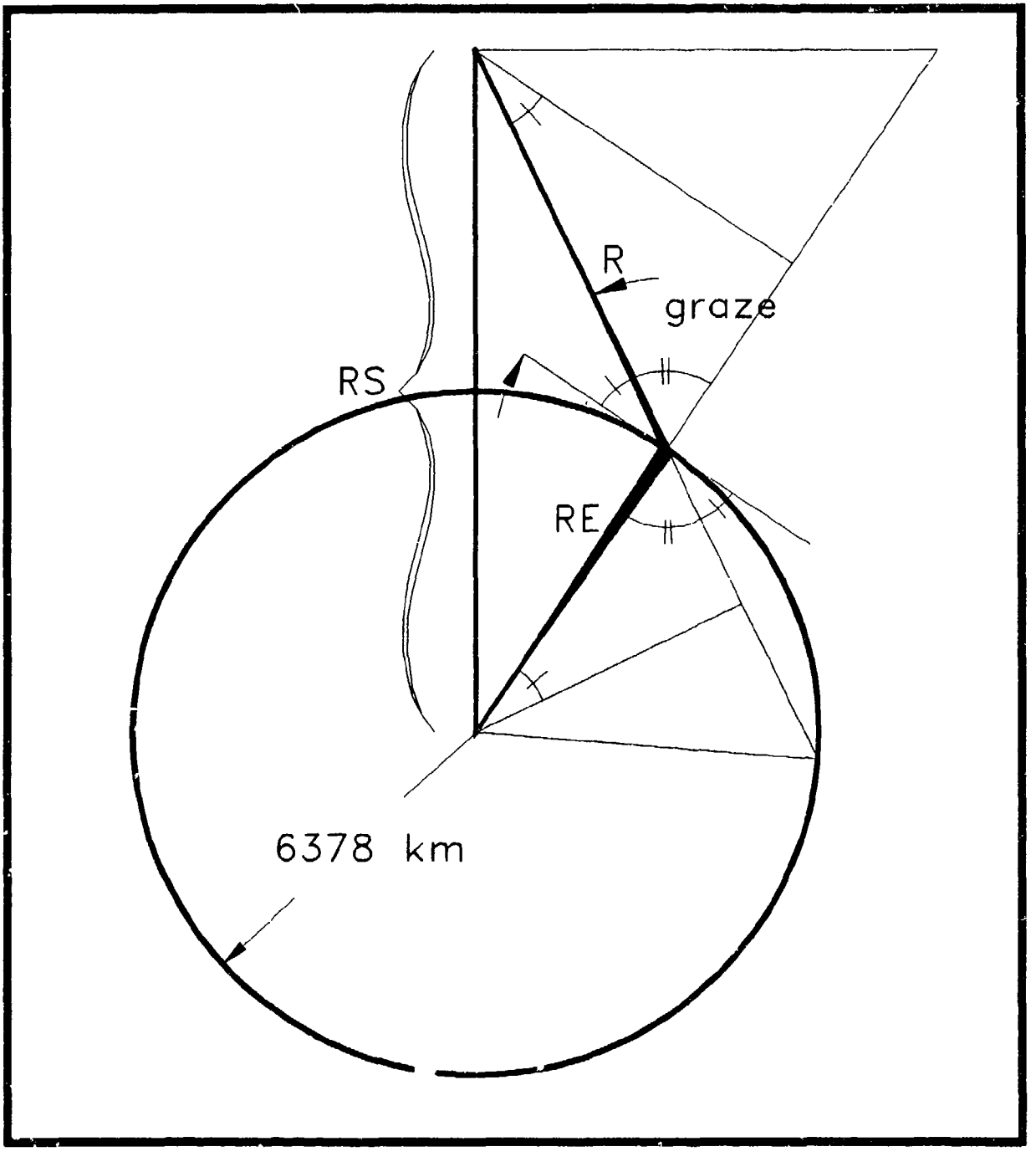

Figure A.1 Encounter Geometry

R = range to clutter patch, RE = earth radius, RS = orbit radius

Figure A.2 Spherical Coordinates with x, y and z Axis Poles

R = range vector from radar to clutter patch or to target

$$x = R\cos\theta_x = R\sin\theta_y\cos\phi_y = R\sin\theta_z\sin\phi_z$$

$$y = R\cos\theta_y = R\sin\theta_z\cos\phi_z = R\sin\theta_x\sin\phi_x$$

$$z = R\cos\theta_z = R\sin\theta_x\cos\phi_x = R\sin\theta_y\sin\phi_y$$

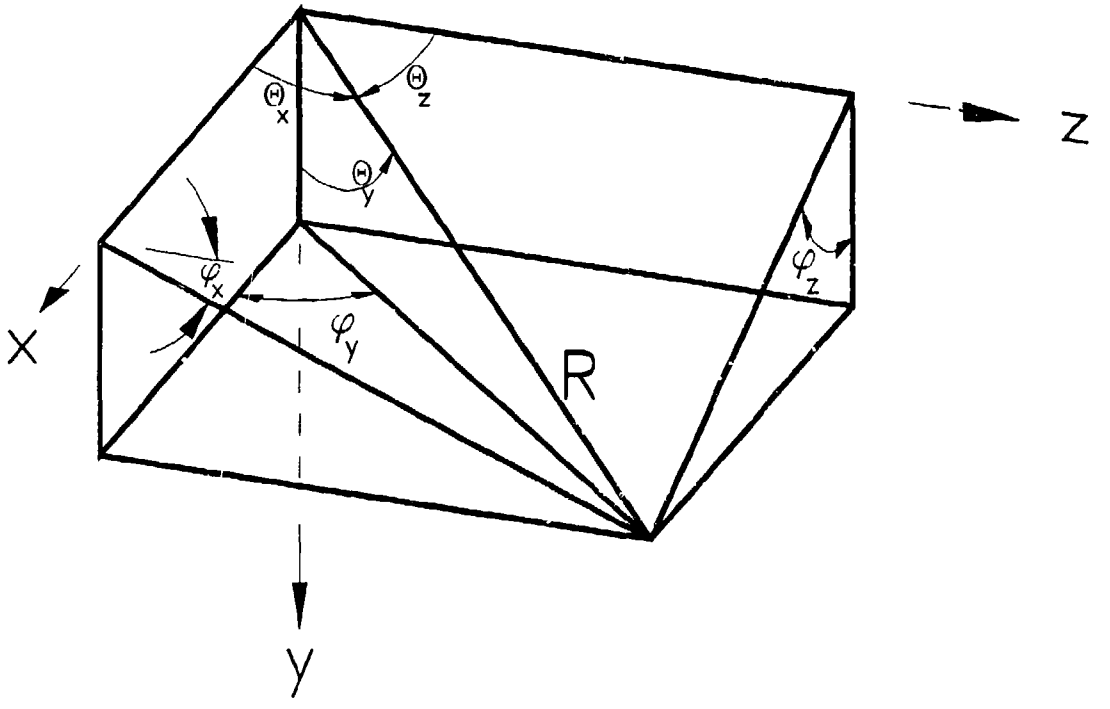

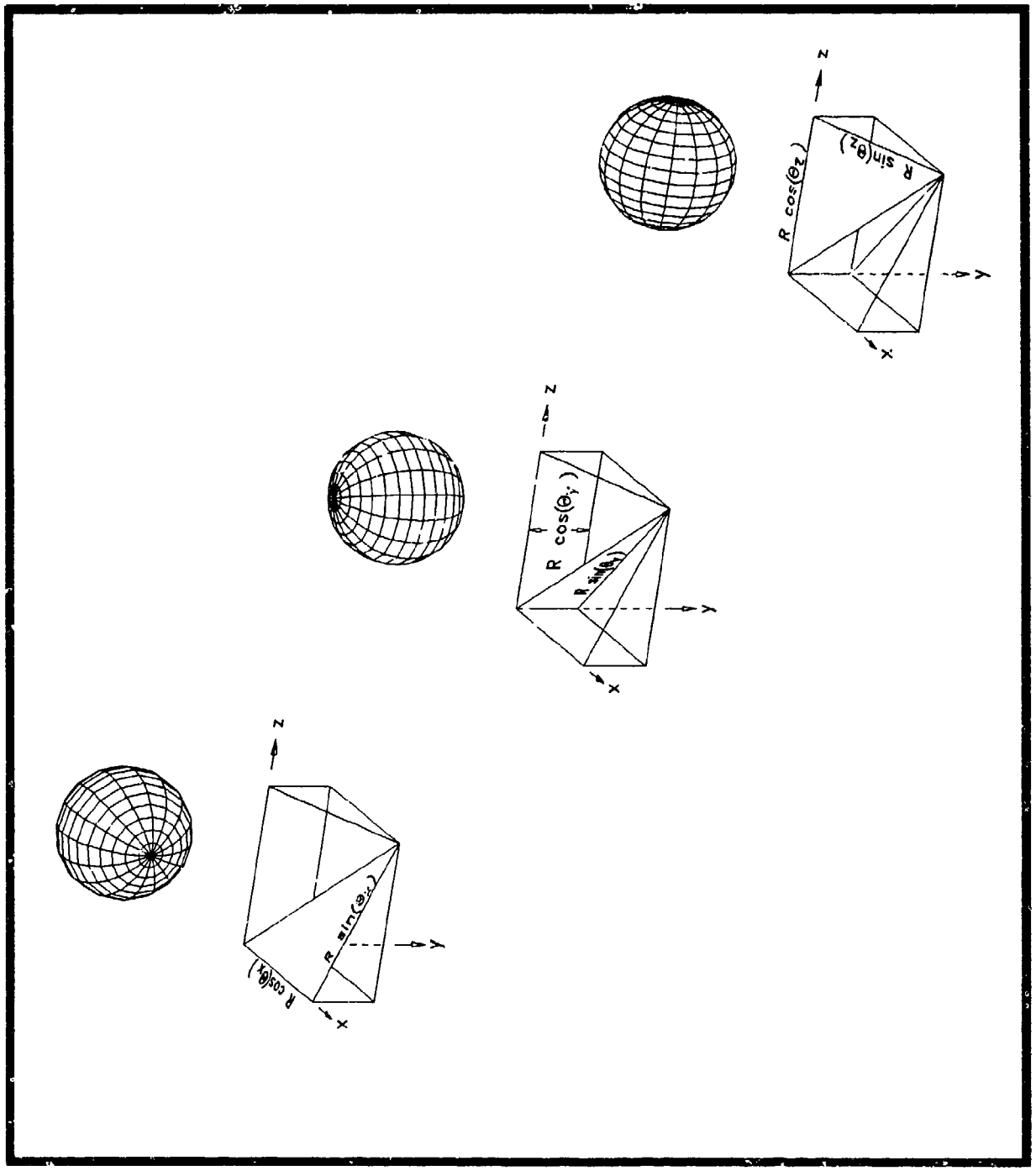

Figure A.3 Candidate Spherical Coordinate Systems

coinciding with each of the coordinate axes (Figure A.2, A.3). In all of the current work, the radar's antenna aperture is presumed to be of rectangular outline aligned with the y and z axes. When the zero crab condition is not met, then the antenna gain functions must be transformed from their platform orientation to the decrabbed coordinate reference.

In all of this work, the spherical coordinate system with the y-axis pole is used because it appears to be particularly appropriate for low PRF waveforms or those with a very modest number of range ambiguities. Other systems are better suited to high PRF waveforms, not subjects of immediate concern.

In the course of developing numerical tools to evaluate surface clutter integrals, it is highly advantageous to compose various examples, using simplified antenna pattern functions, which can be evaluated independently in several coordinate systems and to seek out other examples in which numerical methods can be compared with formally integrated results. The insights developed by these exercises into the relative accuracies of various numerical techniques and of coordinate system selections are invaluable.

Listed on page A-6 are a number of parameters and coordinate relationships used in the clutter analysis formulations of Sections 2 and 3. Note that the letter θ with a subscript is used to represent a polar angle in one of the three spherical coordinate systems whereas θ standing alone is used to represent the earth central angle between the radar and a clutter patch. The second expression from the bottom of the page, relating the range of a clutter patch to θ_y,

$r = r_s \cos\theta_y - \sqrt{r_e^2 - (r_s \sin\theta_y)^2}$, was obtained from consideration of two entwined triangles (Figure A.1), one defined by the radar, the earth center and the clutter patch, one a right triangle including the earth center and the clutter patch. Differentiation and manipulation of that equation leads to the expression following it which facilitates the transformation of the clutter integral from the y-oriented spherical coordinate system to waveform coordinates.

COORDINATE RELATIONSHIPS

Parameter list:

θ_x, Φ_x	polar and longitudinal angles of a spherical coordinate system with its pole sidelooking wrt ground track
θ_y, Φ_y	polar and longitudinal angles of a spherical coordinate system with a downlooking pole
θ_z, Φ_z	polar and longitudinal angles of a spherical coordinate system with its pole parallel to the ground track
r	range from radar to earth clutter patch
θ	angle at earth's center between radar and clutter patch
r_s	orbit radius
r_e	earth radius
r_t	range from radar to a target
r_h	range from radar to earth horizon
graze,g	grazing angle at the earth clutter patch

$$x = r\cos\theta_x = r\sin\theta_y\cos\Phi_y = r\sin\theta_z\sin\Phi_z$$

$$y = r\cos\theta_y = r\sin\theta_z\cos\Phi_z = r\sin\theta_x\sin\Phi_x$$

$$x = r\cos\theta_z = r\sin\theta_x\cos\Phi_x = r\sin\theta_y\sin\Phi_y$$

$$r = r_s\cos\theta_y - \sqrt{r_e^2 - (r_s\sin\theta_y)^2}$$

$$\frac{\partial r}{\partial \theta_y} = \frac{r_s\, r\sin\theta_y}{r_s\cos\theta_y - r}$$

Listed on page A-8 are a number of relationships among the various distances and angles of the downlooking radar encounter (Figure A.1). The expressions of the first three lines of that page are obtained from application of the law of sines to the radar/earth center/clutter patch triangle. Those on the following two lines result from several applications of the law of cosines to same triangle and the identity:

$$r_s^2 = r_e^2 + r_h^2 \ .$$

Another useful identity is the simple one stating that:

$x^2 + y^2 + z^2 = r^2$, corresponding to the familiar result that the sum of the squares of the direction cosines of any point is unity:

$$\cos^2\theta_x + \cos^2\theta_y + \cos^2\theta_z = 1 \ .$$

Following on page A-9 are many of the same associations presented in terms of the normalized waveform coordinates ρ and μ described in Section 2. The range-rate/angle relationship, $\mu = \cos\theta_z$, and its intimate connection with one of the antenna pattern parameters of a suitably deployed and configured array antenna (aligned with the ground trace, rectangular and separably illuminated) is essential in the development of the methods described in this report. Awareness of these relationships can be exploited to achieve far better adaptive clutter reduction than can be achieved otherwise. In retrospect, these relationships are not only simple, but they are perfectly obvious. It's difficult to conceive of how they evaded incorporation, without notice, into the evolution of airborne, clutter limited radar. If they were, it was a well kept industry secret. Nowhere in early airborne radar literature has any reference to them been found. As recently as 1988, when these concepts were briefed extensively to leading experts of the world's most successful pulse-Doppler radar company, they were met with skepticism. (Their own speculations regarding synergistic waveform and antenna patterns, based on fallacious antenna concepts, had been abandoned.)

GEOMETRICAL RELATIONSHIPS

$$\frac{r}{\sin\theta} = \frac{r_s}{\sin(\theta + \theta_y)} = \frac{r_e}{\sin\theta_y} = \frac{r_s}{\cos(graze)}$$

$$\tan\theta_y = \frac{\sin\theta}{\frac{r_s}{r_e} - \cos\theta}: \qquad \tan\theta = \frac{\sin\theta_y}{\frac{r_s}{r} - \cos\theta_y}$$

$$r = r_e \frac{\sin\theta}{\sin\theta_y} = r_e \frac{\cos(\theta_y + graze)}{\sin\theta_y}$$

$$\cos(graze) = \frac{r_s}{r_e}\sin\theta_y: \qquad \sin(graze) = \frac{r_h^2 - r^2}{2\, r\, r_e}$$

$$\cos\theta_y = \frac{r_h^2 + r^2}{2\, r\, r_s}$$

$$\theta + \theta_y + \text{graze} = \pi/2$$

NORMALIZED RELATIONSHIPS

$$\rho = \frac{r_{cl}}{r_h} \qquad \mu = \frac{rdot_{cl}}{v_s}$$

$$\sin\theta_y \, d\theta_y = \frac{1 - \rho^2}{2 \rho^2 \left(\frac{r_s}{r_h}\right)} \, d\rho$$

$$\cos\theta_y = \frac{1 + \rho^2}{2 \rho \frac{r_s}{r_h}} \qquad \sin(graze) = \frac{1 - \rho^2}{2 \rho \frac{r_e}{r_h}}$$

$$\mu = \cos\theta_z = \sin\theta_y \sin\phi_y$$

$$d\mu = \cos\theta_y \sin\phi_y \, d\theta_y + \sin\theta_y \cos\phi_y \, d\phi_y$$

$$d\phi_y = \frac{d\mu}{\cos\theta_x} + \frac{\mu \, d\rho}{\rho \cos\theta_x} \frac{(1 + \rho^2)(1 - \rho^2)}{1 - 2 \rho^2 \left(\frac{r_s^2 + r_e^2}{r_h^2}\right) + \rho^4}$$

The explicit representation for the differential element of angle, $d\phi_y$, is included because it is used in the transformation of the surface clutter integral into waveform coordinates. Except at nadir range where its denominator has a double zero, a few test cases have indicated that its second term can safely be ignored. (The denominator's other two zeros occur at the range of the nadir's antipode.)

The expression for integrated clutter to target ratio developed in Section 2 was evolved from a form:

$$R = \int_{earth's\ area} \frac{(G_1 G_2)_{cl}}{(G_1 G_2)_t} \frac{Æ_{cl}}{Æ_t} \frac{\sigma^c r_t^4}{\sigma_t r_{cl}^2} \sin\theta \, d\theta \, d\phi$$

which can be transformed using previous relationships to:

$$R = \int_{earth's\ area} \frac{(G_1 G_2)_{cl}}{(G_1 G_2)_t} \frac{Æ_{cl}}{Æ_t} \frac{\sigma^c r_t^4}{\sigma_t r_{cl}^2} \frac{1-\rho^2}{2\rho^2 (\frac{r_s}{r_h})} \frac{d\rho \, d\mu}{\cos\theta_x}$$

The analysis domain extends over the right or left half of the earth's cap visible from the radar:

$$\text{Domain of } \mu = \pm \sqrt{1 - \left\{ \frac{1 + \rho^2}{2\rho \ (r_s / r_h)} \right\}^2} = \pm \sin\theta_y$$

$$\text{Domain of } \rho = (r_s - r_c) / r_h \quad \text{to} \quad 1$$

In many circumstances, the integration range can be a small fraction of the analysis domain near the peak of the antenna pattern with essentially zero impact on accuracy and largely diminished run times. In other circumstances adequate

accuracy depends on integrating over the entire domain of μ, for selected range intervals. In others it is essential to integrate to the minimum value of ρ, for selected range-rate intervals.

Depending on the specific encounter, other forms of the clutter integral, obtained by straightforward manipulation, may be advantageous, including:

$$R = \int_{earth's\ area} \frac{1}{2} \frac{(G_1G_2)_{cl}}{(G_1G_2)_t} \frac{Æ_{cl}}{Æ_t} \frac{\sigma^c\, r_t^4}{\sigma_t\, r_{cl}^2} \frac{1-\rho^2}{\rho^2 \left(\frac{r_s}{r_h}\right)} \frac{d\rho\, d\mu}{\sqrt{1-\mu^2-\left\{\frac{1+\rho^2}{2\rho\, r_s / r_h}\right\}^2}}$$

or,

$$R = \int_{earth's\ area} \frac{1}{2} \frac{(G_1G_2)_{cl}}{(G_1G_2)_t} \frac{Æ_{cl}}{Æ_t} \frac{\sigma^c\, r_t^4}{\sigma_t\, r_s r_h} \frac{1-\rho^2}{\rho^4} \frac{d\rho\, d\mu}{\sqrt{1-\mu^2-\left\{\frac{1+\rho^2}{2\rho\, r_s / r_h)}\right\}^2}}$$

which, for the target at horizon range, becomes:

$$R = \int_{earth's\ area} \frac{1}{2} \frac{(G_1G_2)_{cl}}{(G_1G_2)_t} \frac{Æ_{cl}}{Æ_t} \frac{\sigma^c\, r_h^3}{\sigma_t\, r_s} \frac{1-\rho^2}{\rho^4} \frac{d\rho\, d\mu}{\sqrt{1-\mu^2-\left\{\frac{1+\rho^2}{2\rho\, r_s / r_h}\right\}^2}}$$

When the integration extends to the boundary where $\cos\theta_x$ is zero, the integral becomes improper and must be carefully examined for convergence and for computer evaluation problems.

The following forms, exhibiting no waveform dependencies, can be applied to any configuration lacking range-rate processing. They are particularly useful in comparing different evaluation strategies.

$$d\left(\frac{p_{cl}}{p_t}\right) = \left(\frac{g_{cl}}{g_t}\right)^2 \frac{r_h^2\ \sigma^c}{\sigma_t} \frac{1-\rho^2}{2\ \left(\frac{r_s}{r_h}\right)\ \rho^4}\ d\rho\ d\phi_y$$

which, for antenna patterns which are omnidirectional in azimuth, leads to:

$$d\left(\frac{p_{cl}}{p_t}\right) = \pi\ \left(\frac{g_{cl}}{g_t}\right)^2 \frac{r_h^2\ \sigma^c}{\sigma_t\ \left(\frac{r_s}{r_h}\right)} \frac{1-\rho^2}{\rho^4}\ d\rho$$

APPENDIX B
SURFACE CLUTTER DENSITY

Figure 2.9, page 2-10, illustrates a downlooking radar's main beam illuminating an area of the earth's surface and the decomposition of the incident energy into a specular reflection, a component refracted into and absorbed by the earth, and a rescattered component. For monostatic radar, surface clutter occurs because a portion of the rescattered energy is directed back toward the radar and, for near vertical incidence, part of the specular component as well. The depiction of the radar's main lobe being scattered, absorbed and reflected is illustrative only and ought not obscure the fact that sidelobe energy also illuminates the earth and is scattered, absorbed and reflected in identical fashion.

The cross section density of the earth's surface is a measure of what fraction of the power incident on it is retroreflected and contributes to the surface clutter. Two densities have been identified:

σ^c = backscatter RCS of a unit area on the radiation sphere, and

σ^0 = backscatter RCS of a unit area on the earth sphere.

They are related by $\sigma^0 = \sigma^c \sin(\text{graze})$ as illustrated in Figure 2.8, page 2-9. For historical reasons, the clutter cross section is usually described as a density representing the clutter RCS of a unit area on the earth sphere, σ^0. For purposes of this study the density σ^c is a more sensible parameter.

A constant value of σ^c, representing isotropic scattering by the surface, corresponds to σ^0 varying as the sine of the grazing angle, a first order approximation suitable for most of the earth except near the nadir point where the specular component usually dominates. A reasonable model for its behavior adds a term varying as $\sin^{299}$(grazing angle) to account for specular contributions to σ^c (Figure B.1), resulting in a constant surface reflectivity over most of the earth of 0.01 square meters/square meter, or -20 dBsm/sm, smoothly progressing to a fully specular reflection at the nadir point where the grazing angle is 90 degrees.

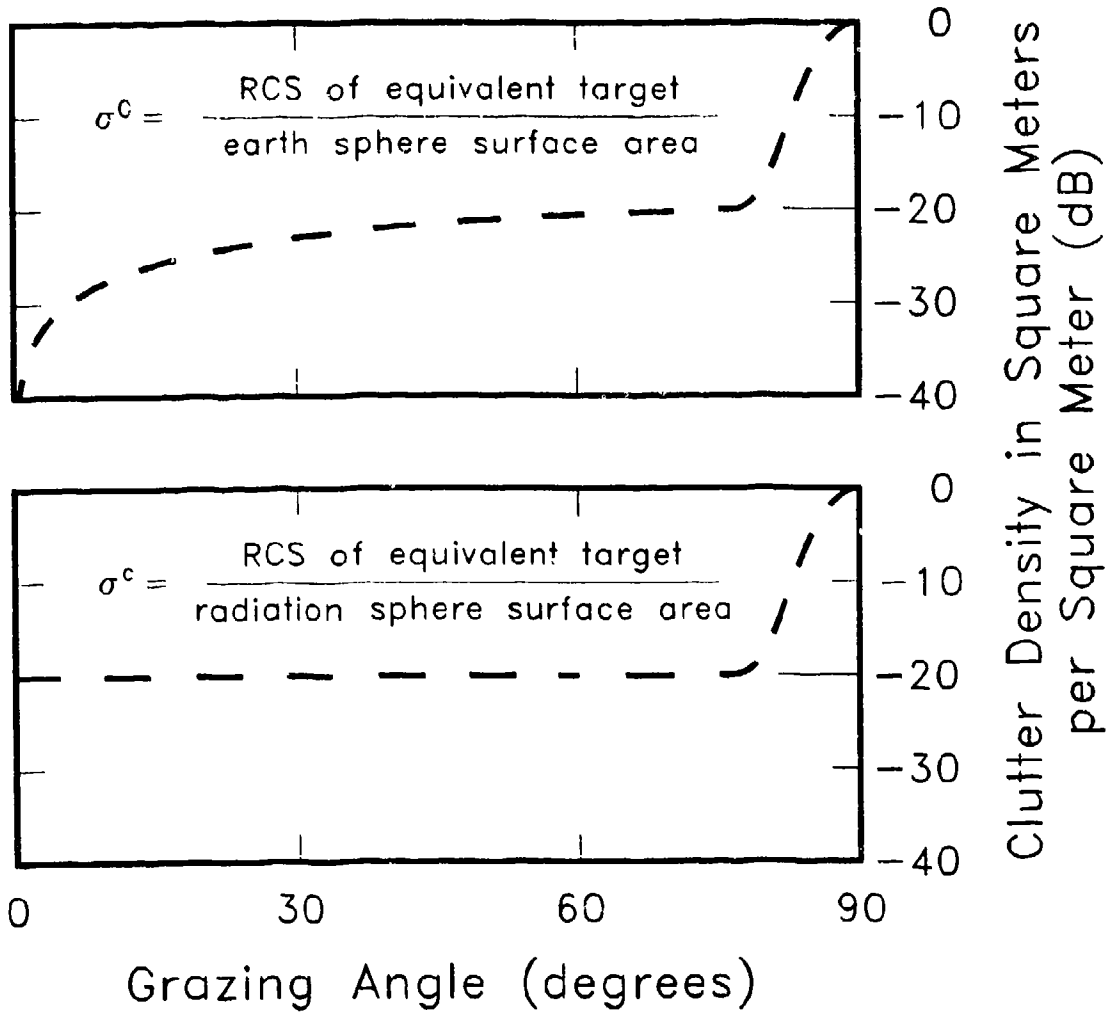

Figure B.1 Clutter Cross Section Densities versus Grazing Angle

In this formulation, differential elements of clutter power are estimated and then integrated non-coherently to obtain complete distributions. Undoubtedly, some differential elements of clutter power exhibit partial coherences, leading to glint and scintillation effects, not considered here. The surface clutter density, described here as varying with grazing angle, also varies with the time of year, the weather, the terrain, frequency, etc. It can exhibit extremely large spikes as, for example, a one square meter patch which is momentarily focussed on the radar and presents it with an X-Band RCS exceeding 10,000 square meters.

For integrating the clutter density distribution over the visible earth in accordance with the analysis developed in Section 2, it is necessary that it be described in waveform coordinates. It is easily converted from a function of grazing angle to an altitude dependent function of range (Figure B.2). The knees at the nadir spike boundaries are exceedingly abrupt in this domain, leading to

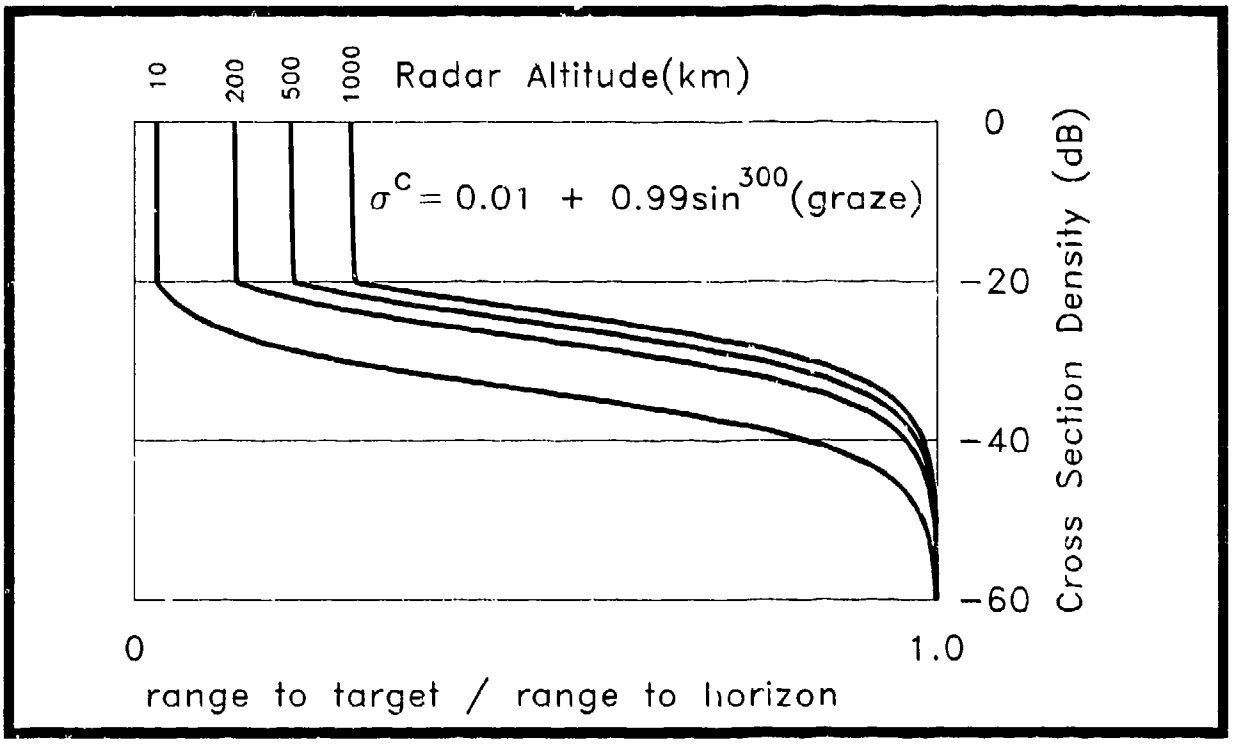

Figure B.2 Clutter Cross Section Density versus Range

some interesting calculation issues in characterizing the complete distribution. Efficient but accurate calculation depends on fine sampling near the horizon, exceptionally fine sampling at the knee and relatively coarse sampling elsewhere. Clutter integrals that extend across the entire domain are best accomplished in segments to minimize computing resources. Brute force approaches that rely on using the finest spacing everywhere are still far too time consuming for efficient utilization of any of the present generation of personal computers and investment in some old fashioned finesse is worthwhile.

Combining these clutter distributions with the geometrical relationships evolved in Appendix A and integrating full circle in azimuth leads to descriptions of the distribution of a one dimensional clutter power density in elevation angle for four radar altitudes ranging from 10 to 1000km using an isotropic radar antenna (Figure B.3). When the process is repeated to describe the distribution of clutter power density in range rather than elevation angle, some intriguing and highly structured properties near nadir, particularly when the radar antenna's power pattern exhibits sin(elevation) or $\sin^2$(elevation) behavior (Figure B.4). The rapid rise of the clutter function at nadir prevents the antenna pattern, as it approaches zero, from completely suppressing the nadir spike. The near nadir behavior for the altitude of 10 km (Figure B.5) suggests that barely perceptible pitch and roll maneuvers of the host aircraft could account for many curious effects that have been observed with high PRF waveforms, certainly including the increased false alarm rate that can accompany finer resolutions in range and range-rate.

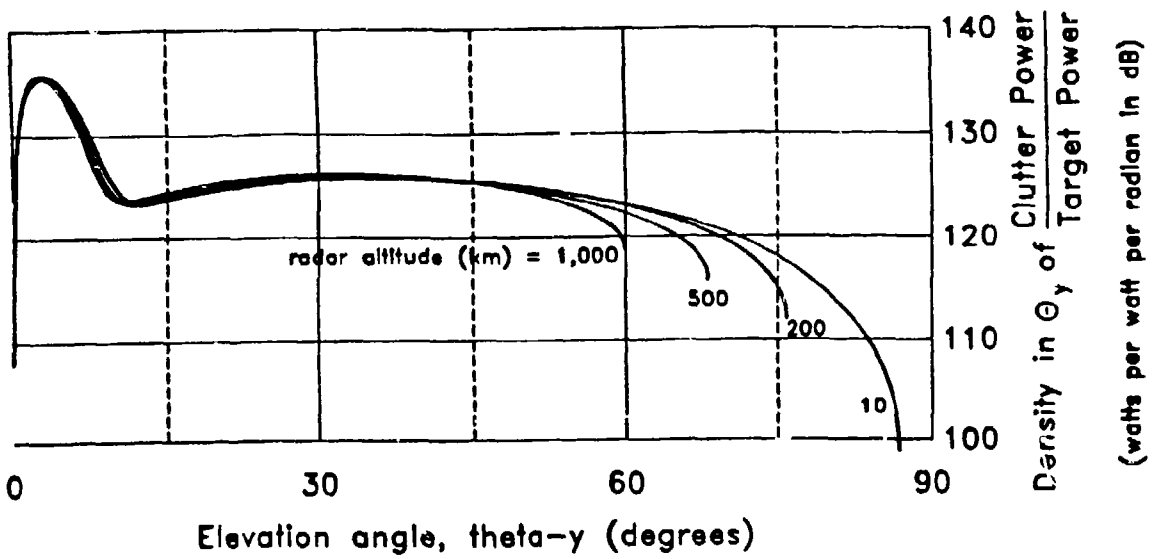

Antenna pattern = isotropic: $\sigma^c = 0.01 + 0.99\sin^{299}$(grazing angle)

Figure B.3 Clutter Densities in Elevation Angle

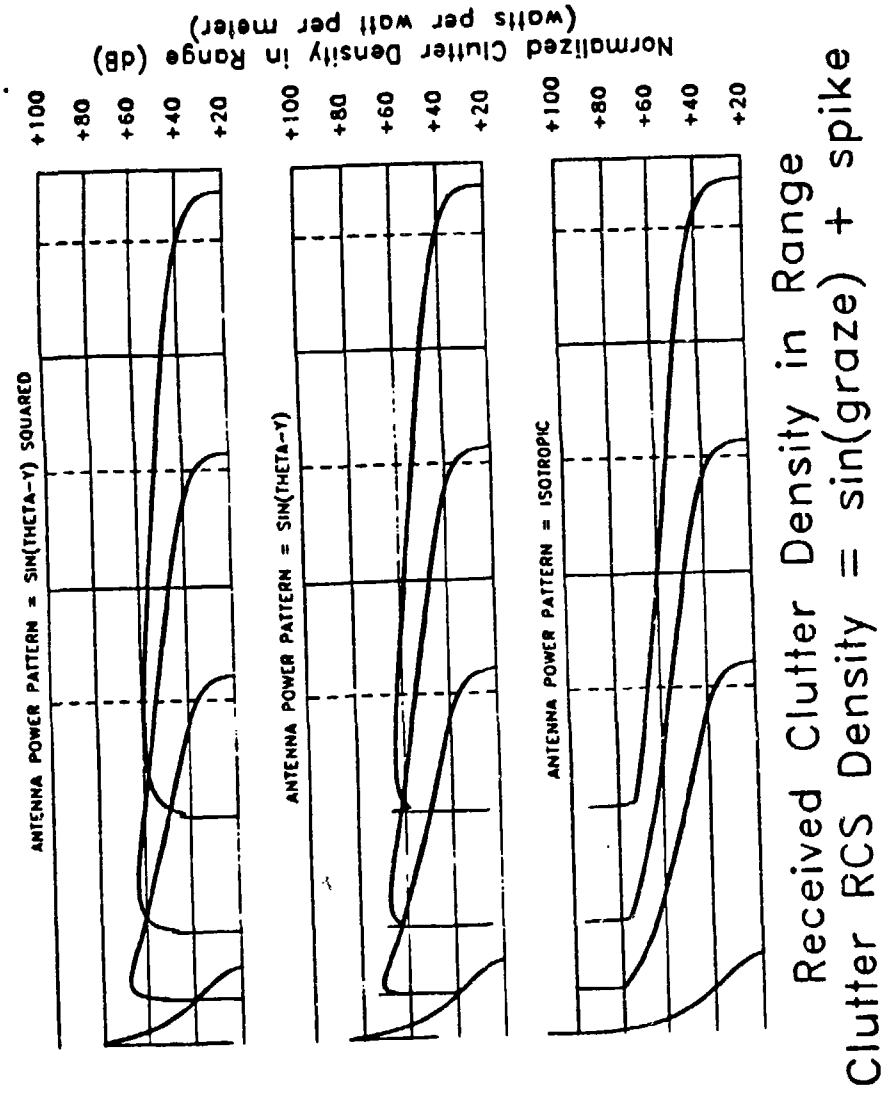

$\sigma^c = 0.01 + 0.99\sin^{299}(\text{grazing angle})$

Figure B.4 Clutter Densities in Range

Figure B.5 Clutter Densities in Range near the Nadir Point
Radar Altitude = 10 km: $\sigma^c = 0.01 + 0.99 \sin^{299}$(grazing angle)

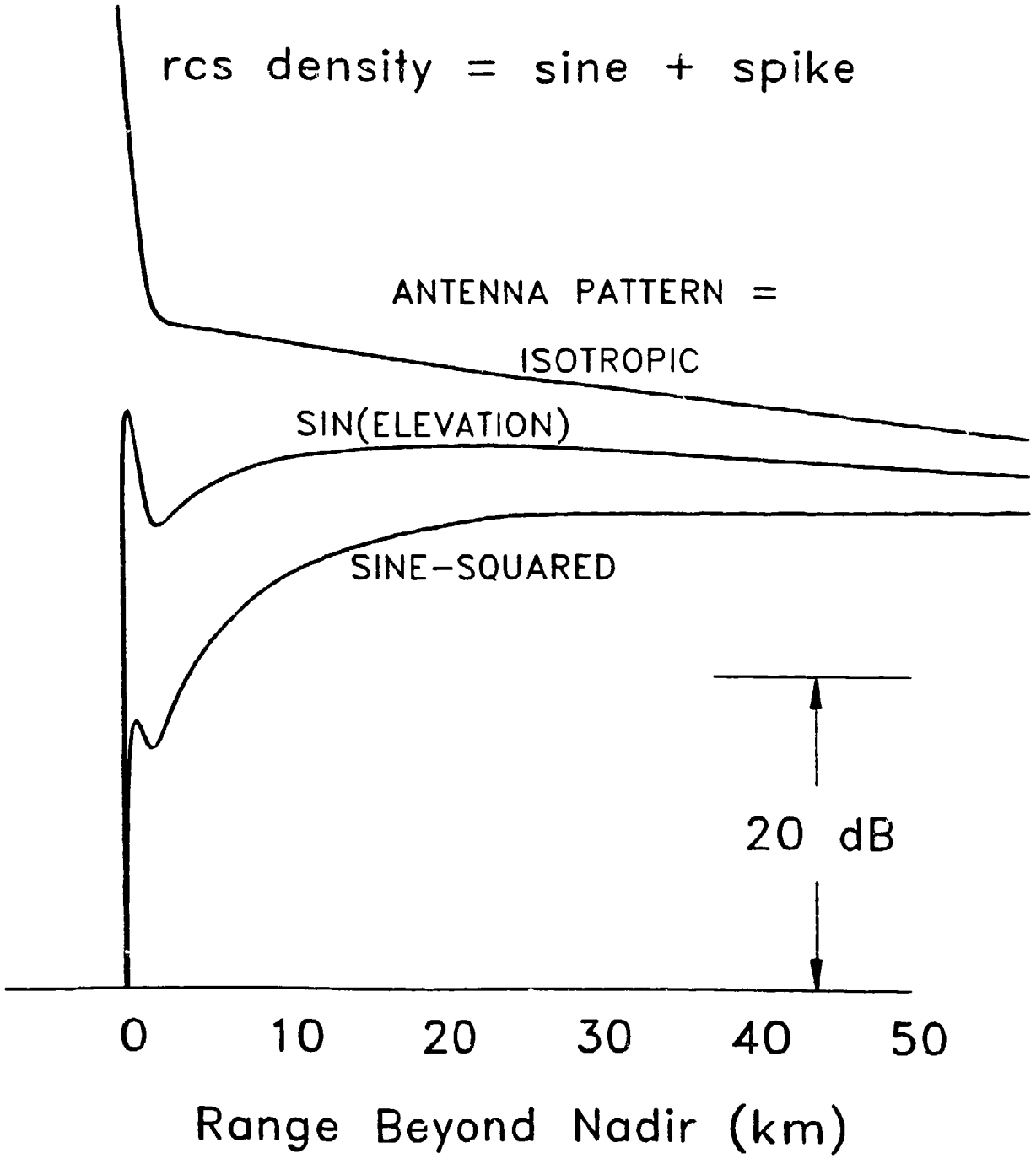

The range distribution of clutter power (still presuming omnidirectional azimuth antenna patterns) is modified profoundly by using an antenna with resolving power in elevation angle only. A vertical line array of sixteen elements, uniformly illuminated and separated by 0.7-wavelength results in the two distributions of Figure B.6, depending on the antenna's elevation pattern peak being directed at the horizon or at 0.3 of horizon range. In both cases the normalizing target was located at the horizon. They illustrate rapid growth in clutter power at nadir, but their accuracy in the sidelobe region has been corrupted because of undersampling. Note that the radar altitude in this case is 60,000 ft.

Scanning the beam even closer to the radar, to 0.2 of horizon range, results in most of the visible surface being illuminated by the first elevation sidelobe above the main beam (Figure B.7). In this case, the normalizing target has been relocated to the peak of the elevation beam. Accuracy in the near in sidelobe is again corrupted by undersampling, but more detailed examination does provide accurate results.

Figure B.6 Clutter Densities in Range (10m Range Interval)
Target at Horizon Range

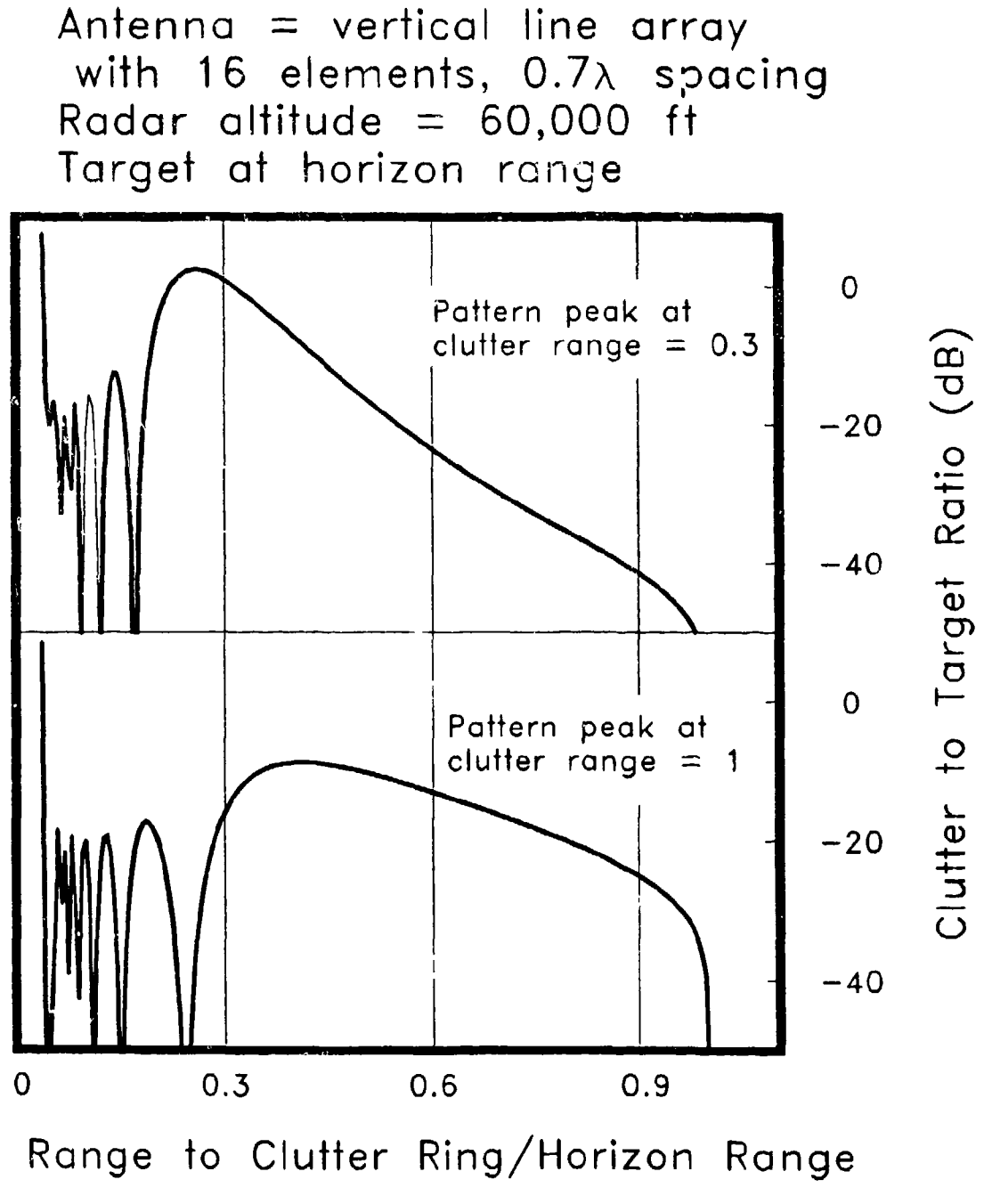

Figure B.7 Clutter Density in Range (10m Range Interval)
Target at 0.2 Horizon Range

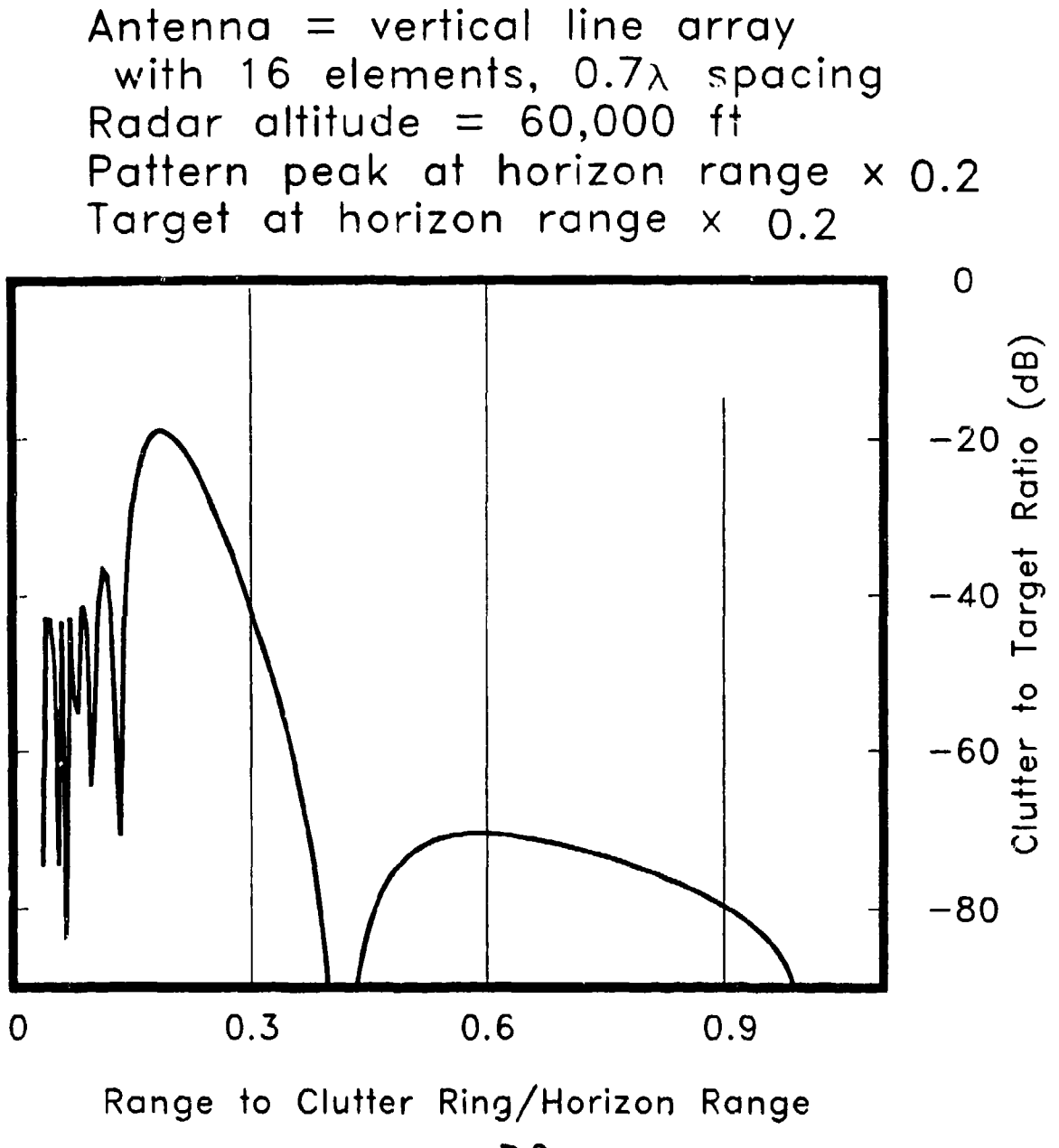

*U.S. GOVERNMENT PRINTING OFFICE: 1994-510-117-50040

MISSION

OF

ROME LABORATORY

Mission. The mission of Rome Laboratory is to advance the science and technologies of command, control, communications and intelligence and to transition them into systems to meet customer needs. To achieve this, Rome Lab:

a. Conducts vigorous research, development and test programs in all applicable technologies;

b. Transitions technology to current and future systems to improve operational capability, readiness, and supportability;

c. Provides a full range of technical support to Air Force Materiel Command product centers and other Air Force organizations;

d. Promotes transfer of technology to the private sector;

e. Maintains leading edge technological expertise in the areas of surveillance, communications, command and control, intelligence, reliability science, electro-magnetic technology, photonics, signal processing, and computational science.

The thrust areas of technical competence include: Surveillance, Communications, Command and Control, Intelligence, Signal Processing, Computer Science and Technology, Electromagnetic Technology, Photonics and Reliability Sciences.